Molecular Mechanics of Cartilage: Quantification of GAG Electrostatic Interactions Via High-Resolution Force Spectroscopy

By

Joonil Seog

M.S., Chemical Technology, 1995
Seoul National University

B.S., Chemical Technology, 1993
Seoul National University

SUBMITTED TO THE DEPARTMENT OF MECHANICAL ENGINEERING IN PARTIAL FULFILLMENT OF THE REQUIREMENTS FOR THE DEGREE OF DOCTOR OF SCIENCE IN POLYMER SCIENCE AND ENGINEERING
AT THE
MASSACHUSETTS INSTITUTE OF TECHNOLOGY

JUNE 2003

Signature of Author:_____
Department of Mechanical Engineering
May 13, 2003

Certified by:_____
Alan J. Grodzinsky
Professor of Electrical, Mechanical, and Bioengineering
Thesis Supervisor

Accepted by:_____
Ain A. Sonin
Chairman, Department of Committee on Graduate Students

Molecular Mechanics of Cartilage: Quantification of GAG Electrostatic Interactions Via High-Resolution Force Spectroscopy

By

Joonil Seog

Submitted to the Department of Mechanical Engineering
On May 28, 2003 in Partial Fulfillment of the
Requirements for the Degree of Doctor of Science in
Polymer Science and Engineering

Abstract

Intermolecular repulsion forces between negatively charged *glycosaminoglycan* (CS-GAG) macromolecules are a major determinant of cartilage biomechanical properties. It is thought that the electrostatic component of the total intermolecular interaction is responsible for 50-75% of the equilibrium elastic modulus of cartilage in compression, while other forces (e.g., steric, hydration, van der Waals, etc.) may also play a role.

To investigate these forces, radiolabeled CS-GAG polymer chains were chemically end-grafted to a planar surface to form model biomimetic polyelectrolyte "brush" layers whose environment was varied to mimic physiological conditions. The total intersurface force ($\leq$ nN) between the CS-GAG brushes and chemically modified probe tips (SO_3^- and OH) was measured as a function of tip-substrate separation distance in aqueous solution using the technique of high-resolution force spectroscopy (HRFS). These experiments showed long-range, nonlinear, purely repulsive forces that decreased in magnitude and range with increasing ionic strength and decreasing pH.

In order to estimate the contribution of the electrostatic component to the total intersurface force, the data were compared to a theoretical model of electrical double layer repulsion based on the Poisson-Boltzmann formulation. The CS-GAG brush layer was approximated as either a flat surface charge density or a smoothed volume of known fixed charge density and the probe tip was modeled as a smooth hemisphere of constant surface charge density.

To further closely mimic physiological condition of the cartilage, the CS-GAG molecules were successfully attached to the AFM probe tip using electric field. The CS-GAG modified tip was characterized by measuring force at various environments and its parking density was also estimated using newly developed molecular level model. The measured force between CS-GAG modified tip and CS-GAG modified substrate showed a long-range interaction that significantly dependent on the ionic strength and pH, indicating the significant role of Coulombic interaction between CS-GAG layers. The equilibrium brush height measured using ellipsometry showed that CS-GAG behaves as an annealed polyelectrolyte that reached its maximum brush height around 0.1 M salt concentration. The equilibrium brush height was compared with the onset of the force increase to obtain further insight on the CS-GAG brush behavior during the force measurement.

Thesis Supervisors:

Christine Ortiz
Title: Professor of Department of Materials Science and Engineering

Alan J. Grodzinsky
Title: Professor of Department of Electrical, Mechanical and Bioengineering

Acknowledgments

First of all, I would like to thank the members of my research committee. I am grateful for them to share time to answer my questions, read drafts, and provide practical advice. It has been my privilege to work with Alan and Christine, my mentor and advisor, during my PhD program. I learned many important lessons that will guide me throughout my life. Alan set me an example as both a skillful researcher and exemplary mentor. From Al, besides fundamentals of electromechanics, I learned that I need coffee, not tea, to stay awake after having truck lunch. If you want optimal results from coffee, you need to make a coffee following the instructions that is written on the top of the coffee maker.(Don't forget to use the right spoon to measure the amount of the ground coffee) I still remember the day when Christine and I opened the AFM box to set it up. Not only did she provide me an opportunity to work on atomic force microscopy, but also she encouraged me to pursue my ideas and guided me with patience. Her suggestion based on her expertise in AFM improved the quality of my papers. Her encouragement inspired me to examine every aspect in further detail and analyze the results in a rigorous way. Prof. Blankschtein enriched my research with his expertise in colloidal science. He provided me with broader perspectives and excellent feedback on key aspects of my thesis.

There have been many friends who have supported me during my doctoral program. Thanks to Han-Hwa and Linda for their support and encouragement throughout my PhD program. I really enjoyed having foods that Han-Hwa brought time to time. Thanks also to my office mate, Delphine, for her help with modeling and emotional support. She also helped me to familiarize with AFM at the beginning of the project. We worked on the chemistry to attach GAG on the surface together and the model that she built has become invaluable for quantitative interpretation of my experimental data. Thanks to Laurel who always cheered me up when I was at a loss. The wonderful GAG image that she obtained has become the first slide of my presentation. I would like to thank Parth for his valuable advice whenever I was having difficulty. I thank Moonsoo, John, Jon, Fitzy, Cindy, Mike, Nora, Diana, and all the members of Continuum mechanics group and Ortiz group members,

Monica, Kuangshin, Kristin, Ben, Jennifer, Celia, Miao, Dong, Reuben, for supporting me always and making my life at MIT more enjoyable.

I am grateful for my parents who have continuously supported and prayed for me. They have always encouraged me and provided me with opportunities whenever I wanted to do something. I could not have completed this work without their love and devotion.

Lastly, I would like to thank my wife, Sunmin Lee. With her love and support, I was able to overcome difficulties and finish this work successfully. She listened, advised, encouraged and made me smile whenever I had concerns, made me laugh when I was stressed out and did everything she could to help me to concentrate on my study.

LIST OF FIGURES

LIST OF TABLES

TABLE OF CONTENTS

Chapter 1

GENARAL INTRODUCTION

1.1 Structure of Cartilage

Articular cartilage is a vascular, dense connective tissue that covers the ends of the bone and functions as a load bearing material in synovial joints (Figure 1.1). Water comprises about 80 % of the wet weight of cartilage and the dense extracellular matrix constitutes the remaining 20 % of the wet weight of the cartilage. Chondrocytes, cells in the cartilage, regulate the synthesis, and degradation of those extracellular materials. The unique composition of this biocomposite shows the complex poroelastic behavior giving the tissue high stiffness, toughness, and shock absorption capabilities. Two major extracellular matrix components responsible for these biomechanical properties are collagen and proteoglycan. Collagen, mainly type II collagen in the cartilage, serves as a structural component giving the cartilage tensile resistance as it does in many other tissues. Aggrecan, a member of the proteoglycan family of molecules in the cartilage are major determinant for compressive resistance due to its highly charged nature, generating significant swelling pressure and contributing up to 50% of the overall equilibrium compressive stiffness of cartilage.(Figure

1.2(a)) [1, 2] The resistance of aggrecan to fluid flow is a major determinant of the tissue' dynamic stiffness under cyclic loading

A single aggrecan molecule contains about 100 *chondroitin sulfate glycosaminoglycans* (CS-GAGs) that are covalently bound to a core protein at extremely high densities (~2-4 nm molecular separation distance) (Figure 1.2(b), schematic picture with HA). Multiple aggrecan molecules assemble further to form *aggregates* by non-covalent attachment to *hyaluronan (HA)*, an interaction stabilized by the adjacent binding of *link protein*.(Figure 1.2(a)) The aggregates form the gel-like component of cartilage that is enmeshed within a network of reinforcing *collagen fibrils.*

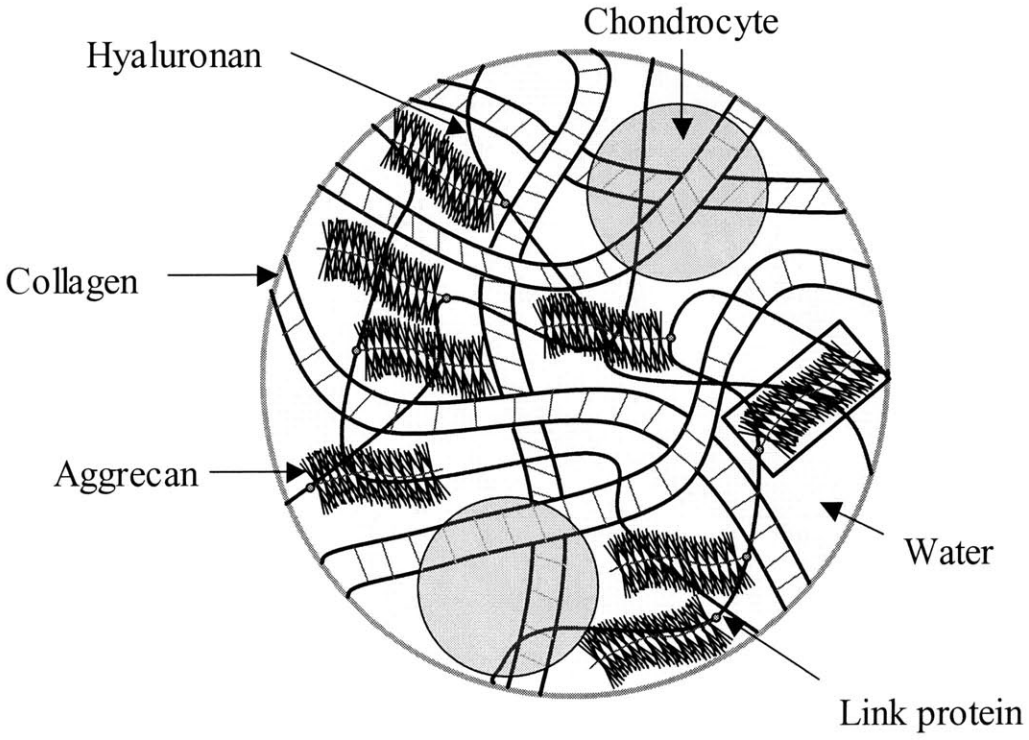

Figure 1.1: Schematic picture of the cartilage in microscopic scale. Chondrocyte maintains the extracellular matrixes of the cartilage. Collagen and aggrecan are two major components of the extracelluar materials that gives a tensile and compressive strength of the cartilage.

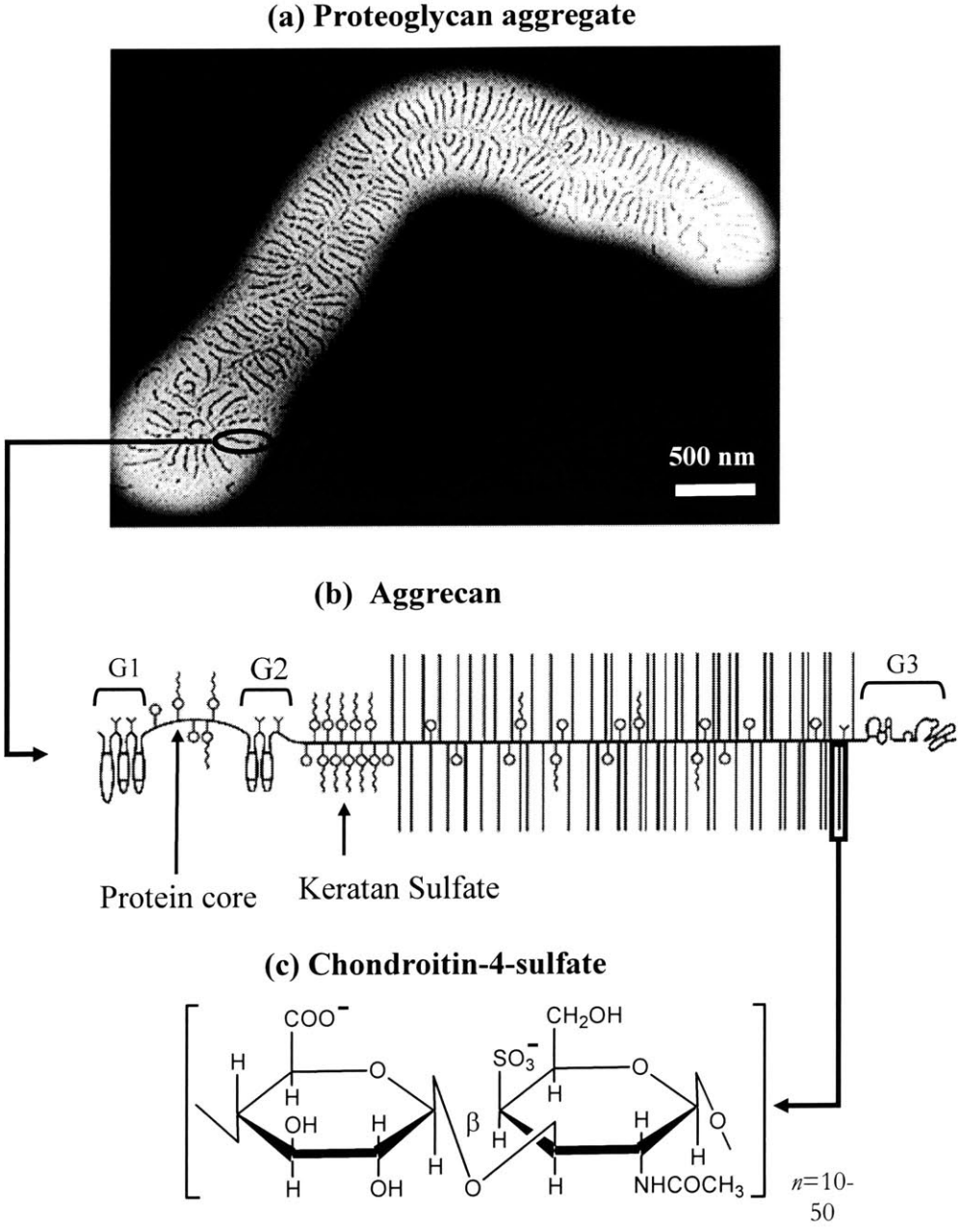

Figure 1.2: Structural hierarchy of aggrecan in cartilage: (a) electron microscopy of aggrecan and the aggregates it forms with hyaluronan and link protein[3]; (b) aggrecan core protein contains 3 globular domains (G1, G2, G3); the CS-GAG attachment region is composed of a variable keratan sulfate region and chondroitin sulfate regions distinguished by their sequence patterns(c) chemical structure of disaccharide repeating unit in chondroitin-4-sulfate glycosaminoglycan (CS-GAG), used in the study

Cartilage aggrecan is an exceptionally complex macromolecule that consists of core protein and CS-GAGs. It has a large core protein contains three globular domains, G1, G2, and G3. (Figure 1.2(b), schematic picture) G1 domain contains one binding site that interacts specifically with HA via link protein. The ternary complex formed among the G1, the link protein, and HA is very stable and provides the basis for anchoring many aggrecans to individual strands of HA. G3 region may interact with carbohydrate ligands on other matrix macromolecules and participate in the organization of the extracellular matrix. [4]

The GAG chains are shown as strands extending out from the core protein.(Figure 1.2(b)) In the major GAG attachment region between G2 and G3, the CS chains are closely spaced, averaging~1 chain per 7 amino acid residues. The CS chains typically have average sizes of 20-30 kDa while the KS chains are generally smaller, 10-15 kDa. CS-GAGs (Figure 1.2(c)) are highly negatively charged, linear polyelectrolytes composed of between 10 and 50 repeats of the disaccharide (N-acetyl-galactosamine and glucuronic acid) which are extensively substituted with sulfate esters at carbons 4 or 6 of the hexosamine residues.[5, 6] As part of the aggrecan macromolecule, individual CS-GAGs have the tendency to assume an extended, rod-like conformation rather than a random coil under normal physiological conditions of 0.15M salt concentration due to intramolecular electrostatic repulsion between neighboring negatively charged carboxylate and sulfate groups (i.e., intercharge distance = 0.64 nm),[6] as well as the high chain packing density.

The unique organization of GAG with such a close intra- and intermolecular distance between the charges in the cartilage was suggesting that the significant portion of the compressive resistance was originated from electrostatic interactions between charged groups in the GAG molecules. Tissue level study and GAG solution study showed

significant dependence of mechanical properties and osmotic pressure on bath salt concentration, which showed the significance of charge-charge interactions in cartilage mechanical properties.[7, 8] Nano-scale modeling of GAG interaction using PB equation showed that electrostatic interaction accounts for half of the equilibrium modulus of the cartilage.[1, 9] It was also found out that non-electrostatic effect of GAG to the cartilage compressive strength was less than 10 % at physiologic condition.[10]

On the other hand it was also found out that the GAG fine structure such as chain length as well as the amount of internal and terminal sulfation of GAG varies with age and degeneration, implying that the nano structure of GAG has pathological importance as well as a functional importance.[5] It was suggested that these structural changes of GAG molecules were related to osteoartheritis development. The relation between these nanostructure of GAG and mechanical properties of cartilage will be a future subject related to this study.

1.2 Specific Aims

The GAGs that are functionally and pathologically important molecules in cartilage biology has been studied in many aspects. It is thought that the unique nanomechanical properties of the constituent CS-GAGs are one of the major determinants of cartilage's biomechanical properties; in particular, electrostatic repulsion due to the electrical double layer, as well as macromolecular "steric" or "overlap" repulsion (Figure 1.3(a)).[11]

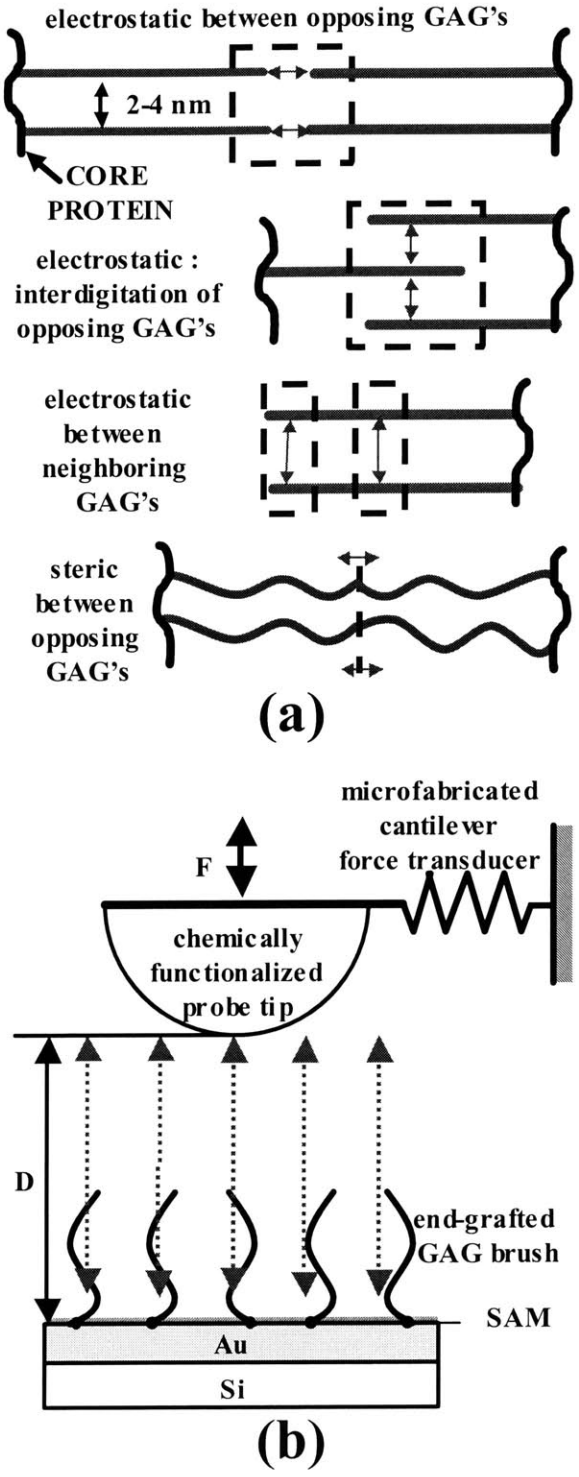

Figure 1.3: (a) Possible components of total CS-GAG andCS-GAG intermolecular interaction. (b) Schematic diagram of high-resolution force spectroscopy experiment of chemically functionalized probe tip versus end-grafted CS-GAG polymer brush

In this study, we focus on mainly the electrostatic repulsive interaction between GAGs, which is the underlying molecular mechanism responsible for compressive properties of cartilage. To achieve this goal we decided to measure electrostatic repulsions between GAG molecules directly using high-resolution force spectroscopy, a variant of atomic force microscopy optimized to measure force at piconewton level.(Figure 1.3.(b))

In order to quantify these molecular-level interactions, CS-GAG polymer chains were chemically end-grafted to planar surfaces to form biomimetic polyelectrolyte "brushes". The nanoscale surface properties of the CS-GAG brushes were then measured directly in aqueous solutions of different ionic strength (IS) and pH using the new technique of *high-resolution force spectroscopy* (HRFS) which employs an extremely soft microfabricated cantilever and probe tip (in our case, chemically modified to known surface chemistry) as a force transducer to record force, F (nN), versus tip-surface separation distance, D (nm). GAG end-grafted AFM probe tip also prepared to measure GAG vs GAG interaction in physiological condition. Our long-term objective is to generalize these methods to address a hierarchy of unsolved nanomechanical problems critical to the understanding of molecular structure/function relations in cartilage and other connective tissues.

Chapter 2

PREPARATION OF BIOMIMETIC, END-GRAFTED POLYELECTROLYTE BRUSHES

2.1 GAG brush layer: Biomimetic System of the Cartilage

The simplest imaginable system to measure intermolecular interaction of GAG is ***polyelectrolyte brushes***, where the GAG chains, carrying a significant number of ionizing groups are anchored by one end on a flat substrate with a reasonable density. In the literature, end-grafted polyelectrolyte brushes have been successfully prepared by four different methods: (1) "grafting to," where (mono)end-functionalized polymer chains are chemisorbed onto a surface from solution,[12] (2) "grafting from," where the polymer chains are generated directly at the surface *in situ*, for example, by using a self-assembled monolayer (SAM) of initiator already covalently attached to the surface to start a radical or anionic polymerization,[13, 14] (3) by using hydrophobically modified polyelectrolyte block-copolymers,[15] and (4) by a Langmuir-Blodgett (LB) technique using polymer-based amphiphile.[16] The major challenge with 'grafting to' technique was that the kinetics of adsorption of chains onto the surface, after an initial rapid increase in coverage, would become very slow because of the barrier to adsorption posed by the molecules already

adsorbed on the surface. Although "grafting to" method does not produce as dense brush layers as other three methods, the "grafting to" method was employed in these studies since its approach was simple and the CS-GAG molecules with relatively short contour length could be readily prepared in (mono)end-functionalized form (with terminal reactive amine groups).

The specific chemical bond that we looked for was determined by the following criteria. Firstly, this bond should be relatively strong so that it can hold the GAG molecules on the surface firmly. Strong immobilization is very important to prevent displacement or removal of the molecules by the tip during force measurement. Secondly, the reaction scheme should be carried out in water with minimal competing reaction. GAG showed very limited solubility for other highly polar organic solvents and water seems to be the only solvent for GAG.[17] It was also found that side reaction of reactive site with water should be avoided to achieve dense GAG brush layer. Thirdly, the GAG molecules should be readily detachable after the force measurement experiment to determine the amount of GAG on the surface. The amount of the GAG on the substrate is very necessary to determine the fixed charge density that will be used later to quantify the measured force.

Thiol(S-H) groups and Au(111) have been shown to form strong-homolytic bond with a bonding strength 44 kcal/mol in water without any side reaction.[18] Some examples of applications of thiol-Au bond are molecular recognition, SAMs as model substrates and biomembrane mimetics in studies of biomolecules at surfaces, patterned surfaces on the micrometer scale, electrically conducting molecular wires and photoresists.[19, 20] Thiol functionalized molecules readily adsorb from aqueous solution onto gold surface to minimize the surface energy of the gold. Once molecules adsorbs on the gold surface, there

is a high chance to obtain the dense brush layer since all the surface is basically reactive site. The size of the GAG molecule is relatively small with 35 contour length so there more chance to obtain a reasonable parking density of GAG on the surface even though there will be a decrease of the reactive area due to adsorption of the GAG onto the surface. The other possible barrier to obtain the high parking density may be the electrostatic interaction between GAG molecules. The PBS buffer with 0.17 M salt concentration was used as an aqueous medium to minimize the intermolecular electrostatic interaction between GAG chains. Thiol-gold bond is also known to be weak at thermal energy, which we can utilize later to detach GAG molecules from the surface to determine the amount of GAG on the surface. Therefore, thiol-gold bond was chosen to be the bond that we are going to use to end-graft GAG on the surface. We attempted to achieve the highest surface grafting density possible by varying the solution conditions of chemisorption (e.g. ionic strength, pH, CS-GAG concentration, incubation time, etc.) To quantify the measured force from GAG brush layer, the parking density of GAG on the substrate was determined using radiolabled GAG. The radiolabeling technique was previously used to measure the coverage of polyelectrolyte brush layer on mica prepared from block copolymer.[21]

2.2 Preparation of End-Grafted CS-GAG Brush Layer.

End-grafting chemistry The radiolabeled GAG molecules were provided by our collaborators. They prepared metabolically radiolabeled ^{35}S-aggrecans from rat chondrosarcoma cell cultures. The protein core of aggrecans were digested with proteinase K, and the resulting amino-acid-terminated ^{35}S-CS-GAG chains were precipitated with ethanol (75%, v/v in 0.001 M sodium acetate), purified by Superose-6® (HR10/60) gel filtration chromatography.[22] The highly pure GAG molecules were then lyophilized and sent to us. The lyophilized GAG was resuspended in 0.01M phosphate buffer, pH=7.4 at 0.1

mg/ml concentration. The molecular weight of the ^{35}S-CS-GAG chains was measured to be 13,428 g/mol by HPLC (Hewlett Packard 1090, Palo Alto, CA, using the Toyo-Pearl HW40F column, 50 cm × 8 mm I.D.[23]), and the polydispersity index was calculated from the chromatogram to be 1.06. The average number of disaccharide units per chain calculated from the number average molecular weight value was found to be 25. Since the disaccharide monomer unit length is 1.28 nm, the contour length, $L_{contour}$, was calculated to be 35 nm, which includes a 3 nm linkage region containing carbohydrate and amino acid moieties.

Since gold-thiol bond was found out to be very appropriate for our purpose, the scheme to add thiol group at the end of the GAG was developed. (Figure 2.1) First, the ^{35}S-CS-GAG chains with their terminal reactive amine groups were treated with 1 μM of dithiobis(sulfosuccinimidyl propionate) (DTSSP, Pierce), producing two GAGs connected by disulfide bond. Then the disulfide bond was reduced to a thiol group using 0.1 mM dithiothreitol (DTT, Pierce). After removal of excess reactants using centrifugal filters (Centricon, Millipore, 3,000 MW cutoff), now thiol terminated GAGs were resuspended in PBS buffer to make a 0.5 mg/ml concentration. Sodium dodecyl sulfate (SDS, Aldrich) was added with a concentration 0.1 % (wt) to minimize nonspecific physisorption. Then 7 μl aliquots of the thiol-terminated ^{35}S-CS-GAG chains were placed on piranha treated 1cm x 1cm gold-coated silicon wafers and incubated in a humidity chamber to prevent drying out.

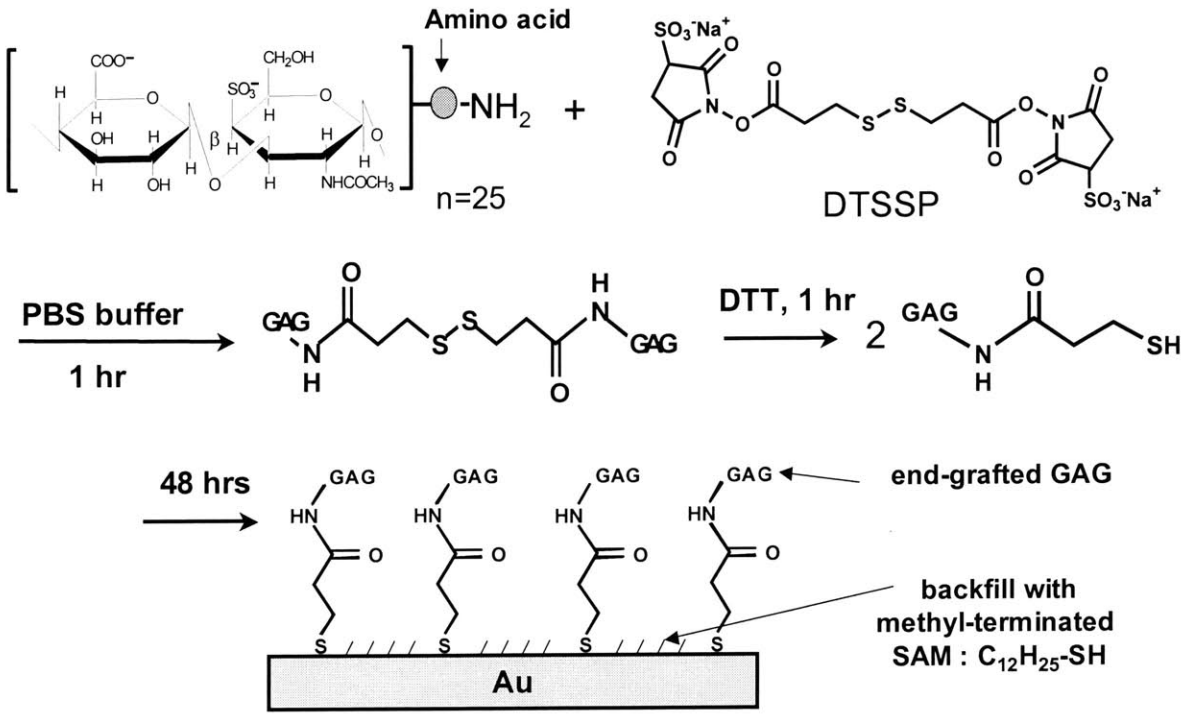

Figure 2.1: Chemical scheme for end-grafting chondroitin-4-sulfate CS-GAG polymer chains to a gold-coated surface.

It was shown that chemisorbed amount of polymer increases as the proportion of poorer solvent increases.[24] For that purpose, an ethanol/water (10/90 volume ratio) mixture instead of pure water was used in the humidity chamber to increase the GAG concentrations on the surface. The humidity chamber was kept at room temperature at various reaction times. 72 hours produced the highest grafting density surfaces. After rinsing, the wafers were placed in 1 mM $C_{12}H_{25}$-SH solution for 15 min to passivate that part of the gold surface not modified with CS-GAG.

Au coated Substrates. Silicon (100) wafers (Recticon Enterprises, Inc., Pottstown, PA; test grade) were cleaned with ethanol and immediately coated with 2 nm of chromium to promote adhesion, followed by 100 nm of Au deposited using a thermal evaporator at 1.5

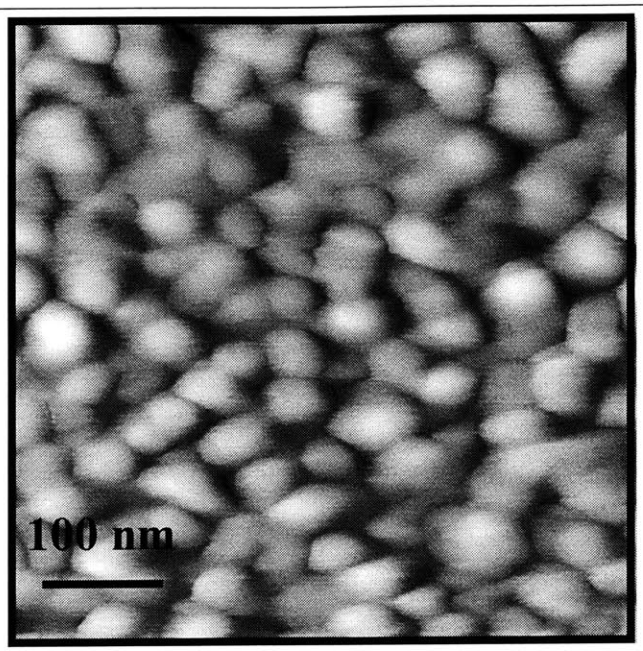

Figure 2.2: Contact mode atomic force microscope topographic image of evaporated gold on silicon wafer taken in air, root-mean-square value for surface roughness ≈ 2.2 nm

Å/s at room temperature at a typical pressure of $2 \cdot 10^{-6}$ Torr. An atomic force microscope (AFM) topographic image (Digital Instruments *Multimode*, Santa Barbara, CA) taken in contact mode in air on $1 \mu m^2$ region of the Au-coated silicon wafer substrate (Figure 2.2) shows a polycrystalline surface structure with a typical root-mean-square (rms) surface roughness of 2 nm and a gold island size range of 25-76 nm. The Au-coated silicon wafers were cleaned using piranha solution (3:1 concentrated $H_2SO_4/H_2O_2(30\%)$) for five minutes just before further chemical modification. *WARNING! Piranha solution is extremely oxidizing, reacts violently with organics, and should be only be stored in loosely tightened containers to avoid buildup of pressure.* Sulfate-functionalized surfaces were produced for control experiments by immersion in a 5 mM ethanol solution of 2-mercaptoethanesulfonic acid sodium salt, $HS(CH_2)_2SO_3Na$ (Aldrich) for 24 hrs and then backfilled with ethanethiol, $HS(CH_2)CH_3$ (Aldrich), also by immersion in a 5 mM ethanol solution for 30 min.

2.3 Characterization of the GAG end-grafted substrate

2.3.1 Scintillation Counting

The presence and amount of GAG on the substrate was verified from scintillation counter using radiolabled GAGs. The GAG attached substrate was placed in the vial and 1 ml of water was added to it. Then the vial was immersed into the water bath and then sonicated at 90 °C for an hour. 4 ml of the scintillation liquid (EcoLume™, ICN, Costa Mesa) was then added to the vial and the amount of the GAG was assessed by then *scintillation counting* (i.e., an assay in which the radioactively labeled ^{35}S-CS-GAG was mixed with a scintillant and the radioactive decay caused emission of fluorescent light from the scintillant which was then detected and recorded) The specific activity (77,317 cpm/μg of ^{35}S-CS-GAG) calculated beforehand was used to determine the amount of GAG on the substrate and the surface grafting density from the total ^{35}S-radioactivity of the detached CS-GAG. The highest grafting density was found to be Γ=0.024 chains/nm^2 or ~(6.5 nm × 6.5 nm)-area per chain.

2.3.2 Contact Angle

Contact angle measurements were carried out to see if the GAG modified substrate changed the surface wettablility of the gold-coated silicon substrate. The gold surface cleaned using piranha solution is hydrophilic at first and then it becomes hydrophobic due to the adsorption of the contaminants from the air within a few minutes. The contact angle between bare gold on silicon and GAG modified gold on silicon was measured after exposed to the air overnight. It was found out that the contact angle measured in static mode decreased from 61 degree for bare gold to 39 degrees for GAG modified gold surface, showing significant drop of contact angle due to the presence of hydrophilic GAG molecules on the surface.

2.3.3 Ellipsometry

The GAG brush substrate was further characterized using ellipsometry to determine the thickness of the GAG layer on the substrate dried in air. Ellipsometry is widely used for thin film thickness measurement in the area of materials science and surface chemistry area. We measured the thickness of the GAG layer on the gold coated silicon substrate in air. First the two important parameters (N_s and K_s) were obtained from bare gold to measure GAG layer thickness. Using these values, the thickness of the GAG layer in air was found out to be 3.18 nm.

2.3.4 Reflectance infrared spectroscopy

IR data were obtained using a Digilab FTS-175 spectrometer (Bio-Rad, Cambridge, MA) equipped with a Universal Reflectance Accessory and wire grid polarizer. The p-polarized light was focused onto the GAG modified surface at a 80° angle of incidence, and the reflected beam was detected by a liquid N_2-cooled mercury-cadmium-telluride detector. After 256 to 1024 scans at $2cm^{-1}$ resolution, characteristic chemical groups that are present in GAGs were identified. The strong peak from carbonyl group at 1670 cm^{-1} and the moderately strong peak from ether group at 1084 cm^{-1}, both present in GAG monomeric unit, were readily identified.

2.3.5 Atomic Force Microscopy Imaging

The atomic force microscopy (AFM) was also used to measure the thickness of GAG layer in contact mode. The 15 μm hexagon pattern on the gold coated silicon substrate was created using soft lithography technique.(Figure 2.3(a)) The outside of the hexagon was

reacted with $C_{12}H_{25}$-SH so only inside of the hexagon was able to react with thiol functionalized GAG. GAG solution was dropped onto the top of this patterned substrate and incubated for overnight. It was clear that the hexagon-patterned area is heightened due to the presence of the GAG inside it. The height of the patterned area was found out to be 1.51 nm in air using cross section analysis tool in the AFM in air. Since we measure the height of the hexagon area that is modified with GAG, we tried to obtain the image of GAG inside the hexagon in contact mode AFM in air. (Figure 2.3(b)) The image of the inside hexagon showed smeared image of gold grains, which is quite different from bare gold surface that we observed in figure 2.2. Without out GAG modifications, the clear images of gold grains were obtained so the smeared image manifested the presence of GAG layers on the surface. The image of GAG at single molecular level could not be obtained probably due to the roughness of the gold coated on silicone. Image analysis of the roughness showed that root mean square value (3.014 nm) of the modified area is much higher than the one of the unmodified area (1.808 nm), indicating the increased roughness of the GAG modified substrate.

Since the gold on mica has atomically flat region of gold grains, it was used to image end grafted GAG macromolecules at single molecular level. Figure 2.4 (a) shows GAG end grafted on the gold coated mica. We were able to see the GAG molecules at single molecular level at high magnification and confirmed the quite uniform presence of the end-grafted GAG on the substrate.(Figure 2.4(b))

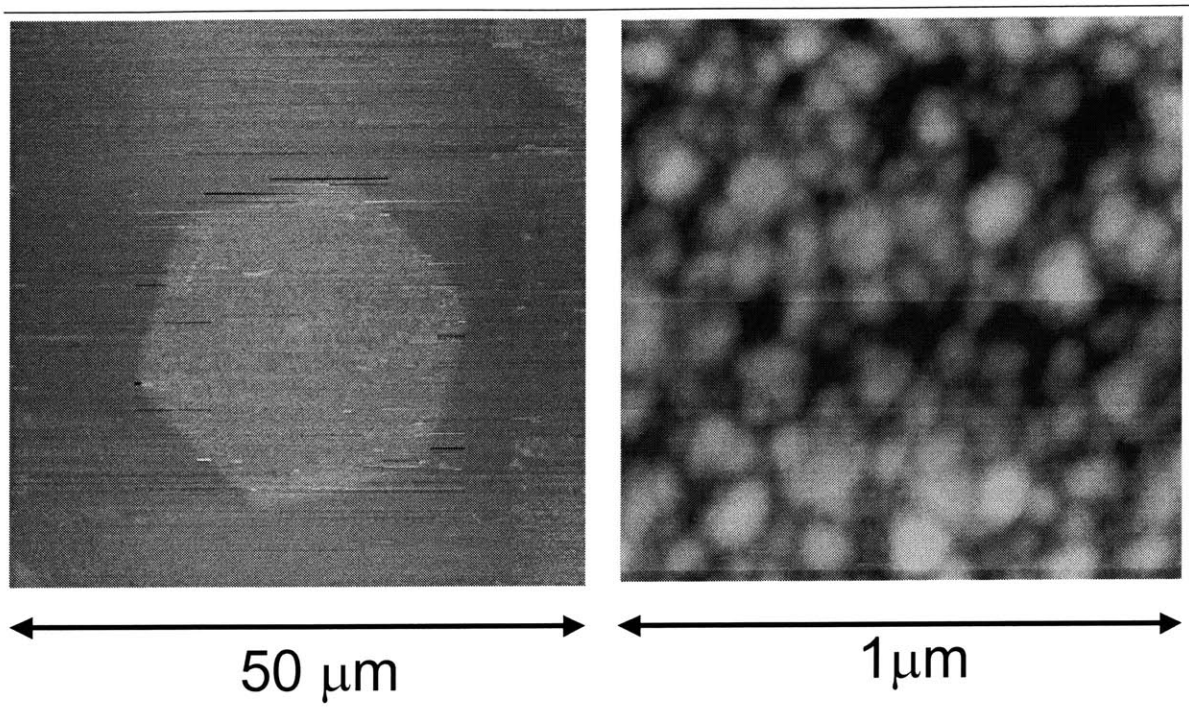

Figure 2.3: (a) AFM image of CS-GAG end-grafted hexagonally patterned area that was created by soft lithography technique, (b) the high magnification image inside hexagon area where GAGs are end-grafted.

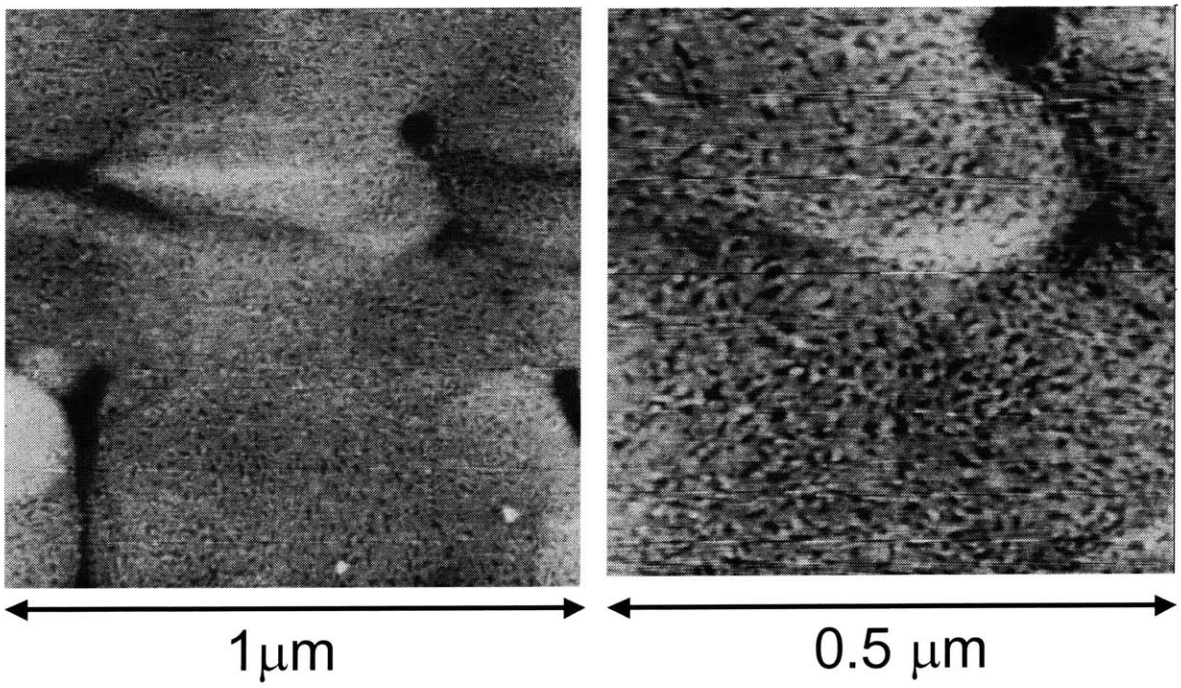

Figure 2 .4: (a) A FM i mage o f G AG e nd-grafted o n gold c oated m ica, (b) t he s ame i mage a t h igher magnification

2.3.6 DMMB Assay

After verifying the presence and quantifying amount of the GAG on the substrate, three different brush parking densities were prepared by varying the reaction time. The 0.58 mg/ml GAG solution with 0.05 % SDS dropped onto piranha treated gold-coated silicon substrate. Then the samples were placed in the humidity chamber (water/ethanol mixture with 90/10 volume ratio) and kept in room temperature for three different times (3 hrs, 24 hrs and 72 hrs). After each time the samples were washed with a plenty of water and then reacted with 5 mM mercaptoundecanethiol for 15 min to passivate the unreacted area of the substrate. To determine the parking density of the GAG brush, the substrate was placed in vial and later about 5 ml of water was added to it. It is well known that the thiol and gold bond is broken at high temperature [18] so we used the thermal energy to detach GAGs from the substrate. The substrate in water was heated until the water boils and kept boiling until the volume of the solution was about 0.5 ml. The volume of about 0.5 ml of solution was recovered from vial, frozen at –80 ^{o}C and then lyophilized. After lyophilization, white power was readily seen, which are the GAG molecules. 25 μl of deionized water was added to each lyophilized samples and mixed well. The volume of 20 μl of the solution was used for dimethylmethylene blue (DMMB) dye assay. The DMMB assay has found wide acceptance as a quick and simple method of measuring the amount of sulfated glycosaminoglycan contents in tissues or fluids. [25] The 240 well plate was used for DMMB assay. The volume of 20 μl of unknown concentration of GAG solution and 200 μl of DMMB dye solution was mixed and the absorption intensity at 525 nm was analyzed by an absorbance reader, Vmax^{TM} (Molecular Devices, Sunnyvale, CA).

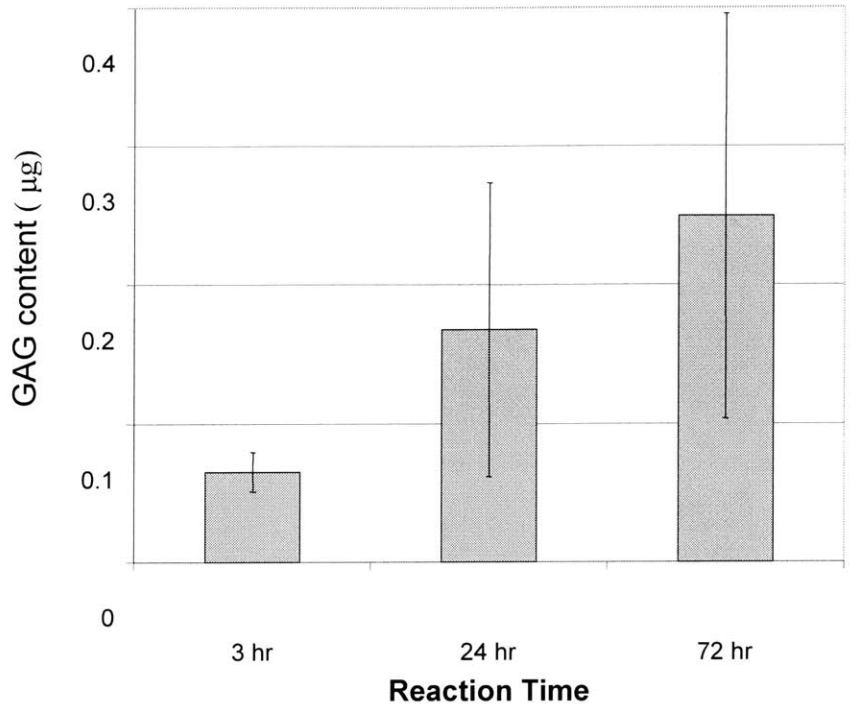

Figure 2.5: The amount of GAG on the substrate determined by DMMB dye bindinganalysis at various reaction times. The bar is the standard deviation and the number of experiments was 5

The complexes of sulfated GAG and DMMB dye start to aggregate and eventually to precipitate as soon as the GAG and dye are mixed so the absorption value was determined in 10 sec after mixing. The amount of GAG determined from DMMB dye analysis at various reaction times is shown in Figure 2.5. The GAG amount increased as the reaction time increased. The parking density difference between 24 hr and 72 hr was not significant considering large standard deviations. The interchain distance that was calculated based upon the grafting density of GAG is in Figure 2.6. As the reaction time increases from 3 hr to 72 hr, the intermolecular distance between GAG decreases from 5.94 nm (Γ=0.028 chains/nm^2) to 3.29 nm (Γ=0.092 chains/nm^2.) The closest interchain distance was in the range of interchain distance in the cartilage at physiological condition. The interchain distance measured using DMMB dye analysis was closer than the one obtained from scintillation counter.

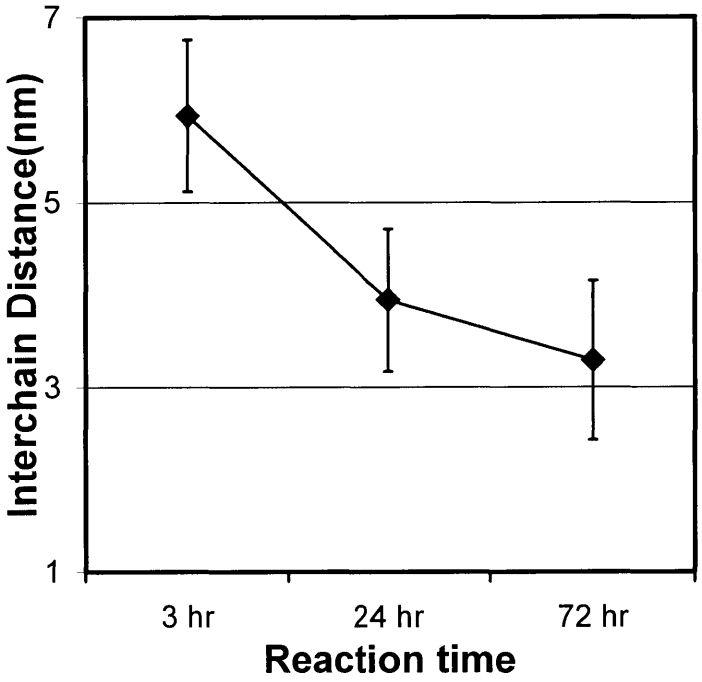

Figure 2.6: Interchain distance between the GAG molecules on the substrate prepared by varying three different reaction times. The bar is the standard deviation and the number of experiment was 5

Chapter 3

INTERACTION BETWEEN GAG BRUSHES AND VARIOUS CHEMICALLY MODIFIED PROBE TIPS

3.1 Introduction

Polymer brushes are a central model in many important problems in polymer science, biophysics and surfactant science, such as polymerically-stabilized colloids, the interaction between membrane proteins and foreign bodies, and surface modification for adhesion and lubrication. Due to its practical importance, its been widely studied theoretically and experimentally.[11, 26-29] Polymer brushes are formed by attaching one end of polymer molecules to a surface with a high density so that chains are obliged to stretch normal to the surface due to their affinity for the solvent. This situation in which polymer chains stretch from the surface is quite different from the typical random-walk behavior of flexible polymer chains in a solution. Colloidal stabilization by end-grafting chains is one of the important examples. In this case particles are maintained in suspension due to the polymer brushes that separates two approaching particles to a distance at which the van der Waals interaction is too weak to keep the particles together.

Whereas this strong favorable interaction between monomer and solvent drives a neutral polymer brush to a highly swollen state, the stretching of the polyelectrolyte brush layer is mainly caused by long-range electrostatic interactions between charged groups. The inter-chain interaction in polyelectrolyte brushes can occur at very low grafting densities far from the actual overlapping regime of neutral brush due to the long range nature of electrostatic interactions.[30] The force measurement in polyelectrolyte brush system showed strong dependence of interaction range and magnitude of the force on salt concentration.[31] It was reported that interactions between two polyelectrolyte brush layers measured using surface force measurement consisted of a long range electrical double layer repulsion and a short-range steric repulsion.[32, 33] Abraham et al investigated the interactions between hydrophobically anchored polyelectrolyte layers and observed the long range interaction and short range steric repulsion. They also found out that the measured long range interaction forces could not be represented by numerical solution of the Poisson-Boltzmann equation.

In this chapter we measured the interaction forces between GAG polyelectrolyte brush layer, the biomimetic system of the cartilage, and chemically modified AFM tips using high resolution force spectroscopy. The experimentally measured forces were compared using newly developed theoretical model based upon Poisson-Boltzmann equation that assumes the brush layer as a volume with a uniform charge density.

3.2 Experimental Methods

3.2.1 High Resolution Force Spectroscopy (HRFS) Measurements.

Instrumentation. HRFS experiments were conducted using a new cantilever-based, piconewton-sensitive instrument; the *Molecular Force Probe* (MFP) (Asylum Research, Santa Barbara, CA) to measure force, F (nN), versus tip-sample separation distance, D (nm). (Figure 3.1) Modeled on AFM technology, the MFP employs a micro-machined soft, flexible cantilever with a sharp tip as a force transducer that deflects in response to the small forces between the cantilever tip and a sample surface. A near-IR laser beam is focused on the backside of the end of the cantilever and directed with a mirror into a split position-sensitive photodiode (PSPD). Depending on the interaction between the tip and the sample, the cantilever bends upward(repulsion) or downward(attraction), which changes the path of the laser to be recorded by photodiode and converted to force vs tip-sample separation distance.

The MFP has an open fluid cell design with an optical (video) microscope located in the base, making it easy to perform an experiment at various aqueous environments and ideal to work on polymeric and biological samples. An adjustable laser focus, novel optic lever geometry, and a low coherence light source optimize response and minimize interference reflections from reflective sample. In AFM periodic pattern was often observed in force measurement due to optical interference if the sample was reflective. A piezoelectric translator (10 μm range) located on a flexure plate in the head incrementally moves the tip towards the sample in the z-direction perpendicular to sample plane ("approach") and away from the sample ("retract") at a constant rate. A LVDT (Linearly Variable Differential Transformer) position sensor (<3Å noise in 0.1-1 kHz bandwidth, 15

μm travel, 0.02% linearity), also located on the flexure plate in the head, quantifies the distance the z-piezo moves the cantilever directly, thus eliminating error due to piezo hysteresis and other nonlinearities, and also reducing or eliminating the effects of thermal drift over long time scales.

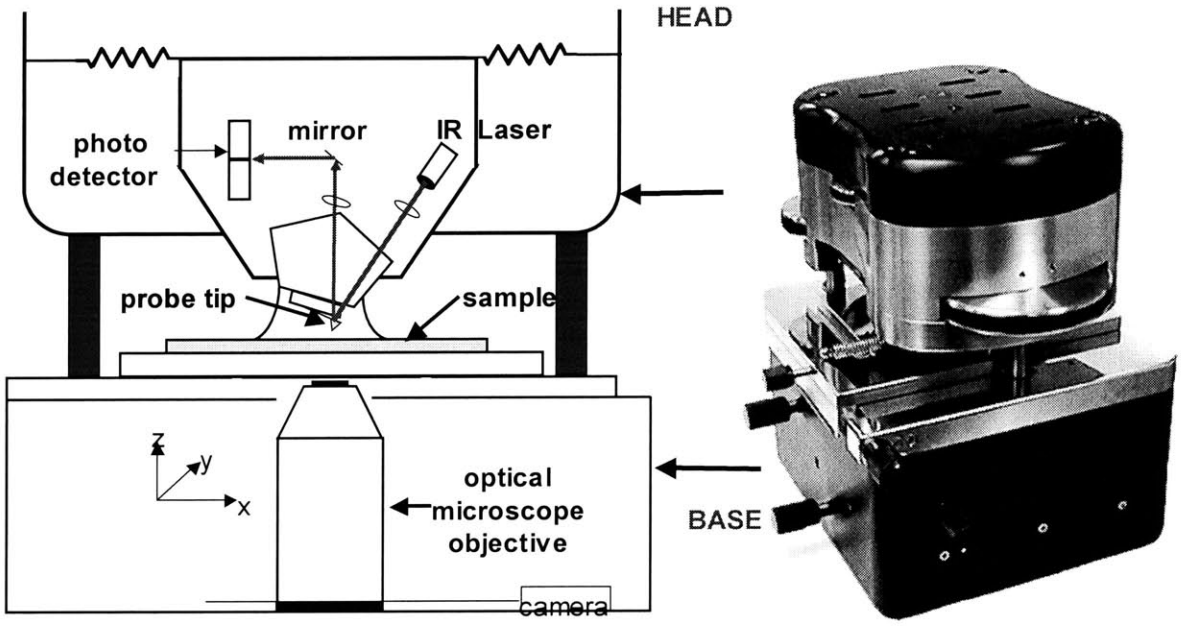

Figure 3.1 Schematic diagram of Molecular Force Probe (MFP)

Conversion of Raw Data and Measurement Errors. Igor Pro software routines (Wavemetrics) were used for conversion of photodiode sensor output voltage (V) into force, F(nN), and LVDT output (nm) into tip-sample separation distance, D (nm). The vertical sensor outputs (V) (i.e., the difference of the top minus bottom quadrants of the PSPD normalized by the total PSPD output, s(V)=(T-B)/(T+B)), were converted into cantilever deflection, δ (nm). This was implemented assuming that the change in z-piezo position dz measured by the LVDT (equal to the change in position of the base of the probe tip) is

equivalent to the change in cantilever deflection, dδ (nm), in the repulsive, contact regime of constant compliance:

$$\delta \text{ (nm)} = s \text{ (V)} \bullet \text{IOLS (nm/V)} \qquad (1)$$

where the IOLS is the "inverse optical lever sensitivity" (nm/V) and is equal to the inverse slope of sensor versus LVDT output curve in the constant compliance regime. The force was then calculated by using Hooke's law for a linear elastic spring:

$$F \text{ (nN)} = k_c \text{ (N/m)} \bullet \delta \text{ (nm)} \qquad (2)$$

where F (nN) is the interaction force and k_c is the cantilever spring constant (N/m). k_c was determined for each individual cantilever according to a nondestructive method described in the literature.[34] The usual convention of positive (+) for repulsive forces and negative (-) for attractive forces was employed. The zero force baseline was taken from data obtained when the cantilever was undeflected far away from the surface (~1000 nm). The error in force measurements is due to calculation of the IOLS (± 5%), the spring constant calibration (± 20%), and nonlinearities of the photodetector associated with the finite size of the laser spot (± 2%). Using the *Thermomicroscopes* probe tips (V-shaped, nominal tip radius ~20-50, length = 320μm, nominal spring constant k=0.01N/m), the MFP is able to achieve a thermally limited force detection of ~5 pN in aqueous solution in a 1 kHz Bandwidth.[35]

The LVDT signal output (volts) was converted into z-piezo distance, z (nm), by calibration at Asylum Research, Inc. via interferometry. The LVDT was found to have a sensitivity of 1.47 μm/V. z (nm) was converted into the tip-sample separation distance, D (nm), by correcting for the cantilever displacement due to the surface interaction force:

$$D\ (nm) = z\ (nm) - \delta\ (nm) \qquad (3)$$

where δ is calculated from eq. *(2)*. The vertical region of apparent infinite slope in the high-force, constant compliance regime was set to D=0, which is due to the fact that the spring constant of the cantilever is much less than the stiffness of the substrate. Yamamoto et al determined the absolute zero distance by AFM imaging across the boundary of a scratched and an unscratched region of the sample surface[36]. They found out that at low grafting density, the brush layer is only compressible up to 0.2 times of the equilibrium distance. Since the brush height measured from force measurement at 0.1 M salt concentration is about 10 nm, the incompressible layer thickness is about 2 nm. Considering that their lowest grafting density is 0.07 chains/nm, the thickness of the incompressible layer in our case should be lower since our grafting density is 0.024 chains/nm. For high-density polymer brushes, it has been shown that there is an inherent error in this assumption due to the presence of a compacted, incompressible polymer layer that is approximately equal to the thickness of the polymer layer in the dry state for lower molecular weights ($M_n \leq$ 25,000).[36, 37]

For the CS-GAG brushes prepared as described above, the thickness in the dry state was measured via ellipsometry and found to be ~3.18 nm. We also used another technique to determine the incompressible layer thickness which involves end-grafting CS-GAG polymer chains to a micrometer-scale chemically patterned surface (prepared via soft lithography technique[20]) and then using AFM isoforce imaging in the constant compliance region of the force versus distance regime to measure the height of the CS-GAG polymer layer, thus locating the D = 0 point. The results yielded an incompressible CS-GAG layer thickness of ~1.5 nm in air, thinner than the dry layer thickness measured via ellipsometry. The surface

chemical patterns were undetectable in deionized water solution, indicating that the incompressible CS-GAG layer thickness was negligible. Each force versus distance curve was obtained by averaging 10-20 curves from 2-3 different spots at each condition. The standard deviation of the force was less than ~30 pN for all ionic strength conditions and separation distances measured.

HRFS Experiments. Force versus distance between CS-GAG polymer brush surfaces and probe tips was measured in 0.0001M to 1.0M NaCl solutions at pH~5.6, using the MFP at room temperature (with z-piezo velocity v= 0.5-1.0 μm/s, z-piezo range = 0.5-1 μm, and rate of data acquisition = 4000 points/s). The NaCl solutions were prepared by mixing NaCl (Mallinckrodt) and deionized (DI) H_2O (18 MΩ·cm resistivity, Purelab Plus UV/UF, US Filter, Lowell, MA). Control studies were performed between sulfate functionalized tips and sulfate functionalized substrates to obtain the surface charge density of the tips. The AFM probe tip functionalized with hydroxy terminated SAM was also used to measure the forces that arise from only GAG brush layer at different ionic strength. In this paper, we focused on data obtained during the approach of the tip to the surface, since we were initially interested in the molecular origins of *compressive* mechanical properties.

Cantilever / Probe Tips. Si_3N_4 V-shaped cantilever/probe tips (Thermomicroscopes, Inc., Sunnyvale, CA unsharpened *Microlevers*) were coated with 2 nm of chromium to promote adhesion, followed by 30 nm of Au deposited using a thermal evaporator at 1.5 Å/s at room temperature. Figure 3.2 shows a scanning electron microscope (SEM, JEOL 6320FV Field-Emission High-resolution SEM) image of the polycrystalline gold-coated probe tip. This image is representative of the probe tips used for the HRFS experiments reported in this paper.

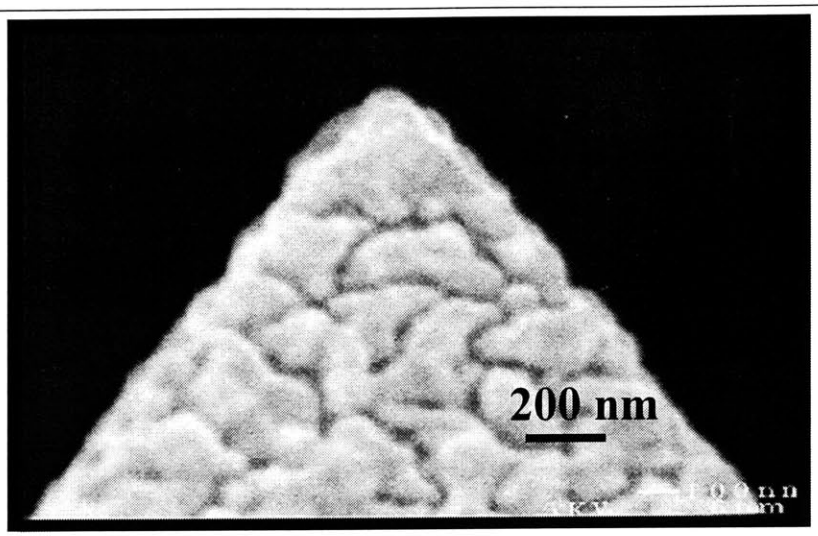

Figure 3.2 Scanning electron micrograph of gold-coated Si_3N_4 probe tip, probe tip radius ≈ 127 nm.

The individual gold grain at the tip apex defines the radius of curvature of the tip, R_{TIP}, and was determined by drawing two intersecting straight lines tangential to the sides of the tip and then drawing a circle tangential to both of them. The radius of this circle was assumed to be R_{TIP}. The radii of curvature were found to be ~127 nm (for the sulfate-modified probe tip used on the sulfate-modified surface as a function of IS), ~25 nm (for the sulfate-modified probe tip used on the CS-GAG-modified surface as a function of IS), ~117 nm (for the sulfate-modified probe tip on CS-GAG-modified surface as a function of pH), and ~25 nm (for the hydroxy-modified probe tip on CS-GAG-modified surface as a function of IS). The Au-coated probe tips were sulfate- or hydroxy- functionalized by reaction with 2-mercaptoethanesulfonic acid sodium salt, (Aldrich) or 11-mercaptoundecanol, $HS(CH_2)_{11}OH$ (donated by Prof. P. Laibinis, MIT, Chemical Engineering) respectively, by immersion of the cantilever probe tips in 5 mM ethanol solutions for 24 hrs. The probe tips that were modified with 2-mercaptoethanesulfonic acid sodium salt were again backfilled with ethanethiol (Aldrich) by immersion in a 5 mM ethanol solution for 30 min

3.3 Results

3.3.1 Interaction between Functionalized Probe Tip and GAG-Functionalized Substrate with Different Parking Densities

The substrates with different parking densities were prepared by varying reaction times. Two different incubation times, 2 hrs and 72 hrs, were used to create two different parking densities. The parking densities determined by scintillation counter using radiolabled-GAG as described in Chapter 1 was found out to be 11 nm and 6.5 nm for 2 hrs and 72 hrs incubation time respectively. The force measured between carboxyl functionalized tip and GAG functionalized substrates with two different parking densities at 0.001 M NaCl concentration showed that the repulsive force from higher parking density substrate was significantly higher than the one from lower parking density substrate.(Figure 3.3) To quantify these repulsive interactions, the exact surface charge density of the tip should be known. The sulfate functionalized tip was chosen for further study since it has a constant charge density in the wide range of pH. The surface charge density of sulfate functionalized tip can be determined by fitting surface charge model to the experimental data as described in the next section.

3.3.2 Interaction Between Sulfate-Functionalized Probe Tip and Sulfate-Functionalized Substrate

Figure 3.3(a) shows a series of (average) Force (nN) and (average) Force/Radius (mN/m) versus Distance (nm) curves measured on approach using a sulfate-functionalized probe tip on a sulfate-functionalized substrate in 0.0001 M – 0.1 M NaCl solutions at pH 5.6. Since the pKa of the sulfate group is ~2-2.5[38] and that of the carboxyl group is 3.5-4,[39] both of the groups should be negatively charged in force measurement condition.

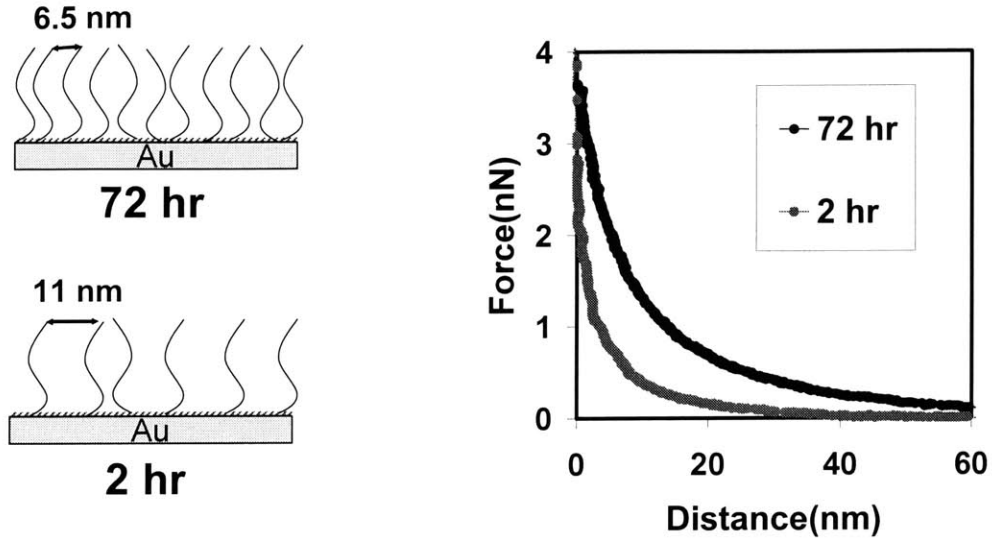

Figure 3.3 Nanomechanical measurement using carboxyl functionalized tip and GAG substrate with different parking densities

Far from the surface, the cantilever remained undeflected and the net force was zero. At lower ionic strength, the probe tip was deflected upwards beginning at approximately D<80, consistent with long range electrical double layer repulsion forces arising from osmotic pressure and Maxwell electric stress.[40] The maximum magnitude of these repulsive forces was measured to be ~0.25 nN (Force/Radius~2.4 mN/m). Even after acquisition of >50 force curves from the same surface site, no significant difference was observed in the data, which suggests that there was no irreversible degradation of the surface functional groups or blunting of the probe tip.

At D≤15 nm, a mechanical instability of the cantilever resulted in an abrupt "jump-to-contact" of the probe tip to the surface at 0.1 M NaCl concentration, due to the gradient of the attractive force exceeding the cantilever spring constant. In this instability region, all accurate data is lost and the slope of this line is equal to the cantilever spring constant,

$dF/dD=k_c$. The (average) jump-in distances were found to be: 4.7 nm (0.0001M), 2.03 nm (0.001M), no jump-to-contact (0.01M), and 5 nm (0.1M). After surface contact was made, the "constant compliance regime" was reached (set to D=0); here, little or no deformation of the sample took place and the cantilever and sample moved together in unison.

With increasing ionic strength, the magnitude and range of the repulsion force decreased due to screening of electrostatic double layer. At 0.1M NaCl, the net interaction was dominated by van der Waals forces and the measured force was attractive over the entire distance range with the minimum force value of 63 pN being a measure of the total surface adhesion. The long-range electrostatic forces in experiments using the sulfate-modified probe tip on the sulfate-modified surface were nonhysteretic, i.e. the approach and retract curves overlapped, at low salt concentrations while the shorter range van der Waals attraction did exhibit hysteresis and increased in magnitude on retraction (data not shown). Similar results have been reported in the literature for 1,2 mercaptoethanesulfonate ($HS(CH_2)2SO_3^-$) in pure water,[41] 11-mercaptoundecanoic acid ($HS(CH_2)_{10}COOH$) as a function of ionic strength,[41, 42] 16-thiohexadecanoic acid (16-mercaptohexadecanoic acid) ($HS(CH_2)_{15}COOH$), 16-thiohexadecane ($HS(CH_2)_{13}CH_3$), 16-thiohexadecanol ($HS(CH_2)_{16}OH$) monolayers on gold in pure water,[43] and 11-mercaptoundecanol ($HS(CH_2)_{11}OH$) and 16-thiohexadecanoic acid in phosphate-buffer (IS=0.01M, pH=7).[44]

Comparison of HRFS Data with Theory. The data of Figure 3.3(b) were compared to predictions based on the Derjaguin-Landau-Verwey-Overbeek (DLVO) theory.[45, 46] The total interaction force was assumed to be a linear summation of attractive van der Waals, repulsive electrostatic double layer, and hydrophilic "hydration" forces:

SULFATE PROBE TIP VERSUS SULFATE SURFACE

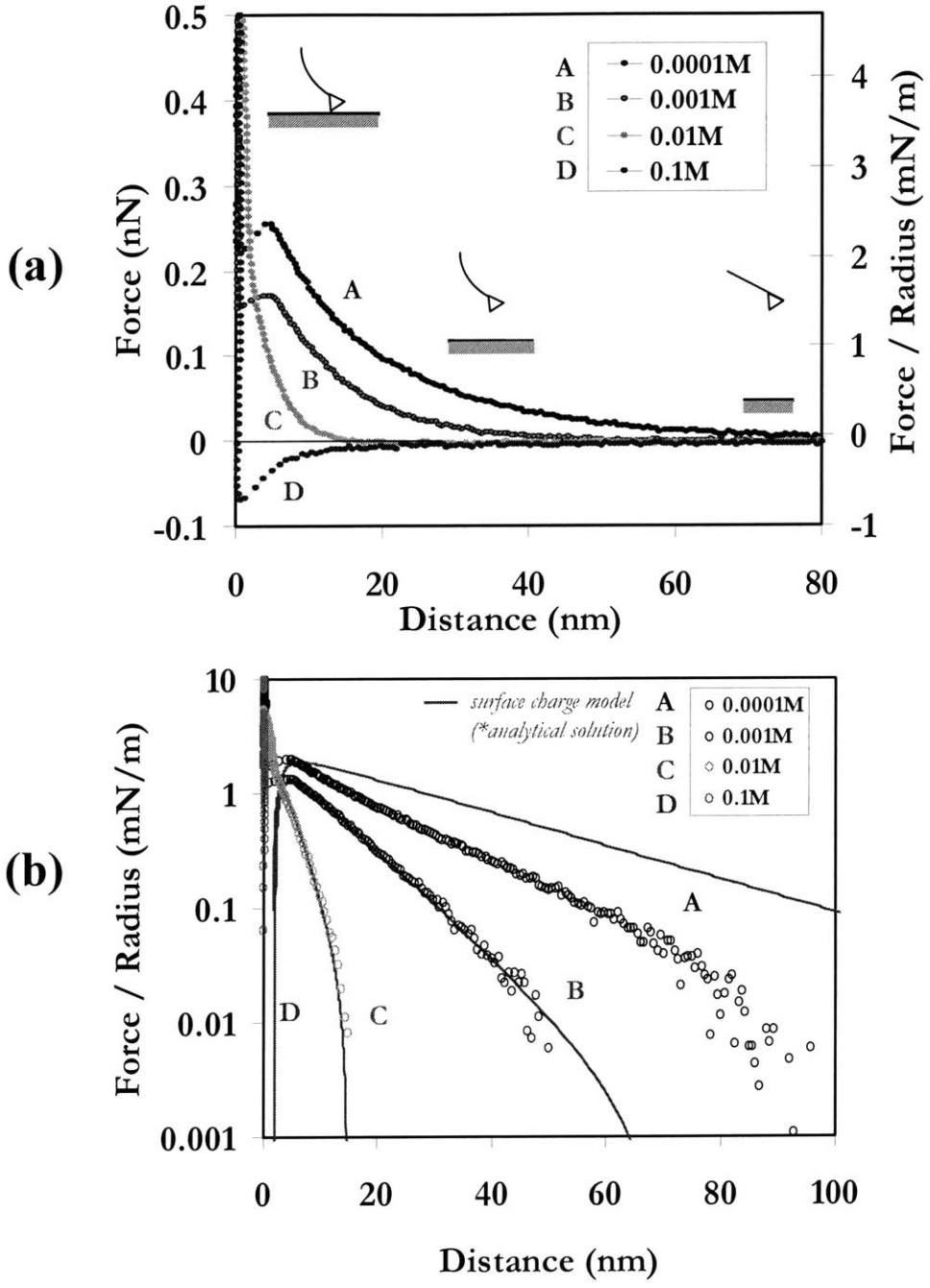

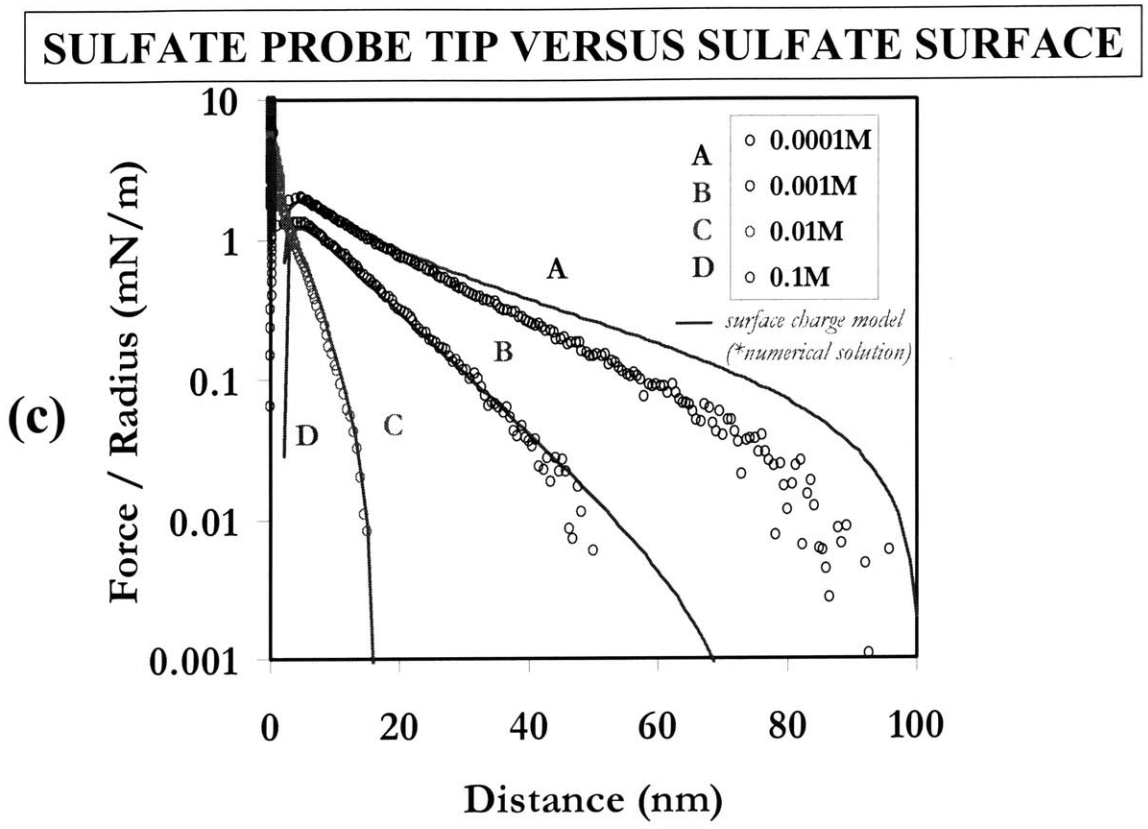

Figure 3.4 HRFS data measured on approach with the MFP between sulfate-functionalized probe tip and sulfate-functionalized surface as a function of ionic strength (IS=0.1M, 0.01M, 0.001M, 0.0001M) at pH≈5.6: (a) (average) Force (nN) and (average) Force / Radius (mN/m) versus Distance (nm), (b) (average) Force/Radius (mN/m) (logarithmic scale) versus Distance (nm) compared to surface charge model (analytical solution, eq. *(A.1.6)* and Appendix Section A.1, using the fitting parameters given in Table 1), and (c) (average) Force/Radius (mN/m) (logarithmic scale) versus Distance (nm) compared to surface charge model (nonlinear numerical solution, Appendix Section B.1) using the fitting parameters given in Table 3.1

$$F_{TOTAL}(D) = F_{VDW}(D) + F_{ELECTROSTATIC}(D) + F_{HYDRATION}(D) \qquad (4)$$

Hydration or Structural Component. A very short range (< 4 nm) monotonic, exponentially repulsive force has been observed experimentally between a variety of different smooth hydrophilic charged surfaces in electrolyte solutions of intermediate and high ionic strength.[47] The origin of this force has been quite controversial and is generally

attributed to the displacement of hydrated, adsorbed surface counterions and is due to the energy needed to dehydrate the bound counterions, which retain some of their water of hydration on binding. Presumably, this force is highly sensitive to and will decrease with increasing surface roughness.[47]

van der Waals Component. The nonretarded van der Waals component of the total interaction force was estimated by fitting the highest ionic strength data (0.1M) to two analytical expressions between 7-20 nm (this distance range is greater than the jump-to-contact cantilever instability region, which was determined as the region where the slope was equal to the cantilever spring constant, but still less than the distances where retardation effects begin to take effect). The first expression was the inverse square power law eq. *(5)* derived using the "Derjaguin approximation":[48]

$$F_{VDW}(D) = -\frac{AR}{6D^2} \qquad (5)$$

where F is the force between a sphere of radius R (assumed to be the probe tip radius, R_{TIP} =127 nm) and a planar surface at separation D, and A is the nonretarded Hamaker constant. The second analytical expression was derived using a more accurate surface element integration (SEI) approach by Bhattacharjee, et al.[49]:

$$F_{VDW}(D) = \frac{d\left[-\left(\frac{A}{6}\right)\left[\frac{R}{D} + \frac{R}{D+2R} + LN\left(\frac{D}{D+2R}\right)\right]\right]}{dD} \qquad (6)$$

A Hamaker constant of $\mathbf{5.2 \bullet 10^{-20}}$ **J** was obtained from the fit to eq. *(5)* and of $\mathbf{35 \bullet 10^{-20}}$ **J** from the fit to eq. *(6)*. These values are close to that predicted using the Lifshitz theory for

gold/H_2O/gold at A=9-30•10^{-20} J (computed from spectroscopic data for gold surfaces).[50] Experimental values have been reported from HRFS data computed using eq. *(5)* for gold/H_2O/gold at A = 25•10^{-20} J, [51]and A = 10•10^{-20} J, [41]$CH_3(CH_2)_{15}OH/H_2O/CH_3(CH_2)_{15}OH$ at A = 3.4•10^{-20} J,[43] and $CH_3(CH_2)_{10}OH/H_2O/CH_3(CH_2)_{10}OH$ at A = 10•10^{-20} J,[43] and at A = 4•10^{-20} J.[41] These results suggest that the gold substrate dispersion interaction dominates over the surface hydrocarbon layer (i.e., only at very short distances (D<1nm) will the less polarizable hydrocarbon layer contribute to the effective Hamaker constant) and, hence, we do not resort to a more complicated multilayer model for the effective Hamaker constant.[44, 51] It has also been postulated that smaller probe tip radii allow penetration through the SAM layer, which in this case is approximately 1.6 nm thick; such a displacement of the hydrocarbon chains upon contact would allow the van der Waals interaction between the underlying gold surfaces to dominate.[51]

Electrostatic Double Layer Component. The electrostatic double layer component of the total interaction force was modeled, first, using a *constant surface charge density approximation* based on the Poisson-Boltzmann (PB) equation in which the substrate is assumed to be a plane of constant charge density (σ_1) and the probe tip is modeled as a hemisphere of radius, $R_{HEMISPHERE}$, also with constant charge density, (σ_2) (see Appendix A.1). Two solutions of the PB equation were obtained and fit to the experimental data shown in Figure 3.3: *(1)* an approximate analytical solution using the linearized PB equation (Appendix A.1.1 eq. *(A1.6)*[52-54]) and *(2)* a more exact numerical solution using the nonlinear PB equation (Appendix A.1.2, eq. *(A1.7)*[55]).

Ionic Strength (M NaCl)	R_{TIP} (nm) FIXED, measure by SEM (BOTH MODELS)	κ^{-1} (nm) FIXED, eq. *(A1.4)* (BOTH MODELS)	$\sigma_1=\sigma_2$ (C/m^2) FREE, LINEAR PB : ANALYTICAL SOLUTION : eq. *(A1.6)*	$\sigma_1=\sigma_2$ (C/m^2) FREE, NONLINEAR PB : NUMERICAL SOLUTION
0.0001	127	30.0	$-2.1\bullet10^{-3}$	$-3.0\bullet10^{-3}$
0.001	127	9.5	$-2.2\bullet10^{-3}$	$-4.0\bullet10^{-3}$
0.01	127	3.0	$-3.2\bullet10^{-3}$	$-15.4\bullet10^{-3}$

Table 3.1: Parameters used in the theoretical models of sulfate-functionalized probe tip versus sulfate-functionalized surface HRFS experimental data. Fits included the van der Waals interaction *(*fixed=parameter fixed to known values, free=fitting parameter allowed to vary in fitting routine)*

Summary of Theoretical Results. The results for the constant surface charge model are given in Figure 3.3(b) (the analytical solution eq. *(A1.6)*) and Figure 3.3(c) (the more exact numerical solution), also taking into account the van der Waals force. In both solutions, κ^{-1} (calculated from eq. *A.1.4*) and R_{TIP} (measured experimentally by SEM) were fixed to their known values, and $\sigma_1=\sigma_2$ was allowed to be a free fitting parameter. The parameters employed for both models are summarized and compared in Table 3.1. The value of σ_1 suggests that mercaptoethanesulfonic acid did not form a densely packed crystalline surface.[56] It is known that alkanethiol with enough number of carbons(>10) adsorb on the gold surface forming 2 dimensional crystalline surface in ethanol because they do not ionize in ethanol despite the high polarity of the ethanol. Force measurement also showed that the interaction force between sulfate or carboxyl terminated SAM remained attractive in ethanol whereas upon flushing with water, strong long-range repulsion was observed.[41] But surprisingly, the potentials generated from sulfate modified surface are quite small. They were unable to obtain potentials much higher than -80 to -100 mV in dilute electrolyte, despite the fact that the sulfonate pKa is about 2. This observation is attributed to incomplete surface coverage due to the shorter alkane chain length.

The 0.1M data were assumed to be dominated by van der Waals interactions and, indeed, including or excluding the electrostatic component of the force changed the Hamaker constant obtained by a negligible amount. For the intermediate ionic strength conditions (0.001M and 0.01M), the nonlinear numerical solution to the surface charge model produced an excellent fit through most of the distance range probed, while the analytical solution increasingly underestimated the force for D<15nm. At the lowest ionic strength value (=0.0001M), the analytical solution could not fit the data over any distance range probed and overestimated the experimental data throughout most of the distance range probed, while the full nonlinear numerical solution improved the fit somewhat for D<25nm. The magnitude of the surface charge density calculated from the analytical solution was 0.35-0.5 times of the magnitude of the nonlinear solution. Interestingly, both models predicted an increase in the surface charge density with increasing ionic strength.

3.3.3 Interaction Between Sulfate-Functionalized Probe Tip and CS-GAG-Functionalized Substrate as a Function of Ionic Strength

The (average) Force (nN), (average) Force/Radius (mN/m), and (average) Stress (MPa) versus Distance (nm) between a sulfate-modified probe tip and a CS-GAG-modified surface is shown in Figure 3.4 for ionic strengths ranging from 0.0001M to 1.0M at pH 5.6. The stress was estimated as the force normalized to the probe tip area (approximated as a hemisphere). Similar to the trends of Figure 3.3, long-range electrostatic repulsive forces were observed which decreased in the magnitude and range with increasing ionic strength. For the lowest ionic strength condition (0.0001 M NaCl), the repulsive force began at D~175 nm >> $L_{contour}$ = 35 nm, and reached a maximum magnitude of ~2.5 nN (~50 mN/m), i.e. much greater than the maximum magnitude of the force reached in the sulfate versus sulfate control experiments at this same IS (i.e. F_{max}~2.4 mN/m). For the highest ionic

strength conditions of 0.1 M and 1 M NaCl, the repulsive forces began at $D < L_{contour} = 35$ nm and reached a maximum magnitude of ~1 nN (~20 mN/m) and ~0.5 nN (~10 mN/m) respectively. The sulfate-CS-GAG net interaction force was purely repulsive at all ionic strengths over the entire distance range probed. The double-layer interaction remained stable even after acquisition of 50 force curves from the same surface site, which suggests that no irreversible surface damage occurred due to the measurement of the force curves themselves. No jump-to-contact of the cantilever due to van der Waals attraction could be observed when the sulfate probe tip made contact with the top of the CS-GAG brush (as observed previously for poly(L-glutamic acid) brushes,[33] or for sulfate probe-underlying gold substrate interaction as we observed for the sulfate versus sulfate data) at any ionic strength value tested. The measured force per unit CS-chain area was of the order ~0.1-0.5 MPa, which scales to the known macroscopic swelling pressures of CS-GAG chains in vivo.[1, 57] The HRFS experiments using the sulfate-modified probe tip on the CS-GAG-modified surface were nonhysteretic throughout the entire distance range probed, as shown in Figure 3.4(b), which shows a typical Force (nN) versus Distance (nm) plot on approach and retract for an individual HRFS experiment at 0.0001M and pH 5.6. The standard deviation of each force profile was less than 20 pN and the force profile with standard deviation at 0.1 M is shown in Figure 3.4(c).

SULFATE PROBE TIP VERSUS GAG SURFACE

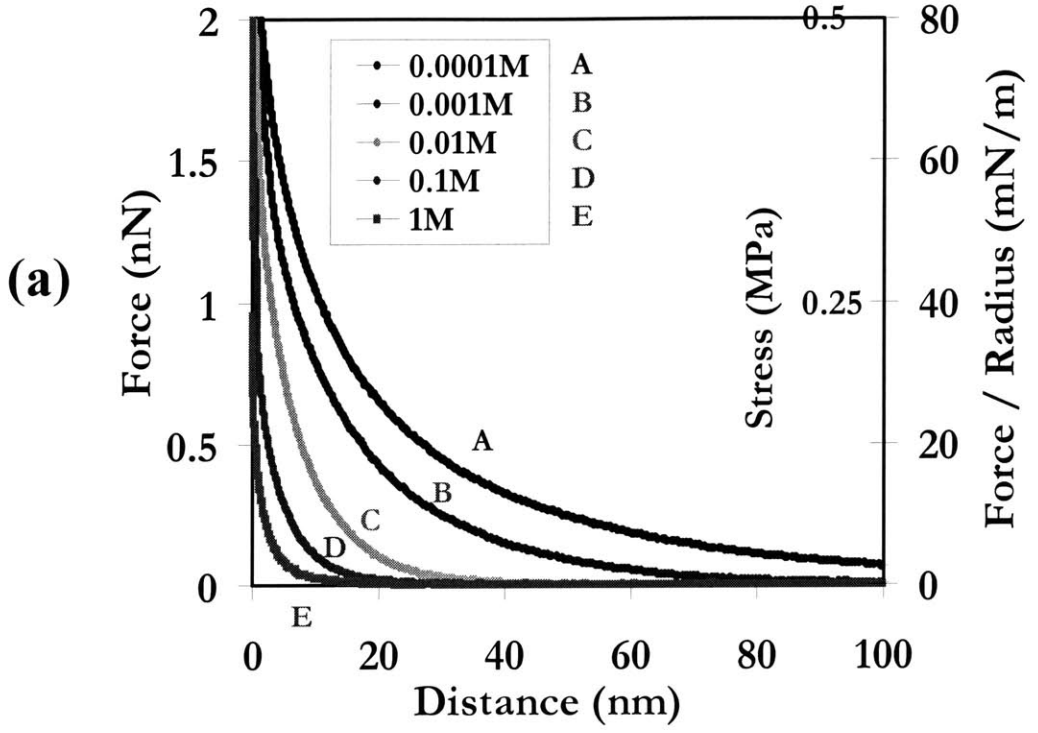

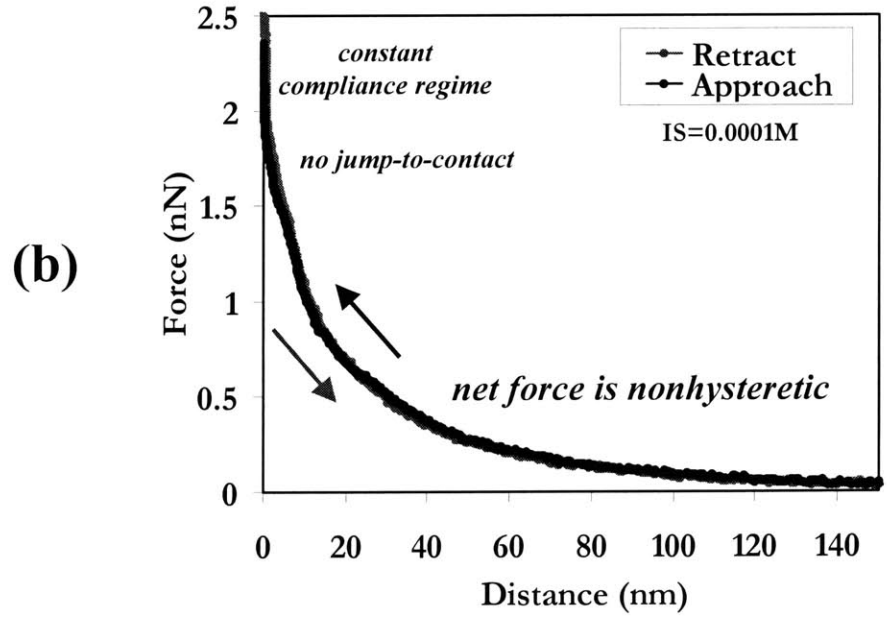

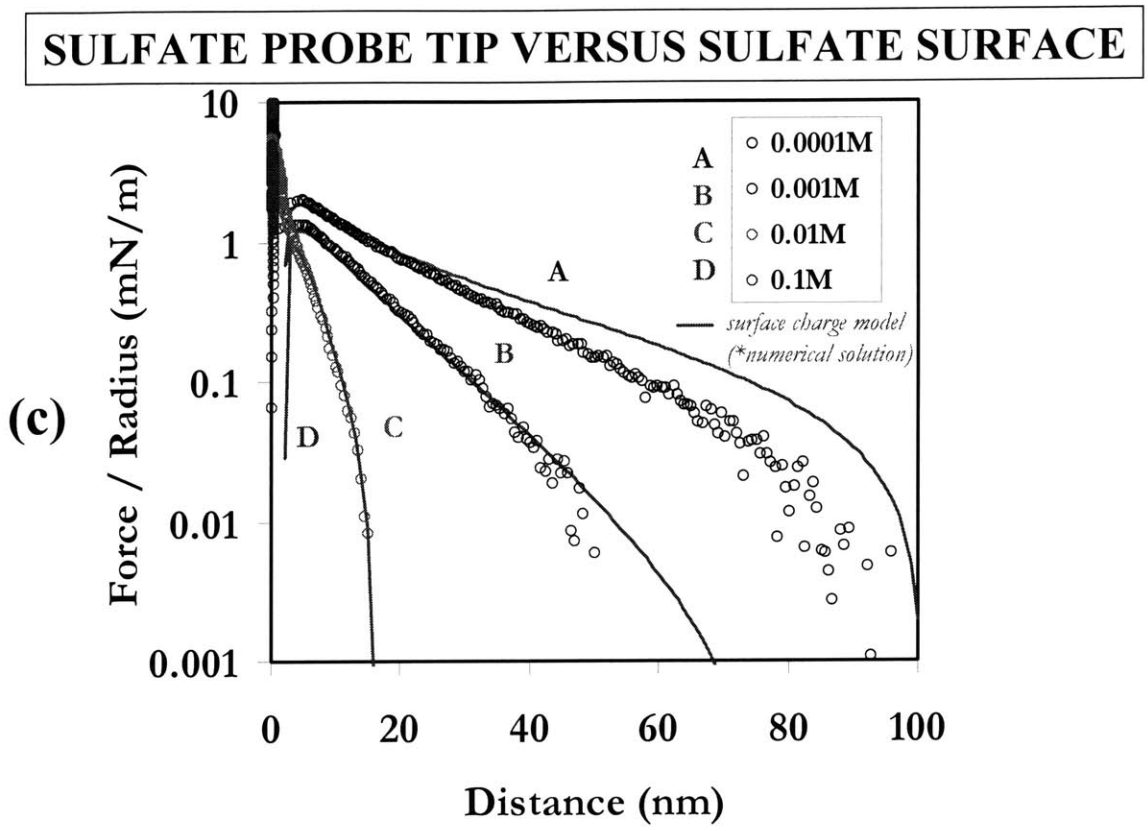

Figure 3.5: (a) HRFS data measured on approach with the MFP between sulfate-functionalized probe tip and CS-GAG-functionalized surface as a function of ionic strength (IS=1M, 0.1M, 0.01M, 0.001M, 0.0001M) at pH≈5.6: (average) Force (nN), (average) Force / Radius (mN/m), and Stress (MPa) versus Distance (nm), (b) Force (nN) versus Distance (nm) on approach and retract for an individual force spectroscopy experiment, pH≈5.6 and IS=0.0001M between sulfate-functionalized probe tip and CS-GAG-functionalized surface, (c) (average) Force/Radius (mN/m) (logarithmic scale) versus Distance (nm) compared to surface charge model (nonlinear numerical solution, Appendix Section 1.B) and volume charge model (Appendix Section 1.C. using the fitting parameters given in Table 2), and (d) expanded plot of Figure 3.4(c), (average) Force/Radius (mN/m) (logarithmic scale) versus Distance (nm), compared to volume charge model.

SULFATE PROBE TIP VERSUS GAG SURFACE

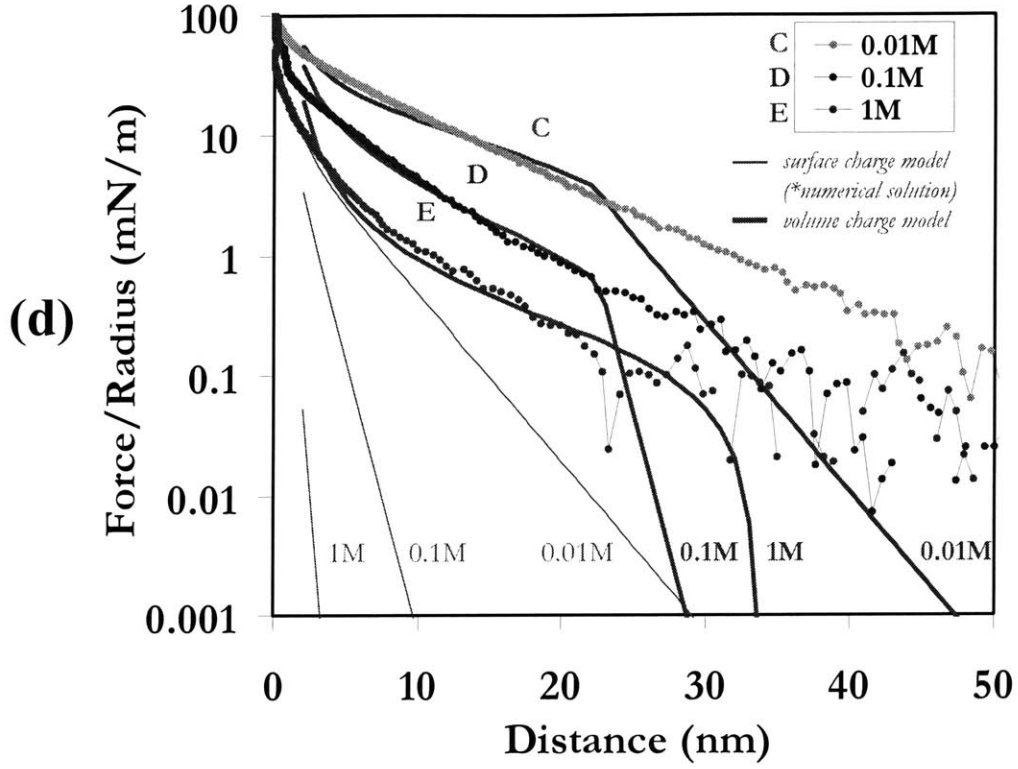

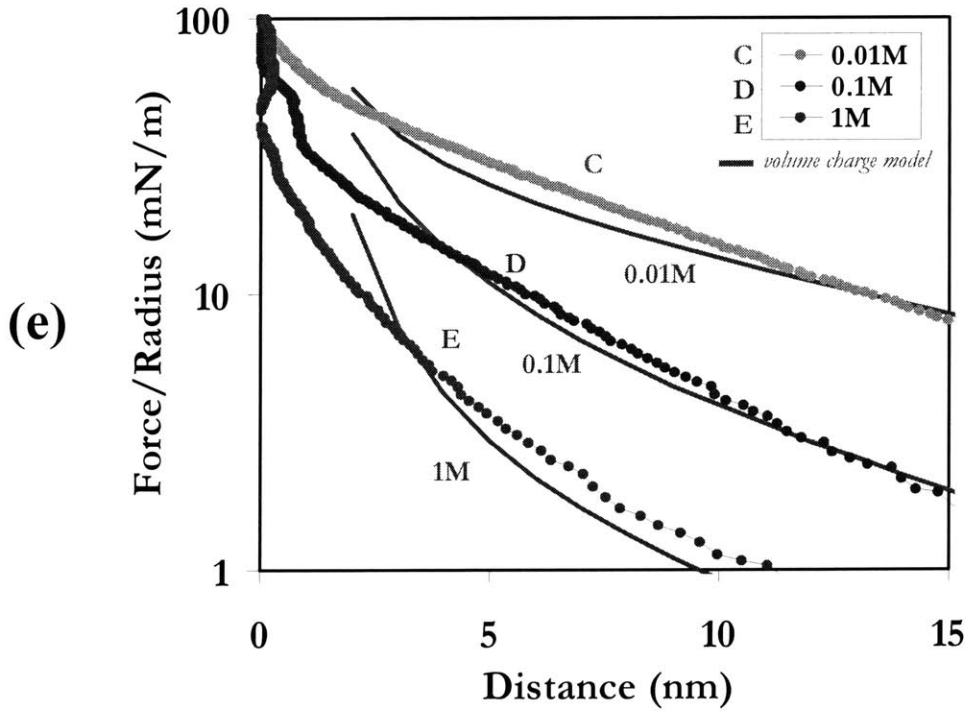

Comparison of HRFS Data to Theory. The total interaction force between a sulfate-functionalized probe tip and CS-GAG-functionalized surface has an additional steric term compared to eq. *(4)* :

$$\mathbf{F}_{TOTAL}(D) = \mathbf{F}_{VDW}(D) + \mathbf{F}_{ELECTROSTATIC}(D) + \mathbf{F}_{HYDRATION}(D) + \mathbf{F}_{STERIC}(D) \qquad (7)$$

where $F_{STERIC}(D)$ is the "overlap" repulsion due to deformation of the polymer layer or brush in compression. For flexible polymer chains, $F_{STERIC}(D)$ has contributions from configurational entropy and osmotic pressure due to a local increase in chain segment concentration at the interface.[11] For rigid-rod like chains, $F_{STERIC}(D)$ includes bending and configurational entropy penalties that is different from configurational entropy of neutral polymers and described in more detail below.[58] No matter what the molecular mechanism, steric repulsion begins when the probe tip comes in physical contact with the top of the polymer layer or brush, L_o (= brush height), which has a maximum value of $L_{contour}$ = 35 nm for the case of the CS-GAG-functionalized substrate. The additivity of steric and DLVO forces has been used extensively in the literature,[59-63] but is questioned by others.[64, 65] It is clear that these two components are interrelated and highly dependent on each other. Since steric repulsion, attractive van der Waals forces, intermolecular electrostatic repulsion between neighboring CS-GAG chains on the surface, and hydration repulsion all come into play at shorter distance ranges,[66-68] the long-range portion of the data (D>10nm) was fitted to the purely electrostatic double layer theories. Only the experiments conducted at the higher ionic strength values (0.01M, 0.1M, 1M) were compared to theory (for reasons described below). Hence, the data of Figure 3.5 were compared to the predictions of: *(1)* the surface charge density model using the nonlinear PB equation solved numerically, and *(2)* a model in which the CS-GAG brush layer was approximated as a smoothed volume of known

fixed charge density (Appendix 1.C.).[59] The latter model represents the chemically-functionalized probe tip as a smooth hemisphere with constant surface charge density, σ_1, and the CS-GAG-functionalized substrate as having a uniform volume charge density, ρ_{fix} = $-5.9 \bullet 10^6$ C/m^3 (0.061M). This volume charge density was calculated from the density of CS-GAG obtained from scintillation counting (0.024 chains/nm^2) and the number of charge groups per CS-GAG chain (2 charges per disaccharide, 25 disaccharides per chain). This model predicts different nanomechanical behavior in two different distance regimes: region *(I)* outside the fixed volume charge region where the PB equation has the same form as the surface charge model, and region *(II)* inside the fixed volume charge region where the PB equation has an extra term added to account for ρ_{fix}.

Summary of Theoretical Data fit Results. The results of fitting the above theoretical models to the data of Figure 3.4 (a) are given in Figure 3.4 (d), including the van der Waals interaction. κ^{-1} (calculated from eq. *A.1.4*), R_{TIP} (measured experimentally via SEM), σ_1 (taken from theoretical fits of sulfate versus sulfate HRFS data, Table 3.1), and ρ_{fix} (calculated from scintillation counting data) were fixed to their known values, so that the surface charge model had no free fitting parameters and the volume charge model had one free fitting parameter, *h*, the height of the volume charge (Figure A1). The parameters employed in both models are summarized and compared in Table 3.2. As expected, the surface charge model greatly underestimated the experimental data throughout the entire distance range probed, while the volume charge model fit better to the data for D<25 nm. For D>25 the force predicted by the volume charge model decreased dramatically, further underestimating the data with increasing separation distance.

Ionic Strength (M NaCl)	κ^{-1} (nm) FIXED, eq. *(A1.4)* (BOTH MODELS)	R_{TIP} (nm) FIXED, measured by SEM (BOTH MODELS)	$\sigma_1=\sigma_2$ (C/m^2) FIXED, NONLINEAR PB : NUMERICAL SOLUTION	ρ_{FIX} (C/m^3) FIXED, VOLUME CHARGE, measured by scintillation counting	*h* (nm) FREE, VOLUME CHARGE HEIGHT
0.01	3.0	25	$-15\bullet10^{-3}$	$-5.9\bullet10^{6}$	21.3
0.1	0.95	25	$-15\bullet10^{-3}$	$-5.9\bullet10^{6}$	21.8
1	0.3	25	$-15\bullet10^{-3}$	$-5.9\bullet10^{6}$	31.8

Table 3.2: Parameters used in the theoretical models of sulfate-functionalized tip versus CS-GAG-functionalized surface HRFS experimental data ***(*fixed=parameter fixed to known values, free=fitting parameter allowed to vary in fitting routine)***

3.3.4 Interaction Between Sulfate-Functionalized Probe Tip and CS-GAG-Functionalized Substrate as a Function of pH

The average Force (nN) versus Distance (nm) between a sulfate-modified tip and a CS-GAG-modified surface for 0.015M ionic strength at pH 3.0 and 7.0 is shown in Figure 3.5. At all distances D, the repulsion force at pH 7 was higher than that at pH 3. Since the CS-GAG carboxylic groups have a pKa ~ 3.5-4, [39]almost half the CS-GAG charge would be neutralized at pH 3, consistent with the lower force that was observed. Thus, the data in Figure 3.5 represents the effect of varying the CS-GAG charge at constant ionic strength, in contrast to the data of Figure 3.4, which represents the effects of varying the ionic strength at nearly constant charge and pH. Interestingly, for the less charged low pH conditions, one can observe the van der Waals jump-to-contact to the top of CS-GAG brush at a separation distance of 8.2 nm.

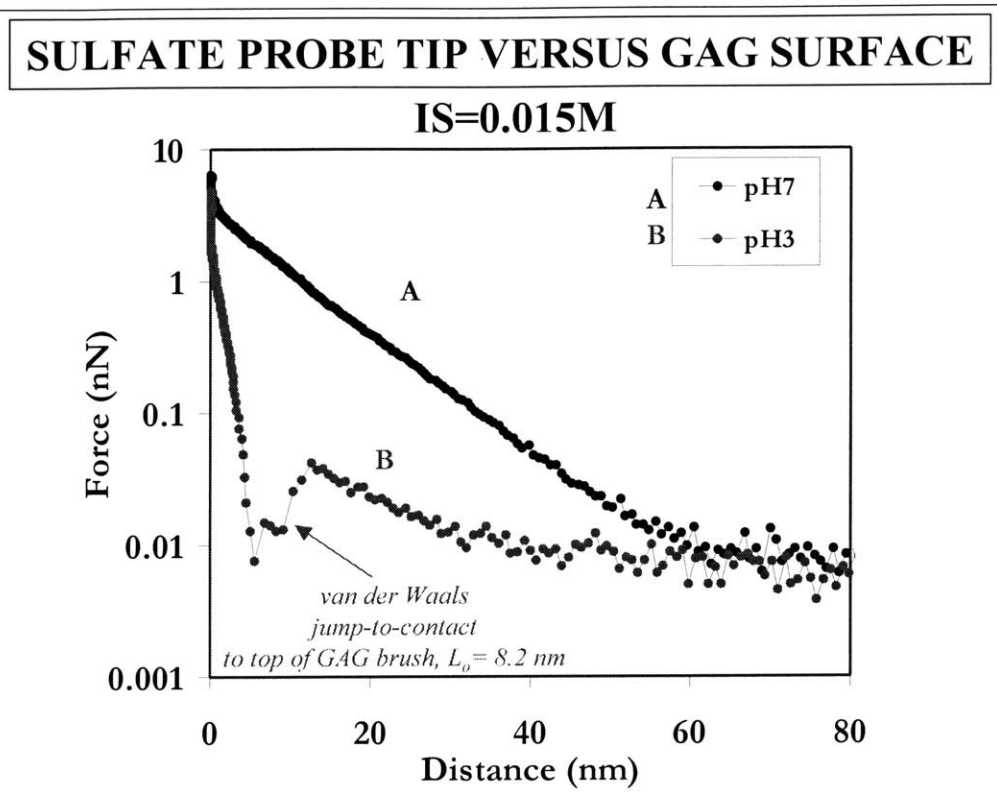

Figure 3.6: Comparison of (average) Force/Radius (mN/m) (logarithmic scale) vs. Distance (nm) curves measured on approach between sulfate-modified tip and CS-GAG-functionalized surface at pH=3 and pH=7 (IS=0.015M).

3.3.5 Interaction Between Hydroxy-Functionalized Probe Tip and CS-GAG-Functionalized Substrate as a Function of Ionic Strength

The (average) Force (nN), (average) Force/Radius (mN/m), and (average) Stress (MPa) versus Distance (nm) between a hydroxy-modified probe tip and a CS-GAG-modified surface are shown in Figure 3.6 (a)for ionic strengths ranging from 0.0001M to 3.0M at pH 5.6 (y-axis on a linear scale) and Figure 3.6 (b) ((average) Force/Radius (mN/m) y-axis logarithmic scale). The neutral, hydroxy-functionalized probe tip is useful because it does not exhibit a pH-dependent change in ionization and is hydrophilic. One can observe

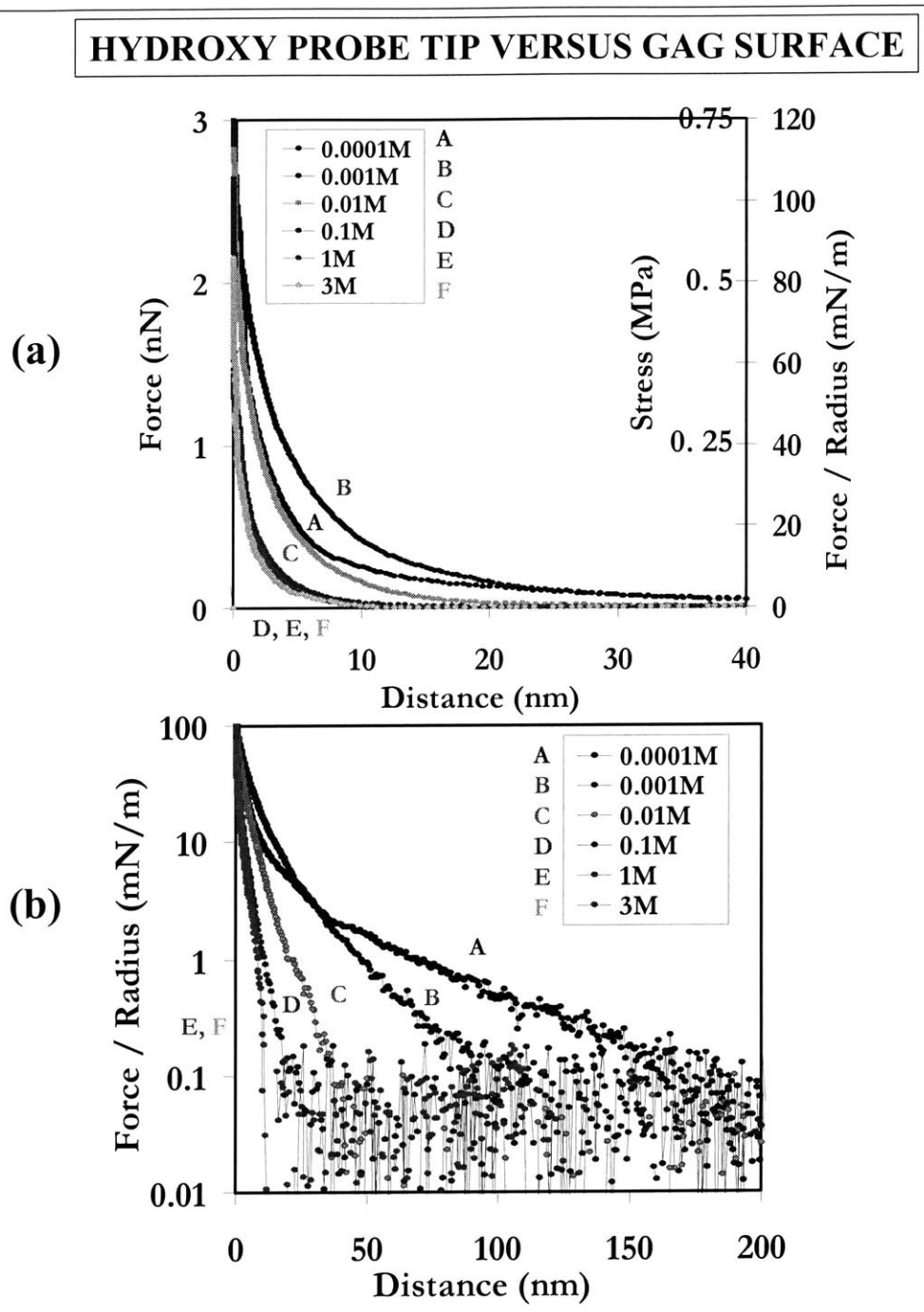

Figure 3.7: HRFS data measured on approach with the MFP between hydroxy-functionalized probe tip and CS-GAG-functionalized surface as a function of ionic strength (IS=3M, 1M, 0.1M, 0.01M, 0.001M, 0.0001M) at pH≈5.6: (a) (average) Force (nN), (average) Force/Radius (mN/m), and Stress (MPa) vs. Distance (nm). (b) (average) Force/Radius (mN/m) (logarithmic scale) versus Distance (nm)

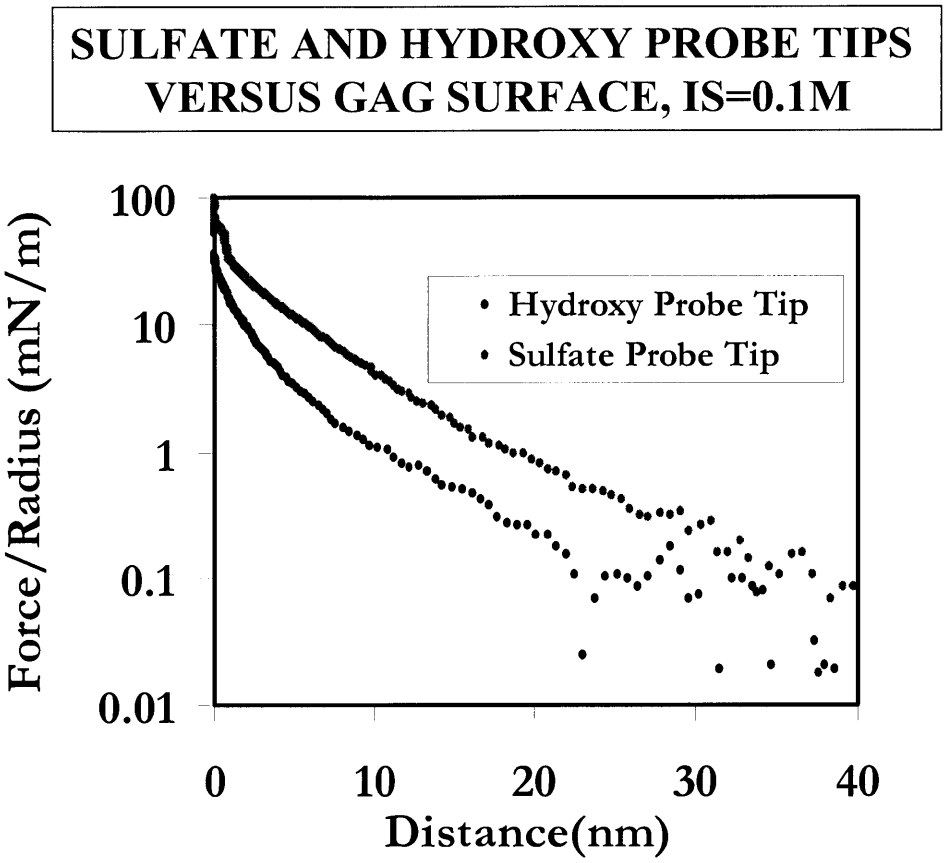

Figure 3.8: Comparison HRFS data measured on approach for sulfate-modified probe tip versus CS-GAG-functionalized surface and hydroxy-modified probe tip vs. CS-GAG-functionalized surface both at pH≈5.6 and IS=0.1M: (average) Force/Radius (mN/m) (logarithmic scale) versus Distance (nm)

that even for this case of the so-called neutral probe tip versus a negatively charged CS-GAG surface, long-range electrostatic repulsive forces are still present up to D=200 nm at the lowest ionic strength conditions, 0.0001M. One possible origin of this electrostatic repulsive force is the nonspecific adsorption of counterions from the solution to the probe tip, which causes the probe tip to have a non-zero effective surface charge. Figure 3.7 shows the (average) Force/Radius (mN/m) on a logarithmic scale versus Distance (nm) for the hydroxy-functionalized compared to the sulfate-functionalized probe tips versus CS-GAG-modified surface at IS=0.1M, pH~5.6. It was observed that the force for the hydroxy-

functionalized tip was always less than that for the sulfate-functionalized probe tip throughout the entire distance range measured. The change of the slope in force vs distance curve was noticed in Figure 3.6 (b) at 0.0001 M. The jump to contact to the top of the brush height was also readily observed around 40 nm at 0.0001 M.

3.4 Discussion

In this study, we prepared highly purified and well-characterized chemically end-grafted polymer brush surfaces of negatively charged CS-GAG macromolecules, and we report the first molecular mechanics measurements in this system using the technique of high-resolution force spectroscopy. A combined experimental and theoretical approach was aimed at understanding the contributions of the four constituent intermolecular interactions (eq. *(7)*) to the total measured force between the brush layer and probe tip.

3.4.1 Control Experiments: Interaction between Sulfate-Functionalized Probe Tip and Sulfate-Functionalized Substrate as a Function of Ionic Strength

In order to interpret our CS-GAG brush measurements, the sulfate versus sulfate control data of Figure 3.4 provided two important pieces of information: *(1)* an estimate of the sulfate charge density of the probe tip, and *(2)* a control to investigate the validity of frequently used theoretical models to represent interaction forces in this relatively simple system. The measurement of repulsive DLVO forces between non-polymeric charged surfaces is well documented in the literature using both the surface force apparatus (and similar instruments)[66-71] and the atomic force microscope.[41-44, 51, 72-82]

All of the theoretical models presented in this paper employ constant surface charge boundary conditions, rather than constant potential, for two reasons. First, both the substrate

and the tip were electrically isolated from each other and from the instrument ground and, therefore, not electrically connected to any source that would maintain them at a constant potential.[83] Secondly, theoretical modeling of the ionization state of surface charges in our system suggests that the CS-sulfate ester as well as carboxyl-derived charge is nearly constant over the range of pH and ionic strength conditions and at all tip-substrate separation distances. In general, the pH at the charged surface and the ionization state of the surface charge groups will depend on bath pH, bath ionic strength, and the pKa's of the charge groups. A lower bound estimate of the surface pH was calculated using the linearized PB equation[52] for our ionic strength range at all distances, given the bath pH=5.6 and the relevant pKa's. The pH at the surface was calculated to be >5, even at the lowest ionic strength, which is much higher than the pKa's of the charge groups. Thus, less than 1% of the sulfate groups would be neutralized (protonated). In addition, we used a model,[84] to calculate the "charge regulation parameter α" that characterizes approaching charged surfaces as maintaining constant charge or constant potential. From our data, this parameter was calculated to always be in the constant charge regime.

The model using eqs. (A1.6) and (A1.7) fit reasonably well to the sulfate-sulfate data of Figure 3.3 (b) and (c), respectively, except at short distances D<15 nm and at low ionic strength for all distances. The overestimation of the data by the linearized analytical solution (A1.6) at low ionic strength is most likely due to *1)* the high values of the potential, which violate the conditions of the linearizing approximation,[85] and *2)* modeling of the tip as an effective hemisphere, while the actual tip geometry is ill-defined and more similar to that of a pyramid. These errors should become increasingly significant at lower ionic strength as the Debye length (the length scale over which electrostatic forces act) approaches R_{TIP}. This tip size-shape problem is also consistent with the apparent increase in predicted surface charge

density with increasing ionic strength (Table 3.1). For the smaller pyramid shape, the model will tend to overestimate the electrostatic force especially at lower ionic strengths. To compensate, the fit values of the surface charge densities will be smaller than the actual values with decreasing ionic strength.

As noted previously, the linearized analytical solution underestimates the experimental data for D<15nm. This is due to the fact that in the constant surface charge model, the magnitude of the potential increases as the tip approaches the surface, and eventually exceeds the values appropriate for the linearization approximation (see Appendix A.1).[49, 86] The linearized solution will then overestimate the data when the tip is far from the surface and underestimate the actual charge density. The nonlinear solution avoids this problem and fits closer to the data (Figure 3.3 (c)). Interestingly, one may note the absence of the van der Waals jump-to-contact at 0.01M data, presumably due to an additional repulsive hydration force

3.4.2 Interaction between Sulfate-Functionalized Probe Tip and CS-GAG-Functionalized Substrate as a Function of Ionic Strength

Several studies have reported the measurement of repulsive forces between surfaces bearing adsorbed[87-91] or hydrophobically anchored[31, 33, 92] polyelectrolyte layers using both the AFM and the surface forces apparatus (SFA). In contrast, the CS-GAG polyelectrolyte chains in our study were *chemically* end-grafted to the surface. Adsorbing polymer layers exhibit significant degrees of hysteresis,[89, 93] while the interaction of the CS-GAGs with the underlying substrate is shown here to be minimal as evidenced by the nonhysteric, reversible overlap of approach and retraction curves (Figure 3.4 (b)). The magnitude of the force was consistent at three different locations and the standard deviation

of the experiment at each ionic strength was less than 20 pN, which indicated the uniformity of the CS-GAG end-grafted substrate. At moderately low ionic strength, we expect the individual CS-GAGs to be in a more extended, rigid-rod -like conformation where the intramolecular repulsion between neighboring charges on the CS-GAG chains outweighs the entropic forces driving the chain to a random coil. As the ionic strength is increased, e.g., to 1M, the chains are expected to collapse into a more random coil-like configuration as the intra- and intermolecular electrostatic repulsion is screened by the salt and the Debye length is reduced,[94] contributing in part to the dramatic decrease in measured repulsive force with increasing ionic strength (Figure 3.4 (a)). A detailed study to investigate the conformation of the CS-GAG chains at the surface directly at various ionic strength conditions using the technique of ellipsometry will be presented in Chapter 5.

Models were fit to the data of Figures 3.4 (d) and (e) at the three highest ionic strengths (0.01M, 0.1M, and 1M). R_{TIP} for these experiments was 25 nm, smaller than that used for the sulfate-sulfate experiments. The approximation of the tip as a hemisphere can only be used when R_{TIP} is much greater than the distance over which the force acts.[47, 49] Therefore, it is not appropriate to use the models described in this paper for the lower ionic strengths (0.001M-0.0001M) at which the Debye length is on the order or larger than R_{TIP} (see Appendix A.1.2).

Constant Surface Charge Model (Nonlinear Numerical Solution). In certain previous studies,[33, 89, 92] a flat surface charge model was used as a first approximation to represent polyelectrolyte layers. However, discrepancies between such a model and experimental data would be expected for the following reasons. Firstly, a flat surface charge may not accurately reflect the distributed charge of the polyelectrolyte chains on the surface,

even for adsorbed layers, since loops (segments terminally bound with the rest in contact with the solvent), trains (series of consecutively adsorbed segments), and tails (having one end bound and the other dangling in solution) are typically present.[95] Secondly, for D<Lo (where Lo=the brush height), steric forces are present. For neutral end-grafted polymer brushes, these forces are due to an attractive elastic restoring force due to configurational entropy and a repulsive osmotic pressure.[11] Upon compression and confinement, the local increase in chain segment concentration at the interface leads to an increase in the osmotic pressure and a decrease in the elastic restoring force, with the osmotic contribution dominating, especially at strong compressions. For rigid-rod like chains, the steric component may also include bending and confinement penalties.[58] Thirdly, lateral intermolecular electrostatic repulsion between neighboring polyelectrolyte chains on the surface may also play a role for decreasing $D<L_o$.

Figure 3.4 (d) compares the flat constant surface charge model pictured in Figure A.1 (a) with our CS-GAG brush data. With all of the model parameters fixed to their known values, the model does predict the correct trend with varying ionic strength but, as expected, it severely underestimates the data over all of the distance ranges measured and gives us a good indication of the magnitude of the additional forces due to the polymeric structure of the CS-GAGs as a function of ionic strength.

Volume Charge Model. Next, we used a "volume charge model" which represents the CS-GAG brush layer as a fixed volume charge density on the substrate (Figure A.1(b)). The height of the volume charge, h, which is equivalent to the brush height, L_o, was the only free fitting parameter in the model, and considerably improved fits were obtained (Figure 3.4 (d), and (e)) compared to flat constant surface charge model for D<25 nm using $h=L_o$ values of

17.6 nm (IS=0.01M), 14.1 nm (IS=0.1M), and 31.8 nm (IS=1M). The values obtained for $h=L_o<L_{contour}$ suggest that the CS-GAG chains are not fully extended, but not completely collapsed on the surface. The h values and, hence, the magnitude of the purely electrostatic forces obtained are most likely overestimated due to the presence of steric repulsion which has not yet been included in the model. This is especially true at IS=1M since the Debye length is small; the electrostatic forces start when the tip is inside the brush in a region where steric forces are most significant. At shorter distances (D<15nm, Figure 3.4 (d)), the model still underestimates the experimental data and, as a first approximation, gives an indication of the magnitude of the steric repulsive component.

For D>25 nm, the volume charge model severely underestimates the experimental data. One reason for this discrepancy is the approximation of the probe tip as a hemisphere, as discussed above. Another source of error is the representation of the CS-GAG brush as a volume of uniform charge density. The CS-GAGs are approximately 6 nm apart and have a nonuniform charge distribution in the space within the brush ($D<L_o$), which will also affect the ionic double layer distribution within and above the brush ($D>L_o$). [96]

The volume charge model predicts a transition in the force versus distance curve at the position $h=L_o$. A sharp transition is not observed in our experimental data, although it has been observed to varying degrees in other polyelectrolyte systems in the literature.[33, 88, 92] This may be due to the relatively low grafting density (Γ=0.024 chains/nm^2) compared to the systems reported in the literature (e.g. Γ=0.13-0.41 chains/nm^2)[33], giving enough room for GAG chains reorganize due to long range electrostatic interaction between GAG brush layer and negatively charged tip. It was noticed that the curve fit of volume charge model extends longer distances at 1M than 0.1 M, which is due to ignoring the steric

component in our model. The curve fit was carried out using a volume charge model that includes only the electrostatic component of force at various salt concentrations. When there exists a region of space in which electrostatic forces dominate (i.e., for ionic strengths ≥ 0.1M), the model is able to predict a value for the brush height that is not significantly affected by the presence of steric forces, consistent with the assumptions of our model. However, at 1M salt concentration, the electrostatic interactions are reduced and may become on the order of steric interactions on the length scale of the brush layer. Therefore, by fitting the electrostatic volume charge model to the total measured force in this regime, the brush height is overestimated. It should also be noted that the volume charge model predicts a significant electrostatic repulsive force even at the highest ionic strength of 1M, a condition typically thought to screen electrostatic interactions.

3.4.3 Hydroxy-Functionalized Probe Tip Versus CS-GAG-Functionalized Substrate as a Function of Ionic Strength

The repulsive interaction between hydroxy terminated tip and GAG brush layer mainly originates from the intermolecular electrostatic interactions since hydroxy tip is supposedly charge neutral. As the ionic strength increased, the repulsive force significantly decreased due to the shielding of intermolecular electrostatic interactions. There was little decrease of the repulsive force as ionic strength decreased from 1 M to 3 M, suggesting that the nature of the repulsive force is rather insensitive to the shielding of the electrostatic interaction at this range.

Repulsion force originated from long range repulsion was observed when the distance between the tip and the surface was longer than the brush height and intermolecular electrostatic repulsion plays a role when the tip was close to the surface. It was observed that

long-range electrostatic repulsive forces are present up to D~200 nm in 0.0001M NaCl, the lowest ionic strength condition. It was postulated that these forces might arise, in part, from an effective surface charge on the probe tip due to nonspecific anion adsorption. In addition, although $\sigma_1 = 0$, the models still predict an electrostatic repulsion force due to the geometry of the tip, bath, substrate system in which the tip surface is impermeable to ions (see Appendix A.1).[53] At 0.0001 M the two regions were clearly observed. At long range the electrostatic force due to adsorbed ions on the tip was shown and then after jump-to-contact to the top of the brush layer around 40 nm, the slope of the force vs distance curve changed as tip penetrate inside the GAG brush. The change of the slope of force vs distance curve was also noticed at 0.001 M without jump-to –contact, which clearly shows that the difference of the measured force in two different regions; one region is beyond the brush due to ionic atmosphere above the brush and the other region due to the fixed charge density of the GAG. At 0.1 M salt concentration, electrostatic and steric repulsion was still strong enough to overcome a short range van der Waal attraction so no adhesion was observed between the tip and the surface.

Crossover point was observed between 0.0001 M and 0.001 M. The distance of the crossover point distance was around 40 nm from the substrate, which is very close to the contour length of the GAG. After the crossover point the force at 0.0001 M is smaller that the force at 0.001 M, indicating that the charge density at 0.0001 M is lower than that at 0.001 M. Simple calculation using the volume charge model developed by Dean showed that the crossover point should occur in case there is a increase of the charge density in the GAG brush layer as ionic strength increases. According to the model, the crossover point was located beyond the brush height due to the long-range double layer interaction that exists above the GAG brush layer. This long-range interaction starts in a further distance at low

salt concentration so force started to increase first. But once inside the brush layer the magnitude of the force is determined by the charge density. So the magnitude of the force is reversed inside the brush because the charge density at higher salt concentration is higher. This assume that the charge density at 0.0001 M probably lower than one at 0.001 M because of less ionization of charge groups. We will examine this issue further in detail in chapter 5.

Although the interchain distance of GAG brush layer that we prepared is longer than the distance in physiological condition, we can achieve the physiological interchain distance by compressing the GAG layer using hydroxy modified tip. If we look at the force in the range of 2-8 nm distances from zero distance, it corresponds to the average interchain distance 2-4 nm when the GAG brush layer is compressed by the hydroxy modified tip. The force started to increase around 10 nm from the surface at 0.1 M. If we assume the uniform GAG density when the brush height is 10 nm, the distance between the GAG is 3.25 nm which is very close to the interchain distance of GAG in cartilage. Within a couple of nm range from the surface, the force reaches 1 nN, which scales to a stress of 250 KPa, which is about half of the swelling pressure of the cartilage and consistent with the unit cell model prediction.[1] The fact that the force was reversible without any hysterisis and jump-to-contact suggests that the repulsive force has the nature of fast relaxation of the compressed state and complete shielding of short range van der Waals attractive interaction. Giasson et al observed that the strong segment-solvent interactions (consequently hydrated segments) due to the hydrophilic nature of polymer backbone dominate the VDW attraction and therefore the measured forces are still in the repulsive regime at small distance

separations.[92] This suggests good solvency of the GAG molecules under the range of salt concentration might also be a reason for the absence of the van der Waals attraction in addition to electrostatic interactions.

To assess the contribution of nonelectrostatic component to the total repulsive force, we compared the force at specific distance at two salt concentrations. The nonelectostatic contribution (entropic and excluded volume effect) to the total force should be independent on the salt concentration. This force is expected to have the highest contribution to the total force at the highest salt concentration, 3 M in this case. If we compare force at 3 M with 0.01 M salt concentration at 5 nm distance from the surface, the magnitude of the force at 3 M (0.0836 nN) is less than 20% of the magnitude of the force (0.441 nN) at 0.01 M. Since the force at 3 M can still have electrostatic component, we can safely say that the steric force at 0.01 M is less than 20% at 5 nm from the surface. If we fit the data from 10 nm to further using the model, the nonelectrostatic component is negligible because the force at 10 nm at 3 M is almost zero.

The contribution of the entropic repulsive force due to the confinement of end grafted rod-like molecules due to incoming spherical particle was calculated using the equation developed by Miller et al.[58] The forces that the incoming spherical particle experiences due to the reduction of configurational entropy of the rod-like molecules is close to our situation at very high salt concentration. We plotted the equation and compared with experimental data but the magnitude was much smaller than the magnitude of the observed force. This suggests that other contribution such as electrostatic interaction and excluded volume plays a more important role in the repulsive forces. The charge-indepednent, entropic contribution of GAG conformation to the equilibrium elasticity is also found out to

be relatively less important at physiologic ionic strength. [10] In 1.5 M salt, the conformational contribution to the swelling pressure of chondroitin sulfate was found to be about 30 %. In physiologic ionic strength, however, the result is closer to 10 %.

3.5 Conclusions

In this chapter, polymer brushes were prepared by end-functionalized polymers with the terminal group selectively adsorbed on the surface. Our system had a 0.024 chains / nm^2 corresponding to the moderately dense regime in which graft chains overlap each other and the volume fraction in the layer may not be high enough to take into account the thickness of the incompressible layer.

The total intersurface force between CS-GAG brush layers and probe tips of known chemistry ($-SO_3^-$, -OH) exhibited a long-range ($D \leq 175$ nm compared to $L_{contour}=35$ nm), nonlinear, purely repulsive behavior that decreased in magnitude and range with increasing ionic strength, and decreasing pH. At physiological ionic strength and pH, the measured stress (i.e., force normalized to the area per chain) is on the order of that reported previously as the proteoglycan swelling pressure within intact cartilage tissue. For $D>L_{contour}$, the inter-surface interaction is dominated by electrostatic double layer forces while, for $D<L_{contour}$, steric interactions also come into play.

At shorter distance ranges, van der Waals and hydration forces may also be present but are expected to be relatively smaller in magnitude. A detailed comparison of interactions between CS-GAG and tip with those between the tip and a sulfate surface charge system ($-SO_3^-$ versus $-SO_3^-$) was further interpreted using two theoretical electrostatic double layer models based on the Poisson-Boltzmann equation. These results provided an improved

understanding of how CS-GAG polymers can sustain compressive loads in macroscopic tissues such as cartilage.

Not surprisingly, the CS-GAG brush layer could not be modeled accurately using a constant surface charge model, which severely underestimated the magnitude of the repulsive force throughout the distance range measured. The volume charge model fit better to the experimental data for reasonable values of the brush height (the only fitting parameter), suggesting that the volume distribution of charge on the CS-GAGs leads to a significant increase in the magnitude of the repulsive force, especially for $D<L_o$. Underestimation of the data by the volume charge theory for $D>25$ nm suggests that the true, nonuniform, rod-like charge distribution along individual CS-GAG chains may be important in understanding the interaction force at these longer range distances. Future experiments to directly determine the brush height as a function of ionic strength will enable us to verify the validity of these fits and to further quantify the distinct contribution of steric and lateral electrostatic interactions to the total force.

Chapter 4

ATTACHMENT OF GAG TO A NANOSCALE PROBE TIP USING AN ELECTRIC FIELD.

4.1 Introduction

The atomic force microscope (AFM) and related high-resolution force spectroscopy (HRFS) instruments have become fundamental tools for studying molecular, colloidal, and surface forces. AFM has become available that has the precision and sensitivity to probe surfaces with molecular resolution in physiological fluid environments and at forces down to piconewton(pN) range.[97] Probing local force at a scale of a single molecule make AFM complementary approach to the surface force apparatus which has been used extensively to measure macroscopic interfacial forces in crossed cylinder geometry.[98] The optical trapping technique also has enough sensitivity to study single molecule mechanics, but its use has been limited to certain samples and to measurements of forces less than tens of pN and it is not suitable for studies where greater applied forces are needed.

A key AFM component is the soft microfabricated cantilever force transducer with a fine probe tip (typically Si_3N_4 with end radii <5-60 nm) that deflects when interacting with a

sample surface. For many AFM studies, controlling the surface chemistry of the probe tip turned out to be extremely advantageous, particularly with regard to probing inter-and intramolecular interactions in biological system as well as enhancing contrast in a friction or phase contrast image. Traditionally, chemically modified tips have been used in lateral force or friction imaging in contact mode, both in fluids and in air, which is often referred as a chemical force microscopy.[99] The AFM probe (silicon nitride) tip is functionalized with a particular chemical species and scanned over the sample to detect adhesion differences between the species on the tip and those on the sample surface. This groundbreaking study opens an entirely new area for force measurements of functional group microstructure in polymers and other materials and binding/recognition interactions in biological systems by developing various strategies for functionalization of the AFM probe.

Although bare silicon nitride tips have been useful in studying single-molecule biomechanics of protein,[100] DNA,[101] and synthetic macromolecules,[102] the functionalization of the tip with biomacromolecules can give much more opportunities to probe various specific molecular interactions as well as single molecules. The AFM tips functionalized by non-specific binding(or physisorption) of biomolecules were used to study molecular recognition between receptors and ligands and stretch single polysaccharide.[103, 104]

Covalent immobilization of specific macromolecules on the probing tip is preferred way to investigate inter- or intramolecular interaction because it enables to control the orientation of the molecules and increases the stability of the molecules on the tip by preventing desorption during the force measurement. The AFM probe tip chemically modified with a wide variety of macromolecules were used to investigate the hybridization

of DNA,[105, 106] binding strength between cell adhesion molecules,[107] discrimination o the chiral compounds,[108] optomechanical property of photosensitive p olymer,[109] and interaction between synthetic macromolecules and polyethylene oxide functionalilzed surface. [110]

However, attachment to probe tips of charged polyelectrolytes with a desired orientation, conformation, and surface density is difficult due to small tip size and polyelectrolyte charge. Appropriate functionalization and subsequent characterization can be critical to interpretation of HRFS data. Parameters including chain-grafting density (Γ, chains/nm^2), the distribution and conformation of chains have a significant impact on the observed interaction force versus separation distance profile.

Our recent studies of the biological polyelectrolyte molecules in cartilage,[5] chondroitin sulfate glycosaminoglycans (CS-GAGs), called for new methods of attachment to nanoscale probe tips in order to out carry out HRFS experiments between two opposing, end-grafted polymer brushes which more closely mimic the physiological conformations found in native tissue. [111] Hence, CS-GAG chains were chemically end-grafted to an Au-coated Si_3N_4 probe tip by means of an electric field applied between the tip and a nearby Pt electrode. Previously, an electric field had been used to attract charged DNA oligonucleotides to an underlying monolayer of single-stranded DNA that had been immobilized to a Au coated sensor surface through a Au-thiol attachment and a 300 mV potential between the sensor and a Pt electrode was found to enhance hybridization of the DNA oligonucleotides to the DNA monolayer.[112]

We extended this to use an electric field to drive CS-GAGs to a nanosized probe tip, thus increasing the local polyelectrolyte concentration in the vicinity of the probe tip and

chemisorption via an end-terminal functionality. The HRFS was used to measure force between GAG functionalized probe tip and SAM modified substrate at various ionic strengths and pH's. The newly developed model[96] that attempts to account for some aspects of molecular geometry and nonuniform molecular charge distribution inside the brush was used to estimate the parking density of the GAG molecules on the tip.

4.2 Experiment

4.2.1 Materials and Methods

Methods described previously[111] for chemically end-grafting mono(thiol)-terminated CS-GAG to Au-coated silicon chips were adapted for grafting GAGs to Au-Si_3N_4 probe tips (square pyramidal geometry, end radius ~ 50 nm) at the end of a soft cantilever (*Thermomicroscopes, Inc,* V-shaped, spring constant, k = 0.01 N/m).

"**Passive functionalization**," involved immersing Au-coated probe tips into 1 mg/ml phosphate buffer solution (PBS, pH = 7.4, IS = 0.17M) containing mono(thiol)-terminated CS-GAG for 9 hrs. After reaction, probe tips were immersed in 5mM 11-mercaptoundecanol, $HS(CH_2)_{11}OH$ ethanol solutions (P. Laibinis, MIT) for 15 min to passivate that part of the surface that did not react with CS-4-GAG.

"**Active functionalization**" involved applying an electric field for 9 hrs between probe tip and a Pt electrode immersed in 1-mg/ml PBS solution of CS-4-GAG[112] in a closed liquid cell of an AFM (*Multimode IIIA*, Digital Instruments, Santa Barbara, CA). The probe tip was grounded, and a negative voltage (-0.15 V) was applied to the Pt cathode via a cap on the piezoelectric scanner (Figure 4.1(a)). The distance between the probe tip and the

Pt electrode was about 100 μm; the sharp probe tip geometry resulted in a 10-fold higher E-field strength near the tip apex (~3000 V/m) compared to 300 V/m at the Pt surface below (calculated using QuickField finite element solver, DK-5700 Svendborg, Denmark, Figure. 4.1(b)).

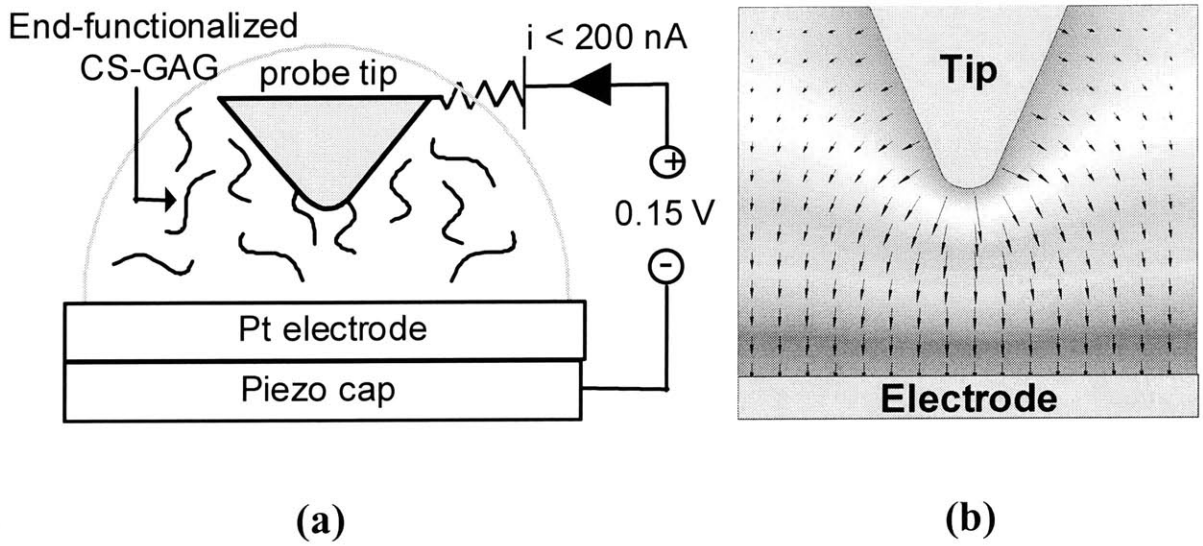

Figure 4.1: (a) End-grafting CS-GAG to a nanosized probe tip using an electric field, (b) 2-D map of E-field lines between tip and electrode; arrow length and direction correspond to E-field magnitude and direction

Figure 4.2(a) and (b) shows the current-voltage curve for the tip-Pt system; at the low voltage used here (< 0.15 V), the resulting small, non-Faradaic current (< 200 nA) minimizes chemical reactions at the probe tip that could lead to electrolysis or disrupt the CS-GAG end-grafting chemistry. The modified probe tip was backfilled as in the passive functionalization method. The planar SAM substrates were prepared using Si (100) wafers (Recticon Enterprises, Inc., Pottstown, PA) coated with a 2 nm-thick Cr layer followed by a 30 nm-thick Au layer, and then immersed in a 1 mM solution of 11-mercaptoundecanol. HRFS measurements were performed using a *Molecular Force Probe* (MFP) (Asylum

Research, Santa Barbara, CA) to measure force versus tip-substrate separation distance, D, at a constant z-piezo displacement rate of 1 μm/s at 23°C. A full description of this instrument, its limit of force and displacement detection in fluids (±5 pN using the present cantilever and ~ 3 Å respectively), and details of measurement errors, were given previously.[111] Data are given as averaged curves of 10 to 15 individual experiments at different locations on the sample surface and have a standard deviation of < 20 pN.

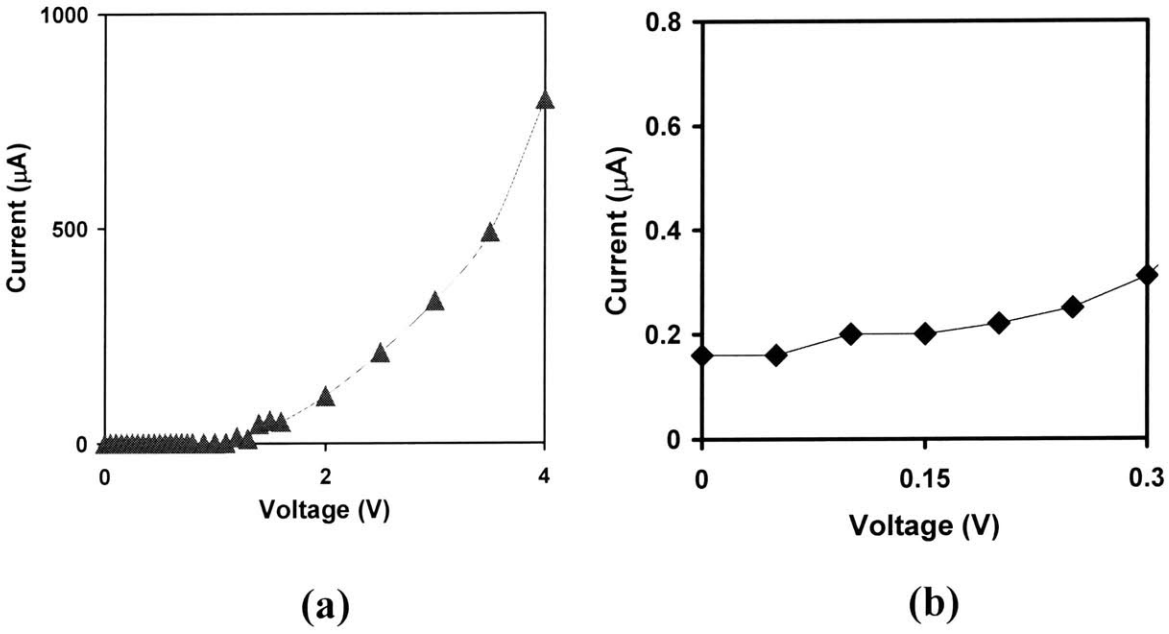

Figure 4.2: (a) Current vs. voltage across tip in 0.1M NaCl, pH=5.6 aqueous solution, (b) Current vs. voltage across tip near the voltage that was used for the experiment. The current was minimized to prevent any chemical reactions at the probe tip.

4.3 Results

4.3.1 Passive vs active functionalization

Figure 4.3 compares averaged force/radius versus distance profiles on approach for the actively and passively functionalized CS-GAG tips vs a OH-terminated SAM planar substrate in 0.1 M NaCl, pH 5.6. The retraction curves overlapped approach curve without showing any hysterisis, which was consistent with the results in the hydroxy modified tip vs GAG modified substrate system. Both probe tips gave a nonlinear, purely repulsive interaction force for D < 40 nm dominated by electrostatic and steric *inter-* and *intra*molecular GAG interactions, with no jump-to-contact due to van der Waals or other nonspecific attractive forces. The electrically functionalized probe tip gave a significantly higher force over a wider distance range, suggesting the presence of a higher density of CS-GAG chains on the probe tip.

4.3.2 Force measurement of GAG functionalized tip vs hydroxy modified substrate

The figure 4.4 (a) shows force/radius, and stress versus distance profiles for the actively functionalized CS-4-GAG probe tip versus a OH-terminated SAM planar substrate on approach at various ionic strength conditions at pH~5.6. The repulsive force was observed to decrease in magnitude and range as the ionic strength increased, consistent with the well-known effect of salt screening of the electrostatic double layer forces. A further validation of the presence of CS-4-GAG on the probe tip is seen in the measured force/radius, and stress versus distance profiles using the same system on approach at pH 7

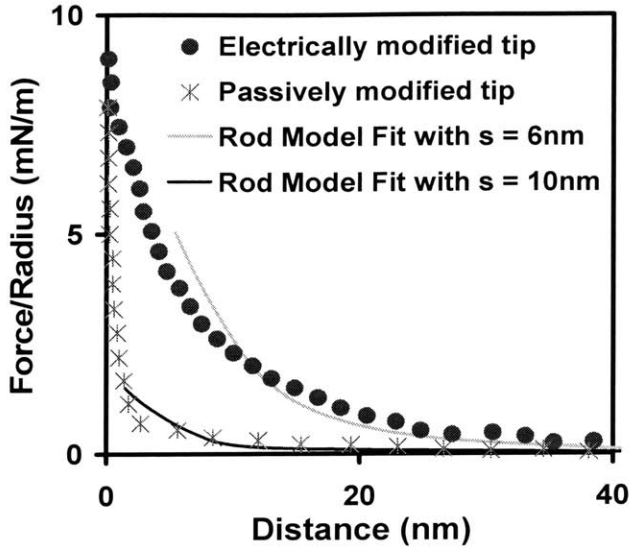

Figure 4.3: Force/radius vs. distance profiles for actively (R_{TIP}=~50nm) and passively (R_{TIP}=~50nm) functionalized CS-GAG probe tips vs OH-terminated SAM planar substrate (IS=0.1M, pH=5.6)

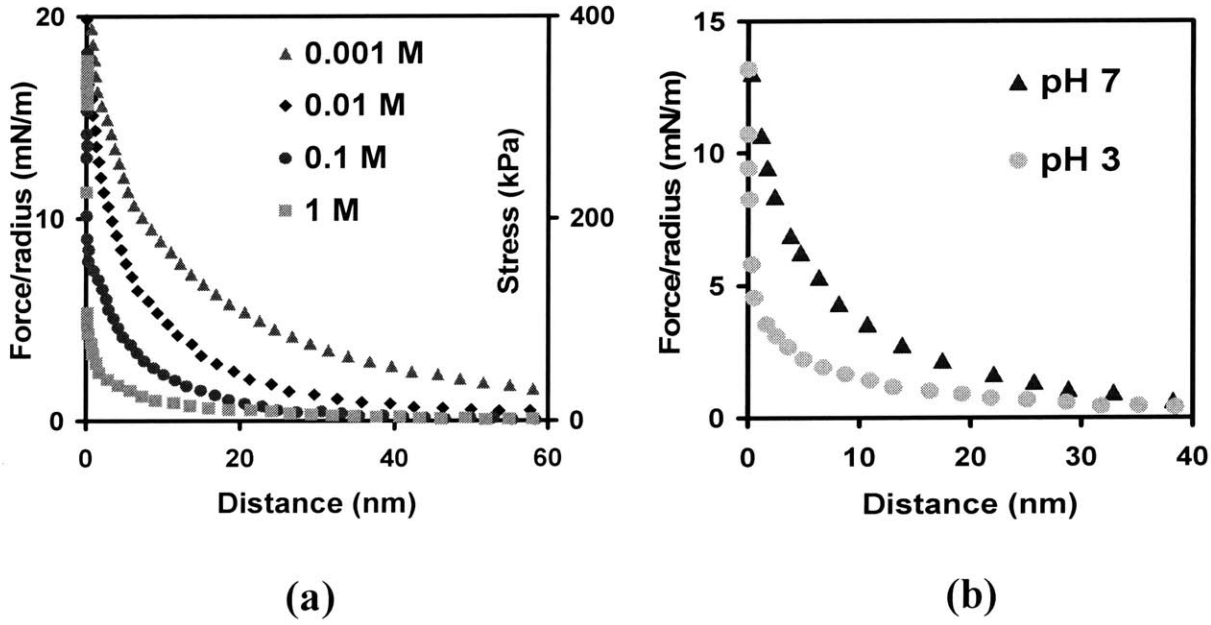

Figure 4.4: (a) Force/radius vs. distance for actively functionalized CS-GAG tip vs. OH-terminated SAM substrate at various IS, pH=5.6 (b) Force/radius vs. distance for the same system as (a) at pH 7 and 3 (IS=0.015M).

versus pH 3 (Figure 4.4 (b), IS = 0.015M). The sulfate and carboxyl groups are both charged at pH 7, whereas only the sulfate group remains charged at pH 3 due to the protonation of the carboxyl group. This reduction of the fixed charge density at pH 3 to about half of its original charge density caused a significant decrease in measured force over the entire distance range, consistent with the hypothesis that the measured repulsive force is due to the presence of the CS-GAG macromolecules on the AFM tip.[111]

4.4 Discussion

The figure 4.3 showed that the repulsive force due to end-grafted CS-GAG molecules on the AFM probe tip was strong enough to completely shield short range attractive van der Waals force at relatively high ionic strength. Since the electrical Debye length, κ^{-1} , is 1 nm at 0.1 M salt concentration, surface anion adsorption to the probe tip, alone, could not account for the long distance range of the forces, which would begin at ~5 κ^{-1}.[51] The ionic strength and pH experiment strongly supported that the nature of the repulsive force is mainly electrostatic origin. The measured force using actively functionalized tip was much higher than the force measured using passively functionalized tip, which shows that the electric field was effective in attracting negatively charged CS-GAG molecules to AFM probe tip.

In order to estimate the grafting density obtained by electrical functionalization, the data of Figure 4.3 were compared to the predictions of a Poisson-Boltzmann based charged rod model (solid curves) for electrostatic double layer repulsion force between a neutral planar substrate and a hemisphere functionalized with a CS-GAG brush. [53] [96] The CS-GAGs were modeled by cylindrical rods that represent the time average space occupied by the individual polyelectrolyte macromolecules in the brush. This model was successfully

applied to quantify the force between GAG end-grafted substrate and various chemically modified AFM probe tips.

The theoretical curves of Figure 4.3 correspond to the force between a planar sulfate substrate and a polyelectrolyte brush composed of cylindrical rods of finite height and uniform charge density, with the Debye length, κ^{-1}, fixed by the NaCl concentration, and the rod radius, r, and distance between neighboring chains, s, fit to the data. The parameters that were fixed in the model included the polyelectrolyte brush height (h = 45 nm, the distance at which the force increased above the noise minus $5\kappa^{-1}$), the rod radius (r = 2 nm, based on our previous study using a functionalized planar substrate [96]), the known charge per CS-GAG chain ($Q = -8.0 \cdot 10^{-18}$ C), and the hemisphere radius (R_{TIP} = 50 nm). The only parameter left adjustable was the distance between neighboring CS-GAG chains (s) and was fit to the HRFS data between D=10-80 nm using the method of least squares. The resulting values, s=10 nm (Γ=0.01 chains/nm^2) for passive and s=6 nm (Γ=0.028 chains/nm^2) for the electrical functionalization, showed that the E-field gave a ~3-fold increase in chain grafting density. The grafting density obtained by electrical functionalization also corresponded well with values obtained from previous measurements of metabolically radiolabeled CS-GAGs attached using the same chemical reaction conditions and measured via the technique of scintillation counting.[111]

We also tried to obtain the relative contribution from the nonelectrostatic component of the total repulsive force in this system. We obtained almost same ratio of the forces at 5 nm between 1 M and 0.01 M as we observed in opposite configuration setup, OH tip vs GAG substrate system. The force at 5 nm at 0.01 M was 0.404 nN that was about 5 times

larger than the force at 1 M, which indicated that nonelectrostatic contribution at 0.01 M is less than 20% of the total repulsive force. The

4.5 Conclusion

To our knowledge, this is the first report of the use of an electric field to enable end-grafting of a high density of charged polyelectrolytes with a desired orientation to an AFM tip to study intermolecular interactions. The sharp tip geometry enhanced the E-field strength near the tip apex which, in turn, facilitated migration of charged GAGs to the AFM probe tip while simultaneously allowing a small total voltage drop and (non-Faradaic) total current. The presence of CS-GAG on the AFM tip was verified by HRFS force measurements at varying pH and ionic strengths in conjunction with a Poisson-based model to characterize the functionalization of the probe tip.

Chapter 5

INTERACTIONS BETWEEN OPPOSING END-GRAFTED GAG BRUSHES IN VARIABLE SOLUTION CONDITIONS

5.1 Introduction

The GAG functionalized substrate and AFM probe tip were successfully prepared as described in chapter 2 and 4. In this chapter we measured interaction forces between GAG end-grafted brush surface and AFM probe tip in various salt concentrations and pH's using molecular force probe. This interchain distance of this system becomes about 4 nm when GAG modified tip approaches GAG modified substrate, obtaining a parking density that is very close to physiological system (~2-4 nm), thus more physiologically relevant than GAGs on substrate only or GAGs on AFM tip only system. The measured force will be compared with the newly developed model that captures the molecular features and sheds light on deformation mechanism(compression vs interdigitation) in the future.

In order to assess the change of the brush thickness as a function of ionic strength and pH, we also performed in-situ ellipsometry measurement. One could call the resulting brush thickness measured by ellipsometry an equivalent optical thickness. The onset of force increase can be a rough estimate of the brush height in dense neutral polymer brush. In the case of the polyelectrolyte, reorganization of the brush layer occurs due to the long range interaction, thus making the correlation of the onset of force to the height of the brush difficult. Here we attempt to correlate the onset of force increase determined from HRFS experiments with optical brush thickness measured from ellipsometry at relatively high salt concentration regime and tried to obtain an insight on the deformation mechanism during compression. And since one of the charged groups of GAG is a carboxylic group, which make GAG as an annealed polyelectrolyte brush, the conformation change of GAG brush layer as a function of ionic strength and pH was also investigated and compared with annealed polyelectrolyte theory.

Background on Polymer Brushes. The system that we prepared to measure GAG vs GAG interaction is fundamentally equivalent with polyelectrolyte brush system. Polymer brushes have been studied extensively both theoretically and experimentally due to their practical and fundamental importance in colloidal stabilization, lubrication, protein resistance and rheology.[113] Typically, most polymer brushes will exhibit a purely repulsive interaction on approach, which is necessary, for example, to maintain stability of colloidal dispersions or to resist nonspecific protein adsorption of biomaterials coatings. For neutral polymer brushes, this repulsive osmotic pressure starts at the equilibrium brush height, Lo, and is due to an increase in polymer chain segment concentration and excluded volume interaction of short-range monomer-solvent affinity and/or monomer-monomer repulsion (sometimes referred to as "steric" forces). Enthalpic penalties may also exist for

certain polymers, such as poly(ethylene oxide)(PEO), for disruption of H-bonding with water and supramolecular structure of PEO.[114] The repulsive interaction between polyelectrolyte (PE) brushes has an additional component; the electrostatic double layer forces that, in certain solution conditions, exist well beyond Los the ionic atmospheres begin to overlap.

The experiments to measure repulsive interaction between polymer brushes have been carried out using surface force apparatus and recently atomic force microscopy.[37, 115] Neutral polymer brushes were prepared using diblock copolymer or surface initiated polymerization that usually produces much higher grafting density than the grafting density obtained by adsorption of diblock copolymer.[31, 36] The range of the measured force was much longer than the equilibrium size of the polymer in solution, a several radii of gyration of the polymer, which indicated that the polymers in the brush layer are highly stretched from its equilibrium state in solution. Taunton et al showed that the range for onset of interaction is roughly twice the equilibrium thickness of the corresponding adsorbed chains calculated from scaling theory.[115] The force measured in good solvent was monotonically repulsive without showing any adhesion or hysterisis at compression or decompression which are characteristic feature of adsorbed polymer layer.[93] The experimental results were explained well quantitatively and qualitatively using scaling theory and mean field theory using brushes with reasonable grafting density.[115] Yamamoto et al obtained exceptionally high grafting density(0.4 chains/nm2) using surface initiated polymerization technique.[37] The true distance between substrate and AFM tip was successfully determined by AFM imaging across the boundary of a scratched and an unscratched region on the sample surface. At this extremely high density brush, they found out that longer

brushes were more resistant to compression than shorter brushes, showing faster force increase.

With charged macromolecules, the stabilization is achieved with a combination of electrostatic and steric interactions. This polyelectrolyte brush-induced pressure is of longer range than the attractive van der Waals force, and, thus, if the grafting density is sufficiently large, it provides a barrier against adhesion near contact. The polyelectrolyte brush layer was successfully prepared by various methods such as adsorption of the diblock copolymer, Langmuir-Blodgett technique or in situ conversion of neutral segment to charged segment.[32, 33, 92, 116] In contrast to neutral brushes that begin to interact only when they are brought into a physical contact, the force measurement between polyelectrolyte brush layers showed long-range electrostatic interaction that begins at the overlap of their ionic atmospheres which extend well above the brush edge.[117] They also observed that the magnitude and range of the monotonic repulsive force decreased as the salt concentration increased due to the shielding of the inter- and intra Coulombic interactions between the charged groups. Tamashiro et al used quenched polyelectrolyte brush system and compared the theoretical predictions for the normal forces between two opposing PE brushes under compression with the experimental measurements. Their mean-field level model was able to explain the ionic-strength dependence of the normal forces qualitatively and quantitatively using parking density as a fitting parameter in their model.

The conformation of the PE brush in aqueous environment provides crucial information to understand and interpret the force experimental data fully using an appropriate model. Therefore, it has been studied using ellipsometry, small angle neutron scattering, small angle x-ray, and neutron reflectivity.[116, 118-120] Ellipsometry has been

employed extensively for the indirect measurement of the thickness and optical properties of thin organic films and recently applied to examine the swelling behavior of polymer brush using simple box model.[118, 121] Habicht et al observed the swelling of a polystyrene brush in cyclohexane as temperature increases using angle dependent ellipsometry, consistent with predictions from mean field theory.[122]

In addition to a neutral polymer brush system, various PE brush systems were studied to examine the effect of the amount of salt, pH and grafting density. PE brushes can be divided into two categories; those with a fixed fraction of charged monomers (quenched PE) and those whose charge density is a variable function of pH, ionic strength, etc. (annealed PE). An example of the former is PE brush consisting of sodium polystyrene-sulfonate. An example of the latter is PE brush consisting of poly(acrylic acid), the charge density of which depends on the pH, the salt concentration, and the grafting density. Since GAG has carboxylic group as well as sulfate group, it is expected to behave as an annealed polyelectrolyte.

Experimental Studies of End-Grafted, Quenched PE Brushes. Mir, et al. determined the interfacial density profile of quenched PE brushes, poly(styrene sulfonate sodium salt) on silica, of two grafting density (interchain distance 4.3 nm for high density sample and 2.8 nm for low density sample) as a function of ionic strength (from 0.1M to 5 M) using small angle neutron scattering (SANS).[116] One striking and unexpected feature was that the mean thickness of the interface, h, was observed to *decrease* with increasing Γ in pure water, in contrast to the prediction of scaling theory where h is found to be independent of Γ [26]. Upon the addition of the salt, the brush layers shrink but never collapse completely. Even at very high ionic strength of 5 M, the chains remain stretched

beyond the Flory radius, R_F and the density profile eventually becomes parabolic with distance from the substrate, z. This effect is due to the fact that strong screening of the long range electrostatic double layer repulsion results in an effective short range excluded volume interaction. Tran, et al. determined the interfacial density profile of quenched polyelectrolyte brushes, poly(styrene sulfonate sodium salt), with interchain distance from 1.3 nm to 2.6 nm using neutron reflectivity (NR). Here it was found out that the chains are strongly stretched due to electrostatic interactions between charged groups and the counterion profile follows quite closely the polymer backbone segment density profile in water. The mean thickness of the brush is proportional to the chain length and does not depend on the grafting density as predicted theoretically. As the bath salt concentration exceeds the concentrations of the counterions in the brush, the PE brush started to shrink but never collapses, even at 5 M salt concentration.[120]

Experimental Studies of End-Grafted, Annealed PE Brushes. Biesalski, et al. studied a polymethacrylic acid brush layer, annealed polyelectrolyte brush, that has variable fraction of charged monomers as a function of ionic strength (from 0.0003 M to 0.3 M) and pH (from 2 to 10) Various parking densities(from 2.4 nm to 11 nm interchain distance) of the brush were prepared using 'grafting from' technique that utilized self-assembled monolayers of an azo initiator on the silicon surface to initiate radical polymerization in situ. Interestingly, the maximum of the brush height occurs at concentration much lower than the average concentration of free ions inside the brush. The theoretical scaling behavior of brush height in osmotic brush regime and salted brush regime were compared with experimental data.[118] Currie, et al. observed that at a given pH the brush thickness behaves nonmonotonically as a function of ionic strength and grafting density. (it initially increases and subsequently decreases with increasing ionic strength). This nonmonotomic behavior

agrees with theoretical predictions for annealed brushes.[123] The experimentally observed scaling exponent in the power law is ~0.1 which is less than that predicted theoretically(1/3) in the osmotic brush regime. [124]

5.2 Experiment

5.2.1 High resolution force spectroscopy measurements

The GAG functionalized substrate and probe tip were prepared as described in Chapter 2 and Chapter 4 respectively. The force between them was measured at 5 different ionic strengths (0.0001 M, 0.001 M, 0.01 M, 0.1 M and 1 M NaCl solution) and 2 pH's (pH 3 and pH 7) using the Molecular Force Probe.

5.2.2 Ellipsometry measurements

The spectroscopic ellipsometry measurements were performed using a variable angle spectroscopic ellipsometry (VASE VB-250 J. A. Woollan Co., Inc., USA) with a rotating analyzer configuration. Ellipsometry measures the change in polarization state of light reflected from the surface of a sample. The measured values are expressed as Ψ and Δ that are acquired versus wavelength at fixed angle (70 degree) of incidence. The two samples with different parking density were prepared as previously described in chapter 1 and were immersed into the liquid cell. The data were collected from 3 different spots for each sample at each salt concentration. The brush heights obtained from fitting of box model were averaged to determine 'optical' GAG brush height. The experiment was carried out in the following order: water, 0.0001 M, 0.001 M, 0.01 M, pH 3(0.015 M), pH 7(0.015 M), 0.1 M, 1 M, and 3 M. The time for equilibrium at each condition was at least 2 hrs.

The simple box model was used as an optical model for ellipsometry data analysis to obtain GAG brush layer thickness. In box model, sample structure was described as three layers that are composed of gold layer, GAG layer, and aqueous environment. The data were fit by varying film thickness with fixed refractive indexes for three layers. Refractive indexes of gold layer, GAG layer, and salt water were used as a fixed parameter for the model fitting. GAG film thickness was an unknown parameter in the optical model and varied to try and produce a "best fit" to experimental data. Regression algorithms are used to vary unknown parameters and minimize the difference between experimental data and theoretical data generated from the optical model.

Strictly speaking, the fundamental equations of ellipsometry are valid for systems consisting of homogeneous isotropic phases with smooth and parallel interfaces. We used a box model to model GAG brush layer; that is, the refractive index, which is coupled to the monomer density, is assumed to be uniform throughout the layer. The assumption of this isodensity of GAG layer may over- or underestimates the brush thickness. Nevertheless surface roughness, graded or heterogeneous composition and anisotropy can be modeled in some cases, it should be kept in mind that the box profile is an input to the optical analysis. More realistic profiles will display a gradual decrease in the segment density.

Modeling of the ellipsometric data requires a good knowledge of optical properties of species on the surface. The refractive index of GAG brush layer was independently obtained from GAG solution measurement. The four concentrations of the GAG solution were prepared and refractive indexes of each solution were measured using a refractometer. As you can see from the table 5.1, the refractive index showed only minor change from 1.3435 to 1.3456 as the GAG concentration varied from 2.5 to 20 mg/ml. Since the density

of the GAG brush layer calculated based upon its known parking density is close to 20 mg/ml, we chose 1.3456 as a refractive index of the GAG brush layer. We also checked the refractive index variation depending on the salt concentration at fixed GAG concentration (20 mg/ml). The refractive index increased about 0.01 when salt concentration changed from 0.01 to 1 M. It was found out that the change of refractive index due to salt concentration change was more pronounced than the change due to GAG concentration.

GAG concentration (mg/ml)	Refractive index at 0.1 M NaCl concentration
2.5	1.3435
5	1.3436
10	1.3444
20	1.3456

Table 5.1: Refractive indexes of various GAG solutions measured at 0.1 M NaCl concentration (pH~5.6)

Salt concentration (M)	Refractive index of GAG solution (20 mg/ml)
0.01	1.3446
0.1	1.3456
1	1.3544

Table 5.2: Refractive indexes of various salt concentrations at 20 mg/ml GAG concentration.

5.3 Results

5.3.1 Force measurement between GAG vs GAG

The interaction forces between GAG functionalized tip and GAG functionalized substrate measured in various ionic strength and two pH's are shown in Figure 5.1. The measured force was monotonically repulsive and showed no adhesion or hysteresis similar to that observed previously for the chemically modified SAM probe tips vs GAG planar substrate. The magnitude and the range of the force were significantly decreased as the ionic strength was increased. At 0.0001 M, the force started to increase for D<140 nm, which is much longer than the twice of the contour length of the GAG molecules, due to the interaction of the electrostatic double layer beyond the GAG brush layer. The force increasing distance decreased as ionic strength increased, finally reaching about 40 nm at 1 M salt concentration. The significant dependence of the magnitude of the force on the ionic strength showed that electrostatic interaction between GAG brush layers is the major component of the repulsive interaction. Although the force at 0.0001 M started at much longer distance than it started at 0.001 M, the force at 0.001 M became bigger than the force at 0.0001 M around 20 nm.

The shape of the curve showed unique behavior at each ionic strength. The force at 0.0001 M was able to be explained with one slope until it is very close to the surface. The force curves measured at 0.001 M and 0.01 M showed two different slopes in force/radius vs distance curves; the slope increased around 80 nm and 40 nm respectively. At 1 M force curve showed a different shape from the other curves judging from the fact that they did not show linear behavior in semilog plot.

The force measured at pH 7 was significantly greater than that at pH 3, due to the deprotonation of carboxylic group at pH 7. The shape of the force at pH 7 was distinctively different from the one at pH 3, suggesting the origin of the repulsive force might be different.

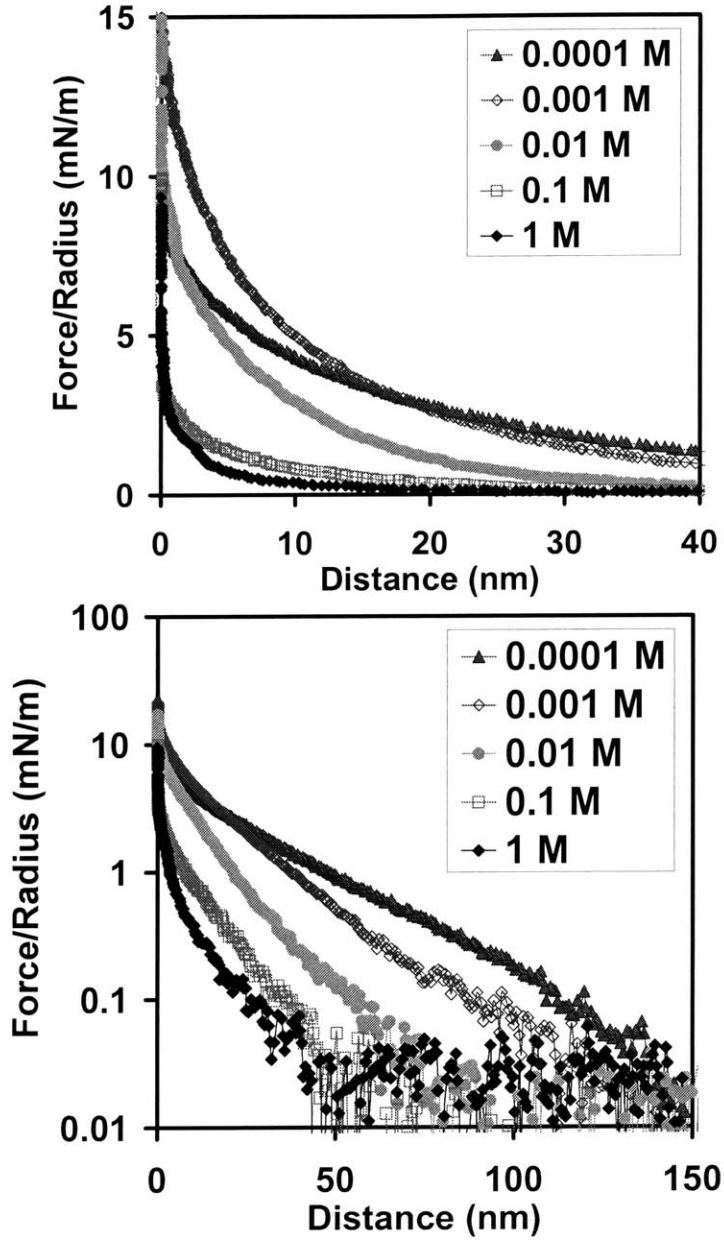

Figure 5.1: (a) The force/radius vs distance curve measured between GAG functionalized tip and substrate at various ionic strength. (b) same curve in semilog scale

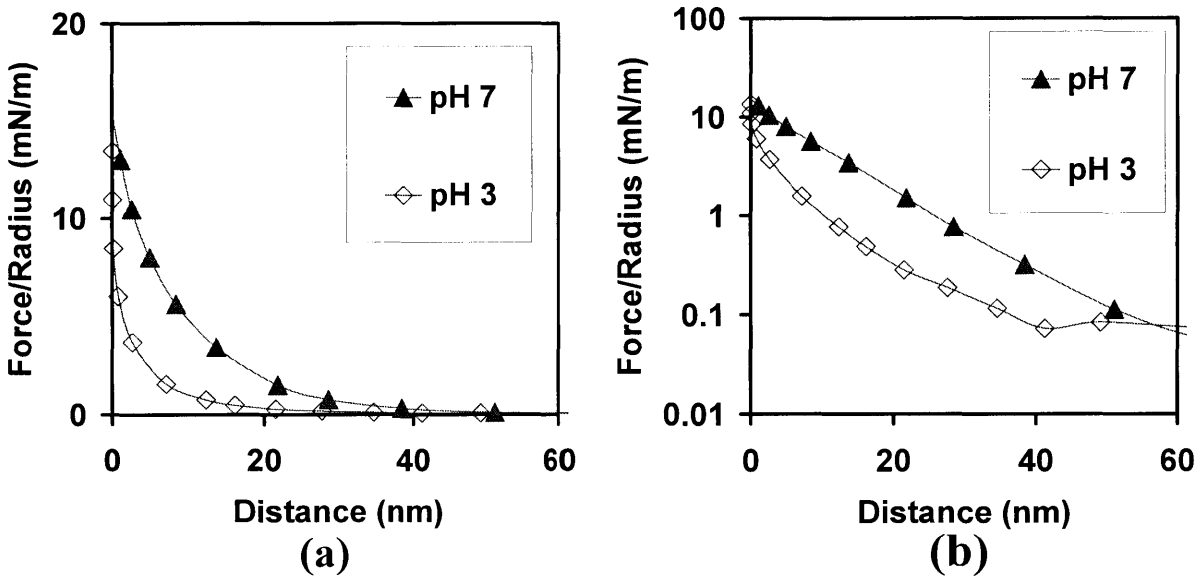

Figure 5.2: (a) Force/radius vs distance curve at pH 3 and pH 7 (b) same curve in semilog scale.

5.3.2 Ellipsometry results

In the box model, the GAG brush layer can be characterized by two unknown parameters; thickness and refractive index. The refractive index of a GAG brush layer can also be calculated using an effective medium approximation. In our case, since we know the parking density of the GAG layer that was determined from scintillation counter analysis, the refractive index for GAG layers was estimated from GAG solution that is about the same concentration of the GAG brush layer. Since the refractive index is related to the monomer number density, changing of the density of the monomer in the brush layer would cause the change of the refractive index of the layer. Styrkas et al found out that changing the refractive index from the crystalline to the liquid-like value (changes of 20% of density) introduces a change of about 3 Å in the total thickness of the layer and results in a fit of the same quality. [125] Since 20% change of density caused only a few Å in thickness, we assume that the variation of the refractive index change due to the swelling of the brush layer has a negligible effect on the model fitting.

The equilibrium brush height of three samples obtained using box model is shown in Figure 5.2. Error bars denote the estimated uncertainty in the fitted value of the brush height. This trend was the same in all three differently prepared samples. The 2 hr sample was prepared by stopping the reaction after 2 hrs and the interchain distance was analyzed to be 11 nm. The two 72 hr samples were prepared by varying the amount of thiol functionalized GAG solution and reacting for 72 hrs for the reaction. The interchain distance for 72 hr sample was found out to be 6.5 nm from scintillation counter analysis.

The brush height of 72 hr sample increased from 20 nm to 28 nm as ionic strength increased from pure deionized water to 0.0001 M. Between 0.0001 M and 0.01 M, the brush height did not change significantly up to 0.01 M and the differences between salt concentrations were within the experimental error. The 24 hr sample showed the same trend; its brush height increased from 11 nm to 18 nm as the ionic strength changes from pure water to 0.0001 M and did not change significantly until the salt concentration reaches 0.01 M. But the absolute value of the brush thickness showed the parking density dependence. The brush height of 72 hr sample was about as twice high as the height of 2 hr sample when the salt concentration varies from 0 to 0.01 M. The maximum brush height achieved around 0.1 M in all samples and then the height decrease as the ionic strength further increased up to 3 M. There was not much difference in the trend and magnitude depending on the amount of GAG dropped on the substrate. The maximum brush height of 72 hr and 2 hr sample was 43 nm and 37 nm respectively.

The pH experiment of 72 hr sample showed the drastic change of the brush height from 23 nm at pH 3 to 48 nm at pH 7, suggesting significant structural change of doubling the brush height occurred due to deprotonation of carboxylic group in the GAG. The

absolute value of the brush height at pH 7 indicated that the GAG molecules are fully stretched, considering that its length is about the same as its contour length. The trend of the brush height variation at various ionic strengths and pH's implied that the GAG is behaving as an annealed polyelectrolyte

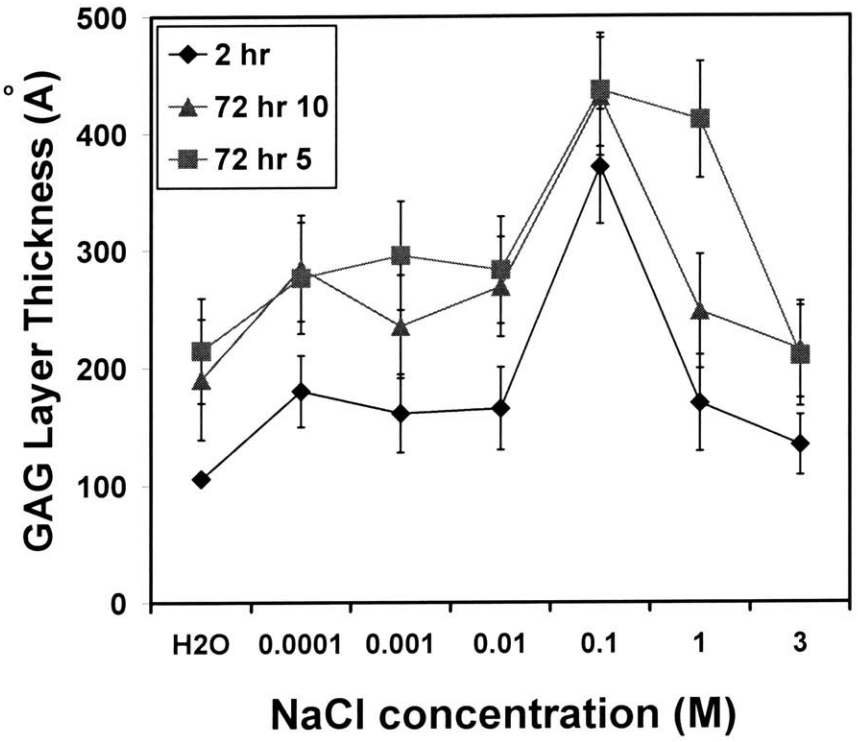

Figure 5.3: The GAG layer thicknesses measured at various salt concentrations using ellipsometry for two different incubation times at pH~5.6. For 72 hr sample, two different volumes (10 µl and 5 µl) of the GAG solution was used and each was labeled as 72 hr 10 and 72 hr 5, respectively.

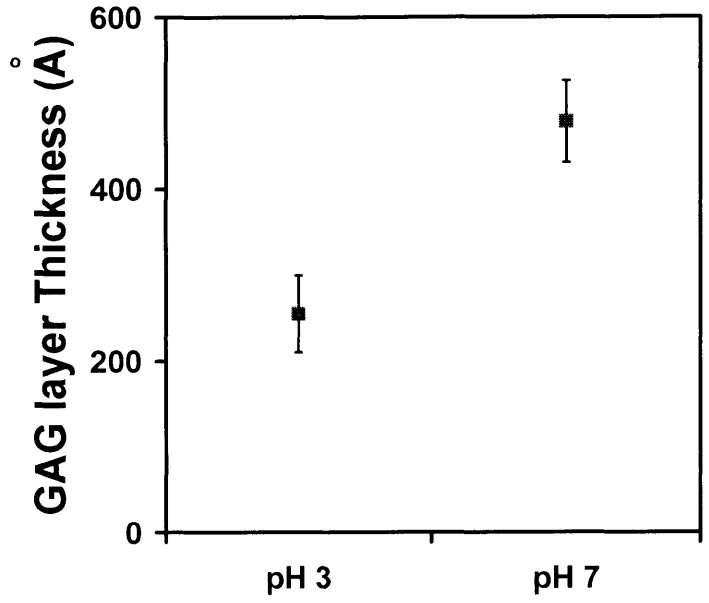

Figure 5.4: The GAG layer thickness measured at two different pH's; pH 3 vs pH 7. (ionic strength: 0.015 M, incubation time: 72 hr)

5.4 Discussion

5.4.1 The force measurement between GAG vs GAG

The repulsive force was reversible without showing any jump-to-contact on the surface even at 1 M salt concentration. No adhesion and no hysteresis during the force measurement in a repeatable manner indicated that GAGs are solidly end grafted on the substrate without adhesion on the substrate, rather stretched out due to Columbic interaction between charged groups with fully hydrated structure. No jump-to-contact at 1 M suggested that GAG brush layer totally shields any attractive surface interactions (e.g. van der Waals dispersion) even at very high salt concentration. The significant dependence of the repulsive force on the ionic strength showed the high contribution of the inter- and intramolecular electrostatic interaction plays a major role in this range of salt concentration.

The range of the repulsive force interaction is well above its contour length due do long range interaction between double layer that exists the above the brush. As pointed out previously by Zhulina et al, in contrast to neutral brushes that begin to interact only when they are brought into close contact, the Coulomb repulsion between polyelectrolyte brushes comes into play at much larger separations, prior to the physical contact of their outer edges.[117] Even without touching each other, the two opposing polyelectrolyte brushes rearrange in order to minimize the grand potential.[126]

The crossover of the force curve between 0.0001 M and 0.001 M occurred around 20 nm and the distance where it happens suggests that there might be the reorganization of the brush due to long range interaction. The crossover of the force curves is believed to be due to the charge increase in the brush layer as the ionic strength increases. [123] If the brush height is fixed, then the crossover of the force curves occurs near the brush height. In the GAG vs GAG experiment, the crossover point was located at about 20 nm which is much less than the brush height, suggesting that there was a reorganization of the GAG brush layer due to long-range electrostatic interaction of the ionic atmosphere above the brush layer. We were able to see the jump to contact to the top of the brush layer in GAG substrate and hydroxy probe tip system at 0.0001 M salt concentration, where the GAG brush layer was less charged and the tip was neutral. No-jump-to contact on top of the brush layer in GAG vs GAG system as well as in case of sulfate tip vs GAG substrate also suggests the possibility of reorganization of the brush before it touches the tip of the brush layer due to double layer interaction that exists between charged surface.

The forces and the configurations of GAG molecules are intimately connected. Information on the configurations of GAGs can be inferred direct measurement of the forces

between two chemisorbed layers that are brought into direct contact. The distance at the onset of detectable force above the standard deviation for the OH and GAG probe tips vs GAG brushes was measured (Figure 5.5) and gives a rough measure of h or 2*h respectively at high salt concentrations(> 0.1 M) where double layer interaction is minimal. It has been shown that equilibrium brush thickness can be determined by AFM force measurement in case of neutral polymer brush with high parking density.[37] Taunton et al showed that the range for onset of interaction is roughly twice of the thickness of the corresponding adsorbed chains using polystyrene-poly(ethylene oxide) diblock copolymers. From the distance for onset of interaction, 2L, which corresponds to the separation at which repulsion can just be detected, an effective layer thickness may be estimated. The onset of force increasing distance was determined by choosing the distance where the force started to increase beyond the standard deviation. The distance where force starts to increase decreased from 70 nm to 41 nm as ionic strength increased from 0.01 M to 1 M in GAG vs GAG system whereas it decreased from 38 nm to 11 nm in the same range of ionic strength variation in GAG substrate vs OH tip. The onset of the interaction showed significant dependency on the ionic strength, which imply an important role of electrostatic interaction in determining the force increase distance. At salt concentrations below 0.001 M, the force increasing distance was well beyond the twice of the brush thickness, indicating that the long-range electrostatic interaction of the double layer above the GAG brush is determining factor of the force increasing distance. Interestingly we observed the long range interaction in hydroxy tip and GAG substrate system. The possible reason would be the adsorption of the ions on the tip surface.

At 0.01 M salt concentration, the force increasing distance (70 nm) was about twice of the contour length of the GAG in GAG vs GAG system whereas it was about 37 nm in

GAG substrate vs hydroxy tip, which is about the contour length of the GAG chain. Considering that the electrostatic interaction starts usually 4 or 5 times of Debye length (3nm at 0.01 M) between two charged surfaces, the fact that force increasing distance is about twice of the effective brush height suggests that there might be an reorganization of the brush layer due to the long-range electrostatic interaction between GAG substrate and GAG tip.[117] However, considering that intermolecular distance between GAG is about 6 nm, just twice of the Debye length, its reorganization due to double layer interaction between GAG brush layers might be limited because intermolecular electrostatic interaction inside the brush layer might be strong enough to compete with the double layer interaction between GAG brush layers.

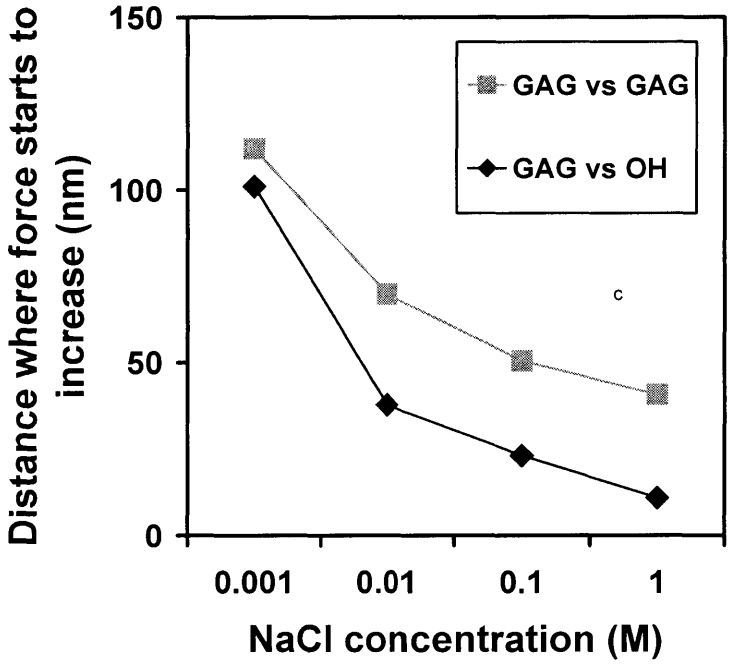

Figure 5.5: The distance where force starts to increase at four different ionic strengths in GAG substrate vs GAG tip and GAG substrate and hydroxy tip.

At higher salt concentration, say 0.1 and 1 M, the force increasing distance in GAG vs GAG system was 50.5 and 40.7 nm respectively, shorter than twice of the GAG contour length. The force increasing distances in GAG vs hydroxy tip system at 0.1 M and 1 M were found out to be 23 nm and 11 nm respectively. These facts suggested that there is an overlap or inter-penetration between the GAG brush layers when the force started to increase. Especially at 1 M, the force increasing distance is about the brush height, implying that there is a significant inter-penetration between GAG layers or compression of the brush layer as the two brush layers approaches. Dean et al compared the repulsive forces between GAG brush layers in two cases; when they interpenetrate each other and when they are squeezed against each other.[96] The comparison of the calculated force of those two models showed that the repulsive force by interdigitation between the GAG layers is smaller than the force by compression of the GAG layer. The fitting of the experimental data using both models showed that interdigitation results fits the data more closely.(paper 3) At 1 M NaCl concentration, the force started to increase at 11 nm, which is far shorter than the contour length of the GAG molecule in GAG vs hydroxy system. The persistence length of the GAG was found out to 9 nm using coarse-grain model at 1 M.[Bathe, 2003 #411] Based upon the distance where force started to increase, which is very close to the persistence length of GAG at 1 M, the bending of the GAG might play a role in the repulsive force.

5.4.2 Ellipsometry measurement.

In situ conformation change of GAG at various salt concentrations is critical to interpret the force measurement data: the brush thickness is essential for molecular scale modeling of our system using PB equation, which is currently used as a fitting parameter. Therefore, the brush height that is mainly determined by inter- and intra- molecular electrostatic interaction is directly probed in situ using ellipsometry. According to theoretical prediction, the polyelectrolyte brush stretching is determined primarily by electrostatic interactions in the layer rather than by steric repulsion between the monomers.[26, 27, 30, 123]The effect of long-range interaction on the orientation of the grafted polyelectrolyte under the conditions of loose grafting was analyzed by Borisove et al.[27] They found out that this stretching of polyelectrolyte brush is determined primarily by electrostatic interactions in the layer rather than by short-range repulsion between uncharged units that plays a major role in the neutral brushes. Moreover, due to the long-range nature of the electrostatic interactions, it was shown that the grafted plolyelectrolyte chains become stretched in the normal direction at grafting densities below the overlapping threshold of the neutral polymer brush.

The polyelectrolyte brushes can be divided into two classes depending on the charged group behavior. In the so-called "quenched" brush, the charge is independent of the local pH so the polyelectrolyte will have a fixed amount of charge. This is the case when the ionizable groups are strong acids, e.g., sulfate groups (SO_3^-). On the other hand, in the so-called "annealed" brush, the ionization of the charged groups does depend on the local pH so the charge density becomes a function of local pH. This case occurs when the charge groups are weak acids, e.g., carboxyl groups (COO-).

In the case of quenched polyelectrolyte that has constant charge without showing any dependence on salt concentration and pH of the bath, the addition of salt into the bulk solution leads to screening of the electrostatic interactions, reducing the electrostatic swelling of the brush thickness from fully stretched state.[116] In contrast, the brush height of annealed polyelectrolyte remains without stretching at low salt concentrations because of the consequence of the following self-regulating mechanism.

At very low salt concentration, even a very small charge density in the brush generates a high potential and a correspondingly high local proton concentration, which opposes further dissociation. In the limit of zero salt concentrations, the proton concentration in the brush is significantly higher than in the bulk phase because the exchange of dissociated protons is limited due to a small number of counterions available in the bulk. As a result, the degree of dissociation in the brush is lower than that of the bulk. This regime is referred to as the annealed osmotic brush regime.[127] In this regime, the brush height of an annealed polyelectrolyte increases as the bulk salt concentration increases due to the increased ionization of the charged groups in the brush.

At high salt concentrations, the proton concentration in the brush is approximately equal to that in the bulk because the dissociated protons in the brush are exchanged with indifferent salt ions from the bulk while maintaining electroneutrality in the brush. This regime is known as the salted brush regime and the brush height decreases as salt concentration increases due to the shielding of the electrostatic interaction. Those two regimes can be distinguished depending on the relation of the ion concentration in the brush to the one in solution. Therefore, whereas the addition of the salt only causes shielding of the electrostatic interaction in the case of fully charged quenched polyelectrolyte brush, it

results two opposite effect in the case of annealed polyelectrolyte brush in two different regimes. In osmotic regime, the addition of salt causes increase of the ionization of polyelectrolytes; increase in the bulk salt concentration results in decrease of the concentrations of H ions in the brush, which induces additional ionization of monomers. In salted brush regime, the increase of the salt concentration enhances the screening of Coulombic interaction as quenched polyelectrolyte case. Due to this opposite effect of adding salt in annealed polyelectrolyte brush, the brush height shows nonmonotonic behavior that shows a maximum brush height between these two different regimes.[127]

GAG has a very unique chemical structure having disaccharide repeating unit that contains both carboxyl group and sulfate group, combination of the quenched and annealed polyelectrolyte structure, in one macromolecule. Since the half of the GAG charged groups are pH dependent, the nonmonotomic behavior of the equilibrium brush height that is typical behavior of the annealed polyelectrolyte is expected. The general trend of the optical brush height change measured using ellipsometry in Figure 5.3 is indeed very similar to the change of the brush height of the annealed polyelectrolyte brush.

Figure 5.3 shows that the brush height slightly increased till 0.01 M and jumped at 0.1 M and then decreased as ionic strength increased supporting the theoretical prediction that annealed polyelectrolyte brush would show the maximum of the brush height as ionic strength increases.[123] Currie et al observed that the brush height slowly increased and then decreased as ionic strength increased in polyacrylic acid brush system which is annealed polyelectrolyte.[124] At very low salt concentration, the counterions, H^+, remain in the brush layer due to high potential inside the layer. Because the local pH inside the brush is low due to localization of the hydrogen ion, most of the charged groups remain protonated.

As ionic strength increased, counterions from salt, say Na^+, is partitioned between bulk and inside of the brush layer, reducing the concentration of the hydrogen ion inside the layer, promoting deprotonation of the uncharged groups. The increased ionization of the charged group with increasing salt concentration make the polyelectrolyte stretched due to electrostatic interaction between charged groups. Further increase of the salt concentration at certain point now starts to shield the interaction between the charged groups of the polyelectrolyte that are fully ionized. The brush height started to decrease as ionic strength increased and finally reach the brush height that was the same as the brush height without any ionization of the charged groups. We observed the same trend showing maximum brush height in our GAG brush system around 0.1 M as salt concentration increased.

The maximum brush height was observed around 0.1M salt concentration. The maximum of the brush height was predicted to be located at osmotic brush/salted brush boundary. Currie et al also observed that the gradual increase of the bush height was evident, reaching maximum around same concentration, 0.1 M, and then it decreased at various parking densities.[124] Ahrens et al also observed that osmotically swollen brush of constant thickness, independent of grafting density, shrinks only at high salt conditions (above 0.1 M) in quenched polyelectrolyte case.[119] In our case the fixed charge concentration of the GAG in the brush layer is about 0.1 M so it is reasonable to observe the maximum brush height at 0.1 M.

Isreals et al predicted that the concentration where the maximum of the brush height occurs depends on the parking density of the polyelectrolyte brush layer.[123] The maximum brush height of 2 hr and 72 hr sample seemed to occur about the same range of ionic strength, 0.1 M although the concentration range that we measured was sparse. It was

predicted that the maximum brush height shifts to higher ionic strength as increasing the parking density.[123] It was found out that increasing the anchoring density by a factor of 5 shifts the maximum to a 5 times higher salt concentration but leaves its maximum height unchanged according to theoretical prediction. That is because ionization is becoming difficult as a result of increasing the mean field in the brush layer due to the increase of the grafting density at specific salt concentration. It was shown that titration curves of the grafted PAA chains shift to higher pH values with increasing parking density, which is an experimental evidence of the above statement.[124] According to the calculation based upon the parking density, the maximum of the brush height of 2 hr sample should occur 0.04 M, not very far from 0.1 M, making it difficult to say whether there was a shifting or not. The another experimental data at various parking densities reported by Currie et al did not show the shifting of the maximum brush height as ionic strength increased and the maximum brush height remained around 0.1 M with wide range of parking densities. This is probably due to neglected excluded volume effect that can play a role in high grafting density brush layer. In our case it was hard to observe the shifting of the maximum because our small parking density variation was small and probably the salt concentration range was too wide to observe the clear trend of the shifting.

In the osmotic brush regime, the brush thickness scales as ionic strength with one third exponent.[123] however, using the experimental results between 0.01 M and 0.1 M, we obtained the exponent close to 0.19 instead of 0.33, which shows that the experimental dependence of the brush thickness on the ionic strength in the osmotic brush regime is significantly less than predicted theoretically. Currie et al also observed that scaling exponent of the brush height was around 0.1, which is also less than that predicted theoretically(1/3).[124]. They attributed the difference to the steric interactions that has a

higher influence at lower salt concentrations. In other words, at low ionic strength the polyelectrolytes are already somewhat stretched due to steric interactions between monomers thus the increase in brush thickness with increasing ionic strength is less than given by the mean field scaling law. On the other hand, Biesalski found out that their polyacid system follows the scaling behavior quite closely in osmotic brush regime.[128]

The exponent in salted brush regime was found out to be -1/3 from scaling theory derived by Pincus.[26] Ahrens et al found out that only at high salt conditions (above 0.1 M), the brush shrinks and the thickness scales with the molecular area and the salt concentration with an exponent – 1/3.[119] It was also that the brush height followed the scaling behavior in the salted brush regime.[126, 129] Tran et al observed that the exponent in their experiment showed the exponent -0.27, a little less than -1/3 predicted by theory. We found that the scaling exponent for brush height vs salt concentration in the range from 0.1 M to 3 M was 0.2, which was smaller than the scaling prediction. Considering the finite size of the molecules of the GAG and NaCl would make the exponent more closer to the theoretically predicted value.

The independence of brush height on the grafting density is a very unusual feature known only for the quenched polyelectrolyte brush in osmotic brush regime.[119] Self consistent field model predicts the shifting of the brush height curve to higher ionic strength as parking density increases without changing maximum in annealed polyelectrolyte brush.[123] But our experimental data showed the brush height from high parking density brush(72 hr) was higher than that of low parking density brush(2 hr) in the range of salt concentrations that we measured. The maximum value of the brush height was also observed to be different between 2 hr sample and 72 hr sample. The 72 hr sample showed

the brush height of 20 nm in pure water with a maximum height of 43 nm at 0.1 M whereas the 2 hr sample showed 10 nm in pure water with a maximum brush height of 37 nm at 0.1 M. For 72 hr sample, the brush height was rather constant around 28 nm from 0.0001 M to 0.01 M. The brush height of the 2 hr sample also showed the same behavior, maintaining similar brush height of 17 nm from 0.001 M and 0.01 M, which implies there is no significant change of charge density that causes structural change of the brush in this range. Although self consistent model calculation predicted that the parking density does not change the maximum brush height, Currie et al and we observed that with relatively high parking density samples, the brush height was dependent on the parking density.[124] [123]

In our experiment the increase and decrease of the brush height was occurred in narrow range compared with the range predicted by theory.[123] And we observed rather abrupt change of the brush height rather than gradual change of the brush height that expands over 3 or 4 orders of salt concentration range predicted by the self consistent field model. The brush height changed little between 0.0001 M to 0.01 M salt concentration and showed rather sudden change of the brush height around 0.1 M salt concentration. Currie et al observed very similar trend with their annealed polyelectrolyte system at similar parking density brush: it showed rather constant brush height at lower salt concentration, then maximum around 0.1 M and then decreased at higher salt concentration with 8 nm^2 parking density, which is closest parking density to our system.[124] The reason for not showing the gradual change of the brush height is not clear at this moment. We think this is because it is hard to detect the weakly stretched polyelectrolyte using ellipsometry at this parking density.

5.4.3 Comparison of optical thickness with onset of force measured using MFP

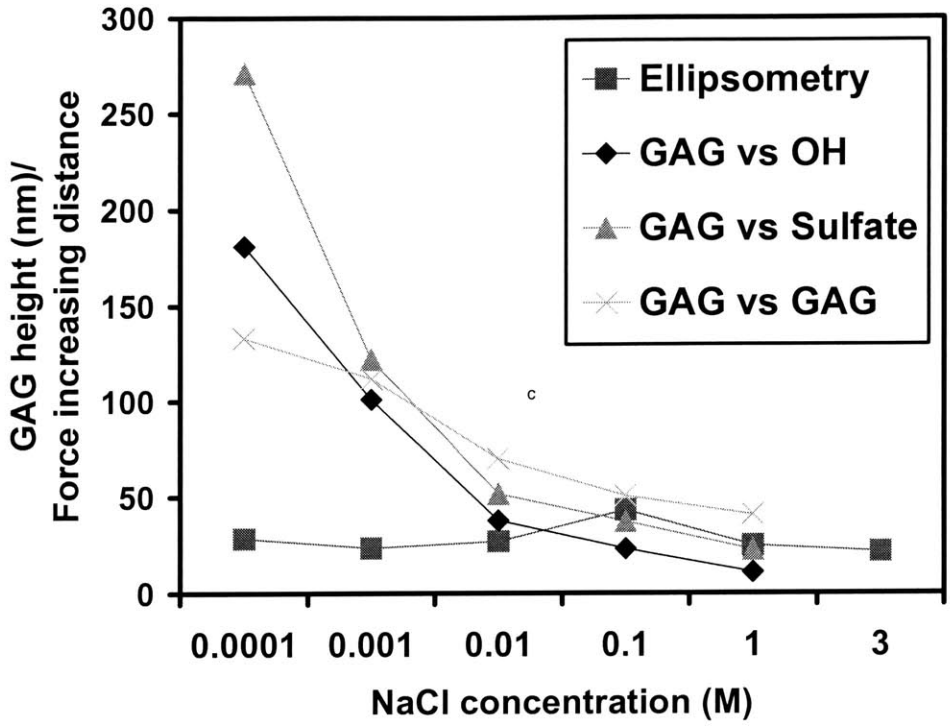

Figure 5.6: The force increasing distance and optical brush height as a function of the salt concentration. The systems include GAG substrate vs hydroxy tip, GAG substrate vs sulfate tip, and GAG substrate vs GAG tip.(pH~5.6)

The force increasing distance in various systems of OH tip vs GAG substrate, sulfate tip vs GAG substrate and GAG vs GAG data showed monotonic decrease as ionic strength increased, whereas the equilibrium brush height measured using ellipsometry showed quite different trend.(Figure 5.6) The force increasing distance in GAG vs sulfate tip was always longer than that in GAG vs OH tip due to the additional electrostatic interaction between the tip and the substrate. Above 0.1 M salt concentration, say, in the salted brush regime, the trend between optical brush height measured from ellipsometry and onset of force increasing distance is same; they decreased as ionic strength increased. The slope of each case turned

out to be in the range of -0.12~-0.20, which is weaker dependence on the salt concentration than the exponent predicted in the scaling theory(-1/3).

In hydroxy tip and GAG substrate system, it was clear that we cannot correlate the force data with optical equilibrium brush height at lower salt concentration, due to the unexpected small charge adsorption on the hydroxy tip. But at relatively high ionic strength above 0.1 M, we can assume distance where the force started to increase due to interaction between GAG brush layers is highly correlated by segment density profile so we can compare the force increasing distance with equilibrium brush height obtained from ellipsometry. The absolute value comparison of the force increasing distance and brush height in OH tip vs GAG substrate system showed that force increasing distance is shorter than equilibrium brush height measured by ellipsometry at higher salt concentration range(above 0.1 M). The GAG molecules at 0.1 M seems to be more stretched out compared to that at 0.01 M based upon the ellipsometry results but due to higher shielding of electrostatic interactions at 0.1 M, the force increasing distance is lower than the GAG brush height. The force measurement suggests that brush layer is compressed by the tip with little resistance that is undetectable by MFP. We also think that splaying of the brush by the pointed tip as a result of shielded intermolecular interaction can be also a reason for shorter range of the onset of force increase at 0.1 M. The optical thickness measured at 3 M was 21 nm which is still as twice as high as the force increasing distance measured at 1 M in OH vs GAG system. This also supports that the force increasing distance is determined when the tip is already inside the brush and there is a depth that tip penetrates with minimal resistance by splaying the brush layer with pointed tip. Although we tried to attempted to correlate the force measurement data with ellipsometry data, the ellipsometry data should be interpreted with care because a presupposed model is necessary to obtain the optical brush thickness. It

was also suggested that the resolution of the ellipsometry might not be enough to resolve the gradual variation of lower parking density sample that weakly stretches as was in our case. In terms of discrepancy between the onset of force increase and optical brush height at higher salt concentration may be due to the box profile which can fail to describe the experiment accurately. Especially in the swollen state, smoother functions like the error function are certainly more appropriate. Because only two parameters(Ψ and Δ) are measured with ellipsometry, it is not possible to deal with such density distributions. Styrkas et al compared the quality of fit using trilayer model with the box model and found out that ellipsometry is virtually insensitive to the roughness on a few nanometer scale unless the refractive index profile of the whole interfacial region is known from other measurements.[125] Due to the insensitivities that can arise from this simple modeling, although ellipsometry measurement provides a good estimate of the brush thickness, additional information from other measurements would be beneficial.

To determine either the counterion or monomer density distribution, one need a scattering technique with a high spatial resolutions; for instance, neutron or X-ray scattering.[116, 119, 120] Neutron reflection measurements is another indirect method to probe the structure of the brush layer. It allows the measurements of the same interface at different contrasts of the ambient phase by mixing deuterated and protonated materials that scatter neutrons with different scattering amplitudes. The future experiment using neutron reflectivity will provide more information of segment distribution that complements the ellipsometry data.

5.5 Conclusion

The force between GAG functionalized tip and GAG substrate was measured at various ionic strength and pH's. The reversible repulsive force was observed without any adhesion and hysterisis. The significant dependence on ionic strength and pH showed that the nature of the repulsive force originated from the Coulombic interaction between charged groups in GAG molecules. The distance where the force started in increase due to interaction between brush layers is compared with optical brush thickness measured using ellipsometry. As we expected, the onset of the force was detected much longer distance that contour length of the GAG at low salt concentration due to the interaction of the ionic atmosphere present above the brush layer. The onset of force increasing distance showed monotonic decrease as the salt concentration increases whereas the optical brush thickness showed a maximum at 0.1 M salt concentration, which indicates that the GAG behaves like an annealed polyelectrolyte brush.

Appendix A

A.1 Theoretical Models for Electrostatic Forces: Diffuse Electrical Double Layer Theory

The Poisson-Boltzmann (PB) equation gives an expression for the electrical potential, Φ (V), between two charged surfaces in an electrolyte solution which, for a mono-monovalent electrolyte has the form:[40, 86]

$$\nabla^2\Phi = \frac{2FC_0}{\varepsilon_w}\sinh\left(\frac{F\Phi}{RT}\right) \qquad (A1.1)$$

where F is the Faraday Constant (=96,500 Coulombs/mole), C_o the bulk concentration of ions (moles/m^3), ε_w the dielectric permittivity of water (=6.9*10^{-10} Coulombs/Nm^2), R the Universal Gas Constant (=8.314 J/mole·K), and T the absolute temperature=298 K. To uniquely determine the potential, two boundary conditions on either the potential or its derivative (the electric field) are required. Unfortunately, the PB equation is nonlinear and therefore is difficult to solve analytically except for simple geometries. The force, F, per unit area acting in the z-direction on the charged surface or, more generally, at any position z=z_0 between the charged surfaces is the sum of two terms: the osmotic pressure due to the ion concentration gradients and the Maxwell electric field stress due to the force of the electric field action on ionic:[40, 86]

$$\frac{\mathrm{F}}{\mathrm{Area}} = \left(2RTC_0(\cosh(\frac{F\Phi}{RT}) - 1) + \frac{\varepsilon_w}{2}(\nabla\Phi)^2 \right)\Big|_{z=z_0} \qquad (A1.2)$$

A.1.1 Constant Surface Charge Density Model: Analytical Solution[47, 52, 53, 72]

This model represents the tip as a smooth hemisphere with constant surface charge per unit area, σ_1 (Coulombs/m^2), and the substrate as a flat plane with constant surface charge per unit area, σ_2. An analytical solution of the linearized PB equation is often used in the literature and can be obtained by first linearizing eq. *(A1.1)* for small enough $F\Phi/RT$ to obtain:

$$\nabla^2\Phi \approx \frac{2F^2C_0}{\varepsilon_w RT}\Phi = \kappa^2\Phi \qquad (A1.3)$$

where κ^{-1} is the electrical Debye length that can be calculated independently from the ionic strength using:

$$\kappa^{-1} = \sqrt{\frac{\varepsilon_w RT}{2z^2F^2C_{io}}} \qquad (A1.4)$$

where the ion valence z = 1 for our experiments. The PB equation has been solved for two infinite parallel planes of charge,[53] and the result integrated to obtain the force between a hemisphere and plane.[72] For two infinite planes of charge with the specified surface charges σ_1 and σ_2, the boundary conditions at these surfaces are: $\frac{\partial\Phi}{\partial z} = \frac{\sigma_1}{\varepsilon_w}$ and $\frac{\partial\Phi}{\partial z} = -\frac{\sigma_2}{\varepsilon_w}$.

As $z \to \infty$, the potential and the electric field approach zero. The force per unit area

between two infinite flat planes of charge having densities σ_1 and σ_2 and separated by a distance D reduces to:[53]

$$\frac{F_{FLAT}}{Area} = \frac{\sigma_1^2 + 2\sigma_1\sigma_2 \cosh(\kappa \mathbf{D}) + \sigma_2^2}{2\varepsilon_w \sinh^2(\kappa \mathbf{D})} \qquad (A1.5)$$

The force on a hemispherical tip of radius $R_{HEMISPHERE}$ is obtained by integrating the force between flat surfaces over appropriately sized concentric cylinders (Fig A.1a). If the surface charge on the tip and the substrate are of the same order and κD is small, then the σ^2 terms can be neglected and the sinh can be linearized, thus yielding:

$$F_{HEMISPHERE} \approx \frac{4\pi\sigma_1\sigma_2 R_{HEMISPHERE}}{\varepsilon_w \kappa} e^{-\kappa D} \qquad (A1.6)$$

This approximation is only valid when $|\Phi|$ is much smaller than the "thermal voltage" $\frac{RT}{F} \approx 25.7\text{mV}$. When $|\Phi| >> 25.7\text{mV}$, the linearized model will overestimate the force. As we are using a constant charge boundary condition, the magnitude of the potential on the surface will increase as the tip approaches the surface. Therefore, when using a constant charge boundary condition, the linearized PB equation may not be accurate for small separations.

A.1.2. Constant Surface Charge Model: Numerical Solution

We used a Newton method on finite differences[55] to solve the full nonlinear PB equation subject to one boundary condition at each surface. The force between two infinite

charged planes was first obtained and then numerically integrated to give the force between a hemispherical tip and planar substrate. Since the problem is one dimensional, the potential in space can be represented as a one-dimensional matrix or vector in which each entry is the potential at evenly spaced points along the *z*-direction. The derivatives in the *z*-direction can be written as differences between neighboring points. The PB equation for each discrete entry plus the boundary conditions give a set of N nonlinear equations, where N is the number of discretizations, all satisfied if the potential at each point is correct. If a close enough initial guess for the value of the potential at all points is given, then that guess can be refined using a Taylor series expansion. This is repeated until the change in potential at each step is smaller than an error threshold. This algorithm is known as a Newton method for solving multidimensional systems. The potential is then converted to a force by taking a bounding box with one surface at point *i* between the two charged planes (where the derivative of the potential is zero; i.e. the electrical field is zero) and the other surface at infinity (where the potential and electric fields are zero). The force on the enclosed surface is then:

$$\frac{\mathrm{F}}{\mathrm{Area}} = \left(2RTC_0 \cosh(\frac{F\Phi[\mathrm{i}]}{RT}) - 1 \right) \qquad (A1.7)$$

The hemispherical tip geometry is approximated by using the calculated force between the flat surfaces and summing up the force on appropriately sized concentric cylinders. In effect, this method, sometimes known as Surface Element Integration (SEI),[49] is the numerical version of the integral for the linearized hemisphere tip solution above. SEI will give the exact interaction if the stress (force per unit area) is normal to the surfaces. This requirement is met if there are constant potential boundary conditions.[49] However, when the boundary conditions are constant charge, the electric field will not be directed normal to the surface

(the surfaces are no longer equipotential) and the stress will not act normal to the surfaces of the tip and substrate. SEI will then underestimate the total force since it does not take the tangential components of the stress into account. Therefore, SEI can only be used to estimate the force between constant charge hemisphere tip and substrate when the radius of the tip is bigger than the Debye length, since the tangential components of the stress will then be small. This method still has advantages over the standard Derjaguin approximation,[47] in which the force between a hemisphere and plane separated by distance D is approximated by calculating the force per unit area between two infinite planes separated by D and then multiplying by $2\pi R_{HEMISPHERE}$. This is only valid when $R_{HEMISPHERE}$ is very large and D is very small. The SEI approximation is valid for any value of D as long as $R_{HEMISPHERE}$ is larger than the Debye length. In addition, SEI can be used for many geometries and not just hemispheres, while the Derjaguin approximation is only valid for convex tip geometries. The above numerical method was implemented in C and run in Matlab (MathWorks Inc., Natick). Space was discretized to 800 increments (i.e. N= 800); the program ran until the solution converged sufficiently.[55]

A.1.3 Volume Charge Model

Since the CS-GAG molecules are approximately 30nm long, they can be modeled as a region of fixed uniform volume charge density using the approach of Ohshima.[59, 126] Adapted to the MFP geometry, this model represents the tip with SAM layer as a smooth hemisphere with surface charge, σ_1, and the substrate with CS-GAG as a smooth volume charge density, ρ_{fix}. (Appendix Figure A.1b) In the electrolyte region outside the fixed volume charge (region I), the PB equation has the form of eq. (*A1.1*). In the region inside the

fixed volume charge (region II), the PB equation has an additional term accounting for the fixed volume density, ρ_{fix}:

$$\nabla^2\Phi = \frac{2FC_0}{\varepsilon_w}\sinh(\frac{F\Phi}{RT}) - \frac{\rho_{fix}}{\varepsilon_w} \qquad (A1.8)$$

As a two-region problem, the solution to eq. *(A1.1.)* in region I and eq. *(A.1.8)* in region II is subject to boundary conditions at the hemispherical and substrate surfaces and at the edge of the volume charge (Appendix, Figure 1b). At the surfaces, the boundary conditions are the same as before: the derivative of the potential is proportional to the surface charge density ($\frac{\partial\Phi}{\partial z} = \frac{\sigma_1}{\varepsilon_w}$ at the tip and $\frac{\partial\Phi}{\partial z} = -\frac{\sigma_2}{\varepsilon_w} = 0$ at the substrate, since there is no longer a surface charge due to the surface monolayer there). There may be some induced surface charge on the substrate but that charge is negligible when compared to the volume charge density due to the CS-GAG and the surface charge density due to the SAM. At the interface between the CS-GAG volume charge density and the electrolyte phase, the potential and its derivative (the electric field) must be continuous. When the distance between the surfaces, D, is less than the height of the volume charge, *h*, and since we assume no interdigitation of the molecules, the model reduces to a single region containing a fixed charge density. The PB equation in this case has the form:

$$\nabla^2\Phi = \frac{2FC_0}{\varepsilon_w}\sinh(\frac{F\Phi}{RT}) - \frac{\rho'_{fix}}{\varepsilon_w} \qquad (A1.9)$$

where $\rho'_{fix} = \rho_{fix}(h/D)$. While the PB equation is nonlinear, the problem is still one-dimensional due to symmetry and, thus, it can be solved numerically using a similar method

as above. This numerical method was also implemented in C and run in Matlab. Space was discretized to 800 increments (i.e. N= 800) and the program ran until the solution converged sufficiently.

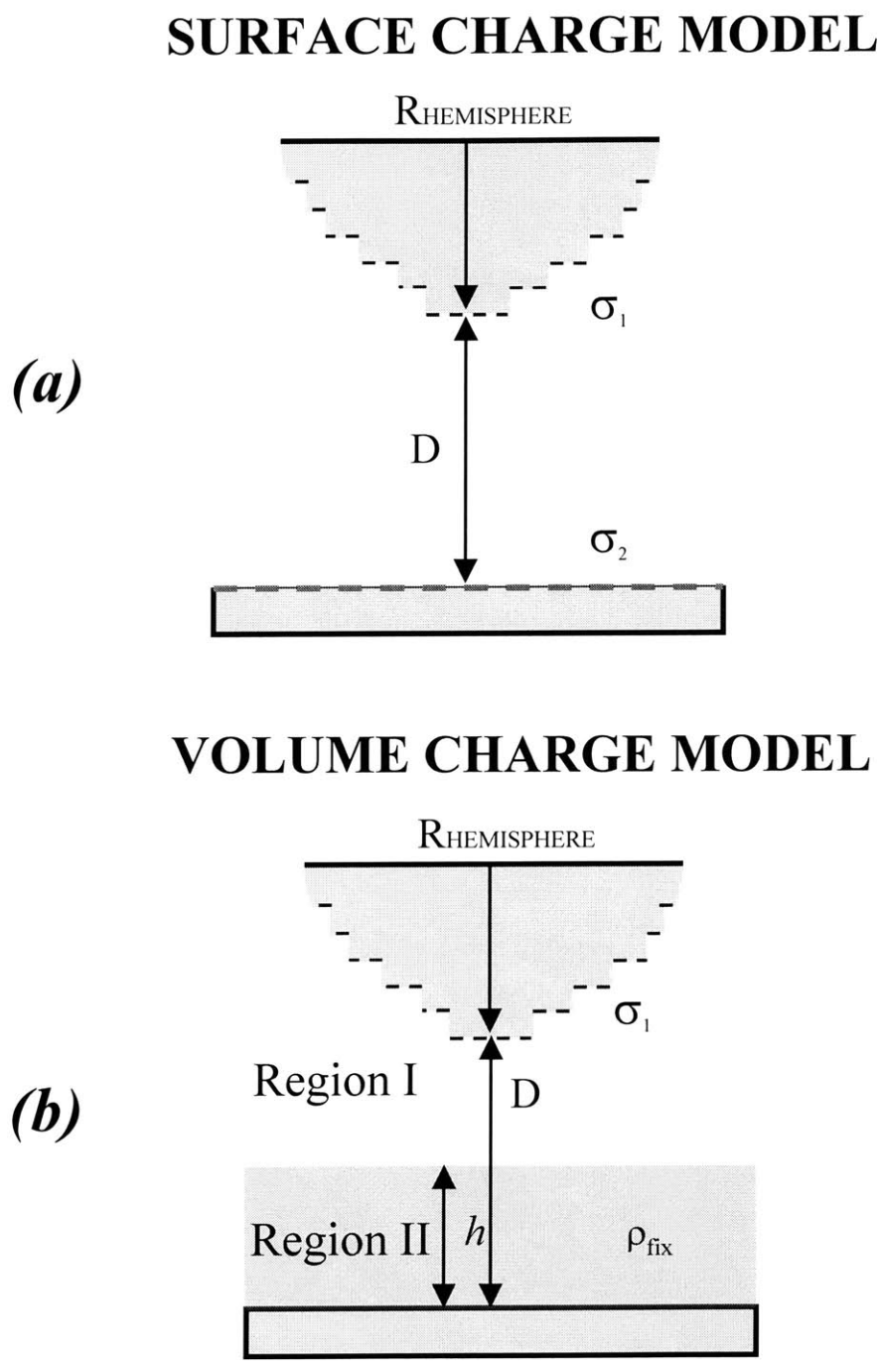

Figure A.1: (a) constant surface charge model, (b) constant volumecharge model

REFERENCES

1. Buschmann, M.D. and A.J. Grodzinsky, *A Molecular Model of Proteoglycan-Associated Electrostatic Forces in Cartilage Mechanics.* J. Biomech. Eng., 1995. **117**: p. 179-191.

2. Jin, M.S. and A.J. Grodzinsky, *Effect of electrostatic interactions between glycosaminoglycans on the shear stiffness of cartilage: A molecular model and experiments.* Macromolecules, 2001. **34**(23): p. 8330-8339.

3. Buckwalter, J.A. and L.C. Rosenberg, *Electron microscopic studies of cartilage proteoglycans. Direct evidence for the variable length of the chondroitin sulfate-rich region of proteoglycan subunit core protein.* J. Biol. Chem., 1982. **257**: p. 9830-9839.

4. Thomas, T.W., K.H. Dick, and C.H. Vincent, *Proteoglycans*, in *Cell Biology of Extracellular matrix*, E.D. Hay, Editor. 1991, Plenum press: New York and London.

5. Plaas, A.H., et al., *Glycosaminoglycan sulfation in human osteoarthritis. Disease-related alterations at the non-reducing termini of chondroitin and dermatan sulfate.* J Biol Chem, 1998. **273**(20): p. 12642-9.

6. Comper, W.D. and T.C. Laurent, *Physiological function of connective tissue polysaccharides.* Physiol. Rev., 1978. **58**: p. 255-315.

7. Eisenberg, S.R. and A.J. Grodzinsky, *Swelling of articular cartilage and other connective tissues: electromechanochemical forces.* J Orthop Res, 1985. **3**(2): p. 148-59.

8. Ehrlich, S., et al., *The osmotic pressure of chondroitin sulphate solutions: experimental measurements and theoretical analysis.* Biorheology, 1998. **35**(6): p. 383-97.

9. Dean, D., et al., *A New Theoretical Model for the Electrostatic Forces Between Polyelectrolyte Brushes.* In preparation.

10. Kovach, I.S., *A molecular theory of cartilage viscoelasticity.* Biophysical Chemistry, 1996. **59**(1): p. 61-73.

11. de Gennes, P.G., *Polymers at an interface: a simplified view.* Adv. Colloid Interface Sci., 1987. **27**: p. 189-209.

12. Sukhishvili, S.A. and S. Granick, *Formation and Characterization of Covalently Bound Polyelectrolyte Brushes.* Langmuir, 1997. **13**(19): p. 4935-4938.

13. Biesalski, M. and J. Rühe, *Preparation and Characterization of a Polyelectrolyte Monolayer Covalently Attached to a Planar Solid Surface.* Macromolecules, 1999. **32**(7): p. 2309-2316.

14. Jordan, R., et al., *Surface-Initiated Anionic Polymerization of Styrene by Means of Self-Assembled Monolayers.* J. Am. Chem Soc., 1999. **121**(5): p. 1016-1022.

15. Amiel, C., et al., *Adsorption of hydrophilic-hydrophobic block copolymers on silica from aqueous solutions.* Macromolecules, 1995. **28**(9): p. 3125-3134.

16. Higashi, N., H. Shiba, and M. Niwa, Macromolecules, 1989. **22**: p. 4650-4652.

17. Kong, J.T., *Measuring the electrostatic repulsionforces between glycosaminoglycans using the atomic force microscope*, in *Department of Materials Science and Engineering*. 1999.

18. Bain, C.D., et al., *Formation of Monolayer Films by the Spontaneous Assembly of Organic Thiols from Solution onto Gold.* Journal of the American Chemical Society, 1989. **111**(1): p. 321-335.

19. Wagner, P., *Immobilization strategies for biological scanning probe microscopy.* Febs Letters, 1998. **430**(1-2): p. 112-115.

20. Wilbur, J.L., et al., *Microfabrication by microcontact printint of self-assembled monolayers.* Adv. Mater., 1994. **6**(7-8): p. 600-604.

21. Parsonage, E., et al., *Adsorption of Poly(2-Vinylpyridine) Poly(Styrene) Block Copolymers from Toluene Solutions.* Macromolecules, 1991. **24**(8): p. 1987-1995.

22. Deutsch, A.J., R.J. Midura, and A.H. Plaas, *Structure of chondroitin sulfate on aggrecan isolated from bovine tibial and costochondral growth plates.* J. Orthop. Res., 1995. **13**(2): p. 230-9.

23. Toida, T., et al., *Detection of glycosaminoglycans as a copper(II) complex in high-performance liquid chromatography.* J. Chromatogr. A., 1997. **787**(1-2): p. 266-70.

24. Marra, J. and M.L. Hair, *Interactions between Adsorbed Polystyrene Layers in Toluene Heptane Mixtures - Effect of Solvent Quality.* Macromolecules, 1988. **21**(8): p. 2349-2355.

25. Farndale, R.W., D.J. Buttle, and A.J. Barret, *Improved quantitation and discrimination of sulfated glycosaminoglycans by use of dimethylmethylene blue.* Biochimica et Biophysica Acta, 1986. **883**: p. 173-177.

26. Pincus, P., *Colloid Stabilization with Grafted Polyelectrolytes.* Macromolecules, 1991. **24**(10): p. 2912-2919.

27. Borisov, O.V., E.B. Zhulina, and T.M. Birshtein, *Diagram of the States of a Grafted Polyelectrolyte Layer.* Macromolecules, 1994. **27**(17): p. 4795-4803.

28. Chen, W.L., et al., *Equilibrium swelling of hydrophilic polyacrylates in humid environments.* Macromolecules, 1999. **32**(1): p. 136-144.

29. Milner, S.T., *Polymer Brushes.* Science, 1991. **251**(4996): p. 905-914.

30. Zhulina, E.B., T.M. Birshtein, and O.V. Borisov, *Theory of Ionizable Polymer Brushes.* Macromolecules, 1995. **28**(5): p. 1491-1499.

31. Kelley, T.W., et al., *Direct Force Measurements at Polymer Brush Surfaces by Atomic Force Microscopy.* Macromolecules, 1998. **31**(13): p. 4297-4300.

32. Hayashi, S., et al., *Polyelectrolyte brush layers studied by surface forces measurement: Dependence on pH and salt concentrations and scaling.* Langmuir, 2002. **18**(10): p. 3932-3944.

33. Abe, T., et al., *Density-Dependent Jump in Compressibility of Polyelectrolyte Brush Layers Revealed by Surface Forces Measurement.* Langmuir, 1999. **15**(22): p. 7725-7731.

34. Hutter, J.L. and J. Bechhoefer, *Calibration of atomic-force microscope tips.* Rev. Sci. Instrum., 1993. **64**(7): p. 1868-1873.

35. Sarid, D., *Scanning Force Microscopy.* 1991, Oxford (UK): Oxford University Press. 48.

36. Yamamoto, S., et al., *Surface Interaction Forces of Well-Defined, High-Density Polymer Brushes Studied by Atomic Force Microscopy. 2. Effect of Graft Density.* Macromolecules, 2000. **33**(15): p. 5608-5612.

37. Yamamoto, S., et al., *Surface Interaction Forces of Well-Defined, High-Density Polymer Brushes Studied by Atomic Force Microscopy. 1. Effect of Chain Length.* Macromolecules, 2000. **33**(15): p. 5602-5607.

38. Kuettner, K. and A. Lindenbaum, *Analysis of mucopolysaccharides in partially aqueous media.* Biochim. Biophys. Acta, 1965. **101**: p. 223-225.

39. Freeman, W.D.S.C. and A. Maroudas, Ann. Rheum. Dis., 1975. **34**(Suppl): p. 44-45.

40. Sanfeld, A., *Thermodynamics of charged and polarized layers.* Monographs in statistical physics and thermodynamics, ed. I. Prigogine. Vol. 10. 1968, Bath(UK): Wiley-interscience publication. 179-185.

41. Kane, V. and P. Mulvaney, *Double-Layer Interactions between Self-Assembled Monolayers of ω-Mercaptoundecanoic Acid on Gold Surfaces.* Langmuir, 1998. **14**(12): p. 3303-3311.

42. Vezenov, D.V., et al., *Force titrations and ionization state sensitive imaging of functional groups in aqueous solutions by chemical force microscopy.* J. Am. Chem. Soc., 1997. **119**(8): p. 2006-2015.

43. Ederth, T., P. Claesson, and B. Liedberg, *Self-Assembled Monolayers of Alkanethiolates on Thin Gold Films as Substrates for Surface Force Measurements. Long-Range Hydrophobic Interactions and Electrostatic Double-Layer Interactions.* Langmuir, 1998. **14**(17): p. 4782-4789.

44. Ashby, P.D., L.W. Chen, and C.M. Lieber, *Probing intermolecular forces and potentials with magnetic feedback chemical force microscopy.* Journal of the American Chemical Society, 2000. **122**(39): p. 9467-9472.

45. Verwey, E.J.W. and J.T.G. Overbeek, *Theory of the Stability of Lyophobic Colloids.* 1948, Amsterdam: Elsevier.

46. Derjaguin, B.V. and L. Landau, Acta Physiochim. URSS., 1941. **14**: p. 633-662.

47. Israelachvili, J.N., *Intermolecular and Surface Forces.* 2nd ed. 1992, London: Academic Press. 275.

48. Derjaguin, B.V., Kolloid Z., 1934. **69**: p. 155-164.

49. Bhattacharjee, S. and M. Elimelech, *Surface Element Integration : A Novel Technique for Evaluation of DLVO Intreraction between a Particle and Flat Plate.* J. Colloid Interface Sci., 1997. **193**: p. 273-285.

50. Parsegian, V.A. and G.H. Weiss, *Spectroscopic Parameters for Computation of van der Waals Forces.* J. Colloid Interface Sci., 1981. **81**(1): p. 285-289.

51. Biggs, S., et al., *Anion Adsorption at the Gold-Aqueous Interface.* J. Am. Chem. Soc., 1994. **116**(20): p. 9150-9157.

52. Ninham, B.W. and V.A. Parsegian, *Electrostatic Potential between Surfaces Bearing Ionizable Groups in Ionica Equilibrium with Physiologic Saline Solution.* J. Theor. Biol., 1971. **31**: p. 405-428.

53. Parsegian, V.A. and D. Gingell, *On the Electrostatic Interaction across a salt solution between two bodies bearing unequal charges.* Biophys. J., 1972. **12**: p. 1192-1204.

54. Butt, H.-J., *Electrostatic Interaction in Atomic Force Microscopy.* Biophys. J., 1991. **60**: p. 777-785.

55. Forsythe, G.E. and W.R. Wasow, *Finite Difference Methods for Partial Differential Equations*, ed. I.S. Sokolnikoff. 1960, New York: John Wiley +Sons, inc.

56. Bain, C.D., et al., Journal of the American Chemical Society, 1989. **111**: p. 321.

57. Maroudas, A., *Physicochemical properties of articular cartilage*, in *Adult Articular Cartilage*, M.A.R. Freeman, Editor. 1979, Pitman Medical: Kent. p. 215-290.

58. Miller, I. and D. Williams, *Steric interaction of an incoming particle with grafter rods: Exact solutions and unusual force profiles.* Phys. Rev. E: Stat. Phys., Plasmas, Fluids, Relat. Interdiscip. Top., 2000. **61**(5): p. R4706-R4709.

59. Ohshima, H., *Electrostatic Repulsion between two parallel plates coverd with polymer brush layers.* Colloid Polym. Sci., 1999. **277**: p. 535-540.

60. van Oss, C.J., *Interfacial Forces in Aqueous Media.* 1994, New York: Marcell Dekker.

61. Everett, D.H., *Basic Principles of Colloid Science.* 1988, London: Royal Society of Chemistry. 51.

62. Sheth, S.R. and D. Leckband, *Measurements of attractive forces between poteins and end-grafted poly(ethylene glycol) chains.* Proc. Natl. Acad. Sci. U.S.A., 1997. **94**(16): p. 8399-8404.

63. Kuhl, T.L., et al., *Modulation of Interaction Forces between Bilayers Exposing Short-Chained Ethylene-Oxide Headgroups.* Biophys. J., 1994. **66**(5): p. 1479-1488.

64. Rijnaarts, H.H.M., et al., *DLVO and steric contributions to bacterial deposition in media of different ionic strengths.* Colloids Surf., B, 1999. **14**(1-4): p. 179-195.

65. Fleer, G.J., et al., *Polymers at Interfaces.* 1993, London: Chapman and Hall.

66. Israelachvili, J.N., *Forces between Surfaces in Liquids.* Advances in Colloid and Interface Science, 1982. **16**(JUL): p. 31-47.

67. Pashley, R.M., *Hydration Forces between Mica Surfaces in Aqueous-Electrolyte Solutions.* J. Colloid Interface Sci., 1981. **80**(1): p. 153-162.

68. Pashley, R.M., *DLVO and hydration forces between mica surfaces in Li+, Na+, K+, and Cs+ electrolyte-solutions - a correlation of double-layer and hydration forces with surface cation-exchange properties.* J. Colloid Interface Sci., 1981. **83**(2): p. 531-546.

69. Israelachvili, J.N. and G.E. Adams, *measurement of forces between 2 mica surfaces in aqueous-electrolyte solutions in range 0-100nM.* J. Chem. Soc. Farad. T., 1978. **74**: p. 975-1001.

70. Horn, R.G., D.R. Clarke, and M.T. Clarkson, *Direct Measurement of surface forces between sapphire crystals in aqueous solutions.* J. Mater. Res., 1988. **3**: p. 413-416.

71. Grabbe, A., *Double Layer Interactions between Silylated Silica Surfaces.* Langmuir, 1993. **9**: p. 797-801.

72. Butt, H.-J., *Measuring electrostatic, van der Waals, and hydration forces in electrolyte solutions with an atomic force microscope.* Biophys. J., 1991. **60**: p. 1438-1444.

73. Ducker, W.A., T.J. Senden, and R.M. Parshley, *Direct measurement of colloidal forces using an atomic force microscope.* Nature, 1991. **353**: p. 239-241.

74. Ducker, W.A., T.J. Senden, and R.M. Pashley, *Measurement of forces in liquids using a force microscope.* Langmuir, 1992. **8**: p. 1831-1836.

75. Biggs, S., et al., *The Role of Colloidal Stability in the Formation of Gold Sols.* J. Colloid Interface Sci., 1993. **160**: p. 511-513.

76. Senden, T.J. and C.J. Drummond, *Surface-Chemistry and tip sample interactions in atomic-force microscopy.* Colloids Surf., A, 1995. **94**(1): p. 29-51.

77. Raiteri, R., et al., *Preliminary results on the electrostatic double-layer force between two surfaces with high surface potential.* Colloids Surf. A, 1998. **136**(1-2): p. 191-197.

78. Zhmud, B.V., A. Meurk, and L. Bergstrom, *Evaluation of Surface Ionization Parameters from AFM data.* J. Colloid Interface Sci., 1998. **207**: p. 332-343.

79. Feldman, K., et al., *Probing Resistance to Protein Adsorption of Oligo(ethyleneglycol)-Terminated Self-Assembled monolayers by Scanning Force Microscopy.* J. Am. Chem Soc., 1999. **121**(43): p. 10134-10141.

80. Teschke, O., E.F. de Souza, and G. Ceotto, *Double Layer Relaxation Measurements Using Atomic Force Microscopy.* Langmuir, 1999. **15**(15): p. 4935-4939.

81. Wang, J. and A.J. Bard, *Direct atomic force microscopic determination of surface charge at the gold/electrolyte interface - The inadequacy of classical GCS theory in describing the double-layer charge distribution.* J. Phys. Chem. B, 2001. **105**(22): p. 5217-5222.

82. Wang, J. and A.J. Bard, *On the absence of a diffuse double layer at electronically conductive polymer film electrodes. Direct evidence by atomic force microscopy of complete charge compensation.* J. Am. Chem. Soc., 2001. **123**(3): p. 498-499.

83. *The Asylum MFP design is such that certain types of highly conducting tips can be grounded via the spring clip that holds the cantilever chip; however this was not the case for our system, Cleveland, J. Asylum Research, Personal communication.*

84. Reiner, E.S. and C.J. Radke, *Double layer interactions between charge-regulated colloidal surfaces: Pair potentials for spherical particles bearing ionogenic surface groups.* Adv. Colloid Interface Sci., 1993. **47**: p. 59-147.

85. Fixman, M., *The Poisson-Boltzmann Equation and its Application to Polyelectrolytes.* J. Chem. Phys., 1979. **70**: p. 4995-5005.

86. Devereux, O.F. and P.L. de Bruyn, *Interaction of Plane-Parallel Double Layers.* 1963, Cambridge, MA: M.I.T. Press.

87. Pederson, H.G. and L. Bergstrom, J. Am. Ceram. Soc., 1989. **82**(5): p. 1137-1145.

88. Kamiyama, Y. and J. Israelachvili, *Effect of pH and Salt on the Adsorption and Interactions of an Amphoteric Polyelectrolyte.* Macromolecules, 1992. **25**(19): p. 5081-5088.

89. Zauscher, S. and D.J. Klingenberg, *Normal forces between cellulose surfaces measured with colloidal probe microscopy.* J. Colloid Interface Sci., 2000. **229**(2): p. 497-510.

90. Biggs, S., et al., *Molecular Weight Dependence of the Depletion Interaction between Silica Surfaces in Solutions of Sodium Poly(styrenesulfonate).* Langmuir, 2000. **16**(24): p. 9242-9248.

91. Le Berre, F., M. Malmsten, and E. Blomberg, *Interfacial Properties of a Model Polyampholyte Studied by Surface Force Measurements, ESCA, and Ellipsometry.* Langmuir, 2001. **17**(3): p. 699-704.

92. Abraham, T., et al., *Direct Measurements of Interactions between Hydrophobically Anchored Strongly Charged Polyelectrolyte Brushes.* Langmuir, 2000. **16**(9): p. 4286-4292.

93. Luckham, P.F. and J. Klein, *Interactions between Smooth Solid-Surfaces in Solutions of Adsorbing and Nonadsorbing Polymers in Good Solvert Conditions.* Macromolecules, 1985. **18**(4): p. 721-728.

94. Hale, G., et al., *Simulation of vascular surfaces: differential saturation with glycosaminoglycans and their quatitative analysis.* Biomaterials, 1988. **9**(4): p. 376-378.

95. Fleer, G.J. and J. Lykema, *Adsorption from Solution at the Solid-Liquid Interface*, ed. G. Parfitt, Rochester, CH. 1983, New York: Academic Press.

96. Dean, D., et al., Langmuir, 2003(accepted).

97. Radmacher, M., et al., *From molecules to cells: imaging soft samples with the atomic force microscope.* Science, 1992. **257**(5078): p. 1900-5.

98. Israelachvili, J.N., *The Forces between Surfaces.* Philosophical Magazine a-Physics of Condensed Matter Structure Defects and Mechanical Properties, 1981. **43**(3): p. 753-770.

99. Frisbie, C.D., et al., *Functional-Group Imaging by Chemical Force Microscopy.* Science, 1994. **265**(5181): p. 2071-2074.

100. Rief, M., et al., *Reversible unfolding of individual titin immunoglobulin domains by AFM.* Science, 1997. **276**(5315): p. 1109-12.

101. Rief, M., H. Clausen-Schaumann, and H.E. Gaub, *Sequence-dependent mechanics of single DNA molecules.* Nat Struct Biol, 1999. **6**(4): p. 346-9.

102. Ortiz, C. and G. Hadziioannou, *Entropic elasticity of single polymer chains of poly(methacrylic acid) measured by atomic force microscopy.* Macromolecules, 1999. **32**(3): p. 780-787.

103. Florin, E.L., V.T. Moy, and H.E. Gaub, *Adhesion forces between individual ligand-receptor pairs.* Science, 1994. **264**(5157): p. 415-7.

104. Rief, M., et al., *Single molecule force spectroscopy on polysaccharides by atomic force microscopy.* Science, 1997. **275**(5304): p. 1295-1297.

105. Lee, G.U., L.A. Chrisey, and R.J. Colton, *Direct measurement of the forces between complementary strands of DNA.* Science, 1994. **266**(5186): p. 771-3.

106. Strunz, T., et al., *Dynamic force spectroscopy of single DNA molecules.* Proc Natl Acad Sci U S A, 1999. **96**(20): p. 11277-82.

107. Dammer, U., et al., *Binding Strength between Cell-Adhesion Proteoglycans Measured by Atomic-Force Microscopy.* Science, 1995. **267**(5201): p. 1173-1175.

108. McKendry, R., et al., *Chiral discrimination by chemical force microscopy.* Nature, 1998. **391**(6667): p. 566-568.

109. Hugel, T., et al., *Single-molecule optomechanical cycle.* Science, 2002. **296**(5570): p. 1103-1106.

110. Jiang, X.P., C. Ortiz, and P.T. Hammond, *Exploring the rules for selective deposition: Interactions of model polyamines on acid and oligoethylene oxide surfaces.* Langmuir, 2002. **18**(4): p. 1131-1143.

111. Seog, J., et al., *Direct measurement of glycosaminoglycan intermolecular interactions via high-resolution force spectroscopy.* Macromolecules, 2002. **35**(14): p. 5601-5615.

112. Heaton, R.J., A.W. Peterson, and R.M. Georgiadis, *Electrostatic surface plasmon resonance: direct electric field-induced hybridization and denaturation in monolayer nucleic acid films and label-free discrimination of base mismatches.* Proc Natl Acad Sci U S A, 2001. **98**(7): p. 3701-4.

113. Klein, J., et al., *Lubrication Forces between Surfaces Bearing Polymer Brushes.* Macromolecules, 1993. **26**(21): p. 5552-5560.

114. Oesterhelt, A.F., M. Rief, and H.E. Gaub, *Single molecule force spectroscopy by AFM indicates helical structure of poly(ethylene-glycol) in water.* New Journal of Physics, 1999. **1**: p. 6.1-6.11.

115. Taunton, H.J., et al., *Interactions between Surfaces Bearing End-Adsorbed Chains in a Good Solvent.* Macromolecules, 1990. **23**(2): p. 571-580.

116. Mir, Y., P. Auroy, and L. Auvray, *Density Profile of Polyelectrolyte Brushes.* Physical Review Letters, 1995. **75**(15): p. 2863-2866.

117. Zhulina, E.B. and O.V. Borisov, *Structure and interaction of weakly charged polyelectrolyte brushes: Self-consistent field theory.* Journal of Chemical Physics, 1997. **107**(15): p. 5952-5967.

118. Biesalski, M., J. Ruhe, and D. Johannsmann, *Segment density profiles of polyelectrolyte brushes determined by Fourier transform ellipsometry.* Journal of Chemical Physics, 1999. **111**(15): p. 7029-7037.

119. Ahrens, H., S. Forster, and C.A. Helm, *Charged polymer brushes: Counterion incorporation and scaling relations.* Physical Review Letters, 1998. **81**(19): p. 4172-4175.

120. Tran, Y., P. Auroy, and L.T. Lee, *Determination of the structure of polyelectrolyte brushes.* Macromolecules, 1999. **32**(26): p. 8952-8964.

121. Azzam, R.M.A. and N.M. Bashara, *Ellipsometry anad Polarized Light.* 1977, Amsterdam: North Holland.

122. Habicht, J., et al., *Swelling of thick polymer brushes investigated with ellipsometry.* Langmuir, 1999. **15**(7): p. 2460-2465.

123. Israels, R., F.A.M. Leermakers, and G.J. Fleer, *On the Theory of Grafted Weak Polyacids.* Macromolecules, 1994. **27**(11): p. 3087-3093.

124. Currie, E.P.K., et al., *Polyacrylic acid brushes: Surface pressure and salt-induced swelling.* Langmuir, 2000. **16**(22): p. 8324-8333.

125. Styrkas, D.A., et al., *Structure of self-assembled layers on silicon: Combined use of spectroscopic variable angle ellipsometry, neutron reflection, and atomic force microscopy.* Journal of Applied Physics, 1999. **85**(2): p. 868-875.

126. Tamashiro, M.N., et al., *Salt dependence of compression normal forces of quenched polyelectrolyte brushes.* J. Chem. Phys., 2001. **115**(4): p. 1960-1969.

127. Borisov, O.V. and E.B. Zhulina, *Structure of weakly charged polyelectrolyte brushes: Monomer density profiles.* Journal De Physique Ii, 1997. **7**(3): p. 449-458.

128. Biesalski, M., D. Johannsmann, and J. Ruhe, *Synthesis and swelling behavior of a weak polyacid brush.* Journal of Chemical Physics, 2002. **117**(10): p. 4988-4994.

129. Guenoun, P., et al., *Freestanding Black Films of Polymers - a Model of Charged Brushes in Interaction.* Physical Review Letters, 1995. **74**(18): p. 3628-3631.